

AD-A059 015

MCDONNELL AIRCRAFT CO ST LOUIS MO

VARIABLE ACUITY DISPLAY DEVELOPMENT. VOLUME I. BASIC PROGRAM. (U)

F/G 14/2

AUG 77 R W FISHER, R HELMICK, G LICIS

F33615-76-C-1031

UNCLASSIFIED

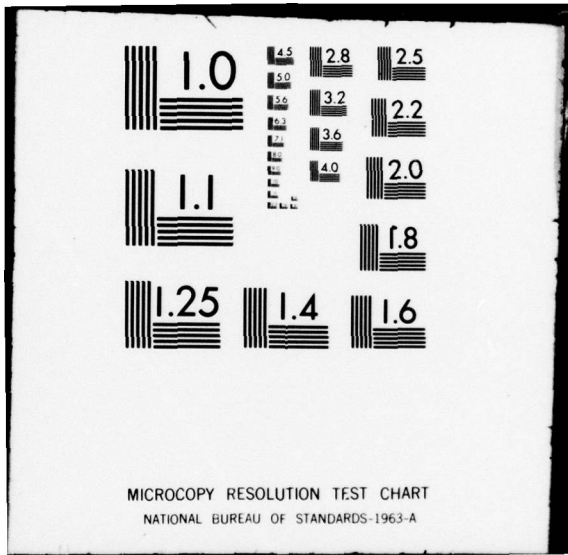
AFAL-TR-77-156-VOL-1

NL

1 OF 1  
AD  
A059015



END  
DATE  
FILMED  
11-78  
DDC



MICROCOPY RESOLUTION TEST CHART  
NATIONAL BUREAU OF STANDARDS-1963-A

AD A059015

DDC FILE COPY

AFAL-TR-77-156  
VOLUME I

LEVEL #



**VARIABLE ACUITY DISPLAY DEVELOPMENT**  
**VOLUME I: BASIC PROGRAM**

MCDONNELL AIRCRAFT COMPANY  
MCDONNELL DOUGLAS CORPORATION  
P.O. BOX 516  
ST. LOUIS, MO. 63166

August 1977

**FINAL REPORT**



APPROVED FOR PUBLIC RELEASE; DISTRIBUTION UNLIMITED.

AIR FORCE AVIONICS LABORATORY  
AIR FORCE WRIGHT AERONAUTICAL LABORATORIES  
AIR FORCE SYSTEMS COMMAND  
WRIGHT-PATTERSON AIR FORCE BASE, OHIO 45433

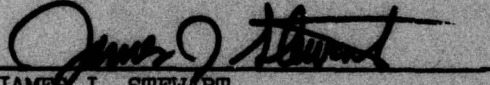
78 09 20 023

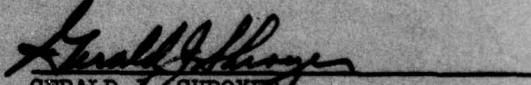
**NOTICE**

When Government drawings, specifications, or other data are used for any purpose other than in connection with a definitely related Government procurement operation, the United States Government thereby incurs no responsibility nor any obligation whatsoever; and the fact that the government may have formulated, furnished, or in any way supplied the said drawings, specifications, or other data, is not to be regarded by implication or otherwise as in any manner licensing the holder or any other person or corporation, or conveying any rights or permission to manufacture, use, or sell any patented invention that may in any way be related thereto.

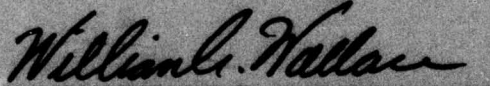
This report has been reviewed by the Information Office (OI) and is releasable to the National Technical Information Service (NTIS). At NTIS, it will be available to the general public, including foreign nations.

This technical report has been reviewed and is approved for publication.

  
JAMES J. STEWART  
Project Engineer

  
GERALD J. SHROYER  
Chief, Thermal Imaging Group

FOR THE COMMANDER

  
WILLIAM A. WALLACE, Lt Col, USAF  
Chief, Electro-Optics & Reconnaissance  
Branch  
Reconnaissance & Weapon Delivery Division

ADDITION BY	
YES	Write Section <input checked="" type="checkbox"/>
NO	Self Section <input type="checkbox"/>
UNANNOUNCED	<input type="checkbox"/>
JUSTIFICATION	
BY	DISTRIBUTION AVAILABILITY CODES
Dist.	ACAL. add. or SERIAL
A	

"If your address has changed, if you wish to be removed from our mailing list, or if the addressee is no longer employed by your organization please notify AEAL/RWI-2, W-PAFB, OH 45433 to help us maintain a current mailing list".

Copies of this report should not be returned unless return is required by security considerations, contractual obligations, or notice on a specific document.

19 TR-77-156-VOL-1

SECURITY CLASSIFICATION OF THIS PAGE (When Data Entered)

REPORT DOCUMENTATION PAGE		READ INSTRUCTIONS BEFORE COMPLETING FORM
1. REPORT NUMBER AFAL-TR-77-156, Volume I	2. GOVT ACCESSION NO.	3. RECIPIENT'S CATALOG NUMBER
4. TITLE (and Subtitle) VARIABLE ACUITY DISPLAY DEVELOPMENT Volume I, Basic Program		5. TYPE OF REPORT & PERIOD COVERED FINAL TECHNICAL REPORT
7. AUTHOR(s) R.W. Fisher, R. Helmick, G. Licis A. Rosenfeld		8. CONTRACT OR GRANT NUMBER(s) F33615-76-C-1031
6. PERFORMING ORGANIZATION NAME AND ADDRESS McDonnell Aircraft Company McDonnell Douglas Corporation P.O. Box 516, St. Louis, MO 63166		10. PROGRAM ELEMENT, PROJECT, TASK AREA & REPORT NUMBER Project 2004/06/06
11. CONTROLLING OFFICE NAME AND ADDRESS Air Force Avionics Laboratory United States Air Force Wright-Patterson AFB, Ohio 45433		12. REPORT DATE August 1977
14. MONITORING AGENCY NAME & ADDRESS (if different from Controlling Office)		13. NUMBER OF PAGES 89
		15. SECURITY CLASS. (of this report) Unclassified
		15a. DECLASSIFICATION/DOWNGRADING SCHEDULE
16. DISTRIBUTION STATEMENT (of this Report) Approved for public release; distribution unlimited. 12 94 p.		
17. DISTRIBUTION STATEMENT (of the abstract entered in Block 20, if different from Report) v. 2 A058458		
18. SUPPLEMENTARY NOTES		
19. KEY WORDS (Continue on reverse side if necessary and identify by block number) Variable Acuity Displays Optics Vision		
20. ABSTRACT (Continue on reverse side if necessary and identify by block number) A small compact direct view display was designed and fabricated for the Variable Acuity Remote Viewing System. This display is 20 times smaller, 50 times brighter, and has 3 times better resolution than the only other existing display for the system, a real image projection display.		

403 111 78 09 20 023

slf

FOREWORD

This is Volume I of a two-volume final report of Contract F33615-76-C-1031. The objectives of this contract was to design, fabricate, and test a small compact direct view display for the Variable Acuity Remote Viewing System (VARVS).

The display was successfully fabricated and found to have satisfactory performance. The contributions, technical guidance, and suggestions of Mr. V. Diehl, Project Manager, Air Force Avionics Laboratory are gratefully acknowledged.



TABLE OF CONTENTS

<u>Section</u>	<u>Title</u>	<u>Page</u>
1	INTRODUCTION & SUMMARY	1
2	BACKGROUND AND APPROACH	3
	2.1 Eye Control (Fully Gimballed Display)	5
	2.2 Head Control (Helmet Mounted)	5
	2.3 Hand Control (Fixed Display)	5
	2.4 Selected System	6
3	ANALYSIS	9
	3.1 Optical Requirements	9
	3.2 Electronic Requirements	14
4	DISPLAY DESIGN & FABRICATION	18
	4.1 Optical Design and Fabrication	18
	4.2 Approach Development	18
	4.3 Mechanical Design and Fabrication	28
	4.4 Electronic Design and Fabrication	28
5	ASSEMBLY AND TEST OF VIEWER	32
	5.1 Electronics	32
	5.2 Optical Assembly Tests	32
6	CONCLUSIONS AND VARVS SYSTEM PERFORMANCE PREDICTIONS	41
	REFERENCES	46
	APPENDIX A DIRECT VIEW PHOTOMETRIC ANALYSIS	47
	APPENDIX B APPLICATION OF THE NIGHT VISION LABORATORY (NVL) THERMAL VIEWING SYSTEM STATIC PERFORMANCE MODEL TO THE RVS	49
	B.1 MTF's	49
	B.2 Noise Equivalent Modulation (NEM)	54
	B.3 MRM Calculations	56
	B.4 Conclusions	57
	APPENDIX C COMPUTER DESIGN DATA	59

LIST OF ILLUSTRATIONS

<u>Figure</u>	<u>Title</u>	<u>Page</u>
1	VARVS Display Systems	2
2	MCAIR Display Systems Studies	4
3	Approach	7
4	Performance vs Display Brightness	10
5	Performance vs Optical Blur	11
6	VAD Distortion and Focal Length Requirements	12
7	Distortion Design Tolerances	13
8	Cue Generation (Optical Distortion Correction)	16
9	IMC Mechanization - Optical Distortion Correction	17
10	Optical Design and Fabrication Work Flow	18
11	Direct View Geometry	19
12	Diffuse Screen Viewer	20
13	Effect of Small Pupil Test Setup	23
14	Basic Components of the Direct View Display	24
15	Optical Elements of VAD	26
16	Predicted Performance from Design Raytrace	27
17	Variable Acuity Aspheric Viewer	29
18	Optical Assembly	30
19	CRT and Electronic Mounting Structure	30
20	Final Mechanical Assembly	31
21	Optical Evaluation	33
22	Measured Image Height Accuracy	34
23	Measured Optical Blur	36



LIST OF ILLUSTRATIONS (Continued)

<u>Figure</u>	<u>Title</u>	<u>Page</u>
24	Electronics and System Test Setup	37
25	CRT Test Setup for Display System Resolution Testing	38
26	Measured Viewer Performance Limit	38
27	Display Optical Performance Comparisons	40
28	Variable Acuity Display System Performance with ONR Camera	42
29	Variable Acuity Display System Performance with ONR Camera	43
30	Variable Acuity Display System MTF's for Perfect Display	44
31	Variable Acuity Display System MTF's for Design Goal Optics and Existing CRT and Electronics	44
32	Variable Acuity Display System MTF's for Completed Display	45
33	Variable Acuity Display System Total MTF's	45
A-1	Direct View Geometry	47
B-1	Scan Distortion Introduced by Foveal Lens	50
B-2	Optical Relay Parameters	52
B-3	NVL Model Adapted to VARVS for Visual Spectrum	58

## Section 1

### INTRODUCTION & SUMMARY

This final report documents the results of Contract No. F33615-76-C-1031 where the objective was to design and build a compact direct view display for the VARVS (Variable Acuity Remote Viewing System). It contains the analysis design, fabrication, and testing data.

Prior to this effort the only way to display wide field variable acuity imagery was a large gimbaled projection system developed under Navy (ONR) contract. This system required a 9 foot diameter dome and an expensive light valve projector and a sophisticated servo control system. The direct view display developed under this contract has 1/20 the size and is about 1/10 as expensive as the projection system. In addition, the display fabricated under this effort is about 50 times brighter than the projection display, has uniform illumination over the entire field-of-view (FOV), has twice the on-axis acuity of the projection display, and has much better contrast capabilities because the projection system suffers from an integrating sphere effect that significantly reduces contrast. These two concepts and their relative sizes are illustrated in Figure 1 which shows the basic elements of the two display systems. The figure also shows a potential for helmet mounting of a reduced size version of this direct view display.

The measured performance of the completed direct view Variable Acuity Display (VAD) is listed below.

o Field of View	120°
o Distortion	1%
o On-axis Acuity	1 arc minute
o Dynamic Range	10 shades of grey ( $\sqrt{2}$ )
o Brightness	50 footlamberts
o Brightness Uniformity	<u>+10%</u>

This performance was achieved even though the optical quality of the display was approximately 1/4 of the design raytrace prediction. The problem appears to be caused by poor radial surface quality of the lens spline surfaces.

In order to reduce size and weight of the VAD further for helmet mounting, it appears that a state-of-the-art improvement must be made in fabrication and testing of the spline or aspheric lens surfaces. If such improvements can be made, a size reduction of 1/2 to 1/3 would be feasible. With plastic optics and a solid state linear array source, it appears that this display design could be helmet mounted in the manner shown on Figure 1.

This report has six sections including this Introduction. The second section provides the background and the approach to the development of the viewer. The third contains the analysis. The fourth contains display design and fabrication data. The fifth section contains viewer assembly and tests and finally the last section contains the conclusions and performance predictions.

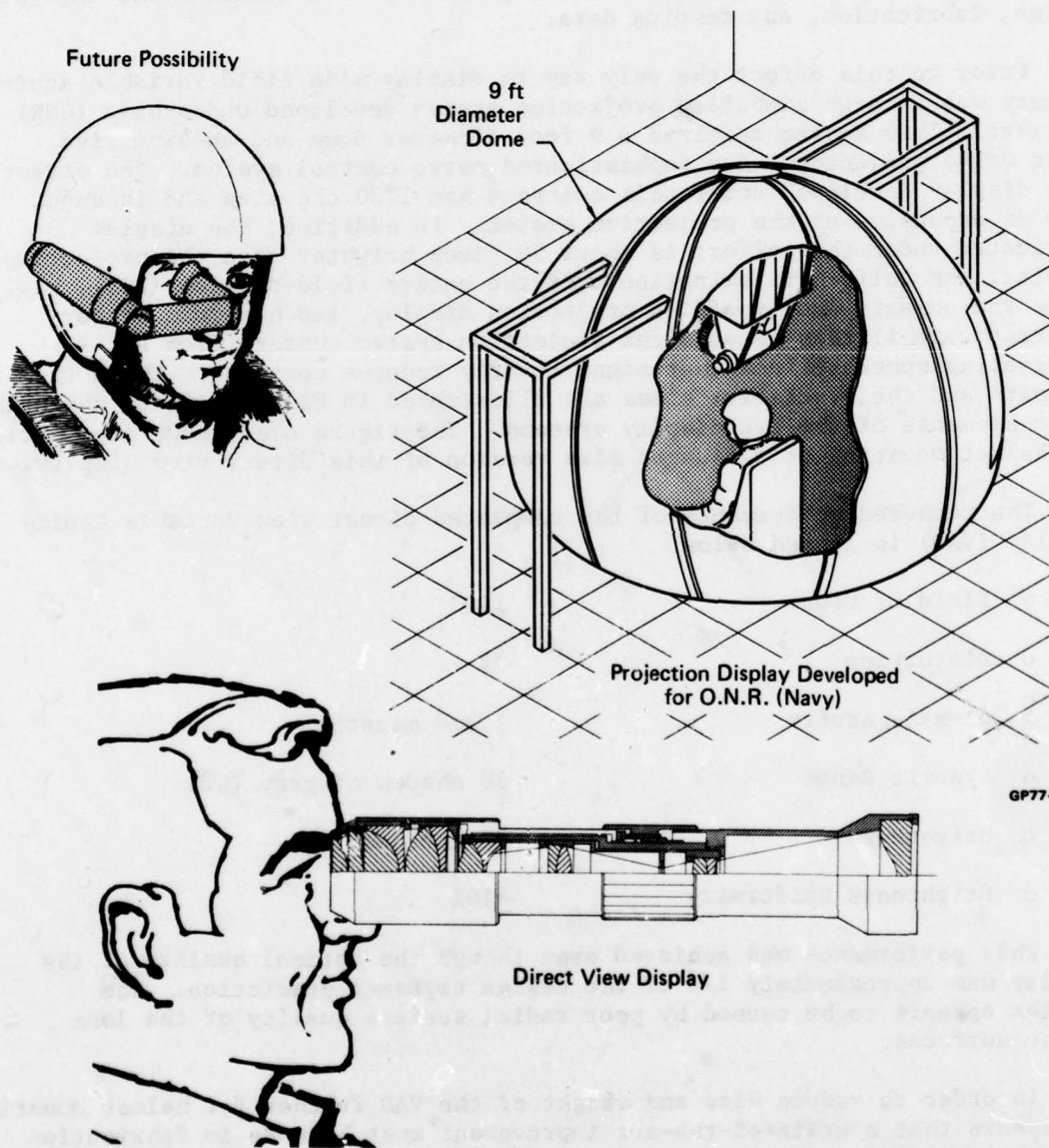


**FIGURE 1**  
**VARVS DISPLAY SYSTEMS**

## Section 2

### BACKGROUND AND APPROACH

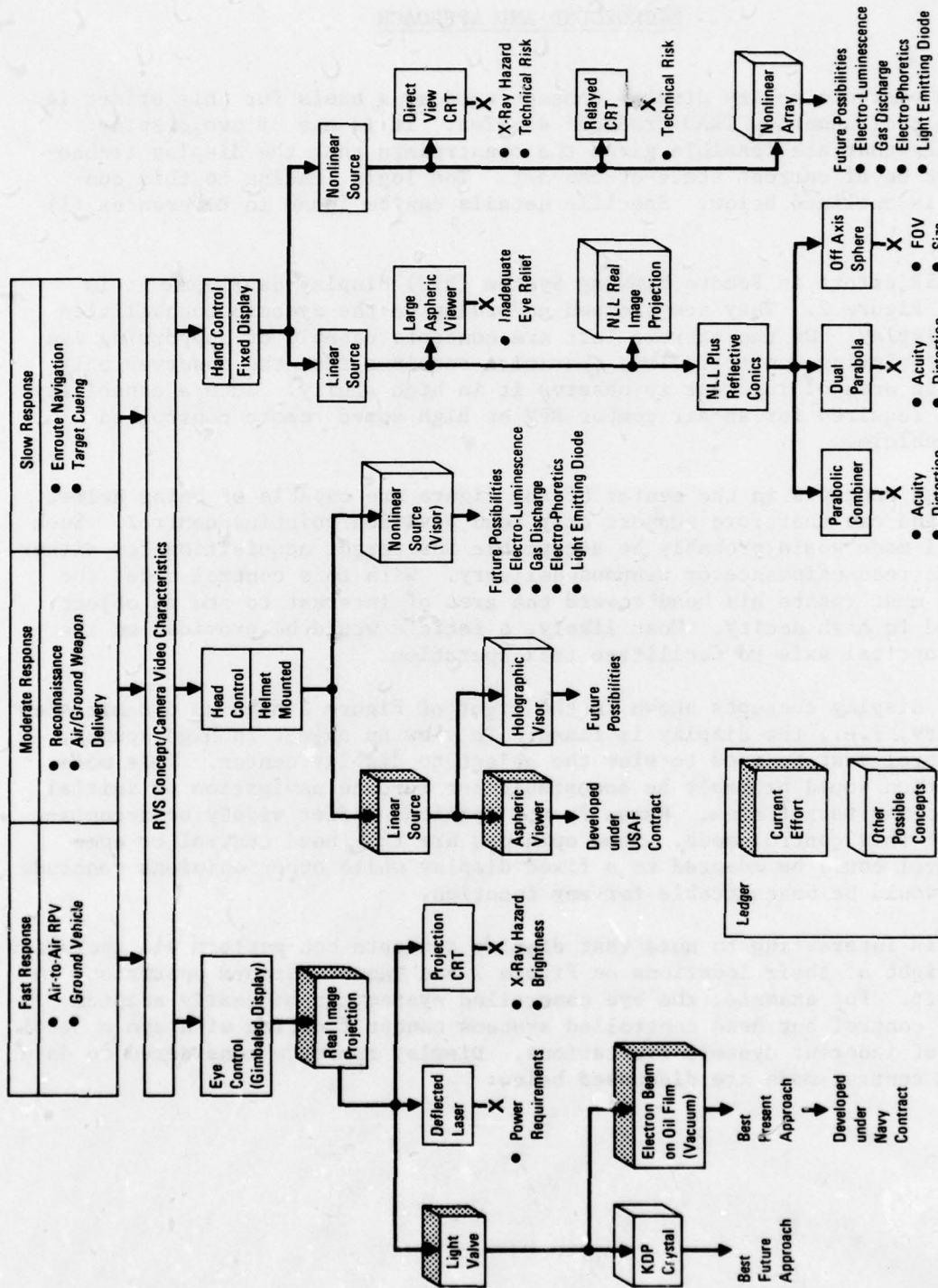
The variable acuity display concept used as a basis for this effort is the result of numerous IRAD tradeoff studies. It is one of two display approaches that are feasible given the constraints that the display technology must be of current state-of-the-art. The logic leading to this conclusion is outlined below. Specific details can be found in References (1) and (2).

MCAIR effort in Remote Viewing System (RVS) display development is shown in Figure 2. They are grouped according to the dynamic capabilities of the display. On the extreme left are concepts capable of supporting eye position/pointing control. This operation requires that the observer only look at an area of interest to observe it in high acuity. Such a capability might be required for an air combat RPV or high speed remote controlled ground vehicle.

Those concepts in the center of the figure are capable of being helmet mounted and can therefore support only head position/pointing control. Such a control mode would probably be acceptable for target acquisition for either real-time reconnaissance or weapons delivery. With this control mode, the observer must rotate his head toward the area of interest to see an object displayed in high acuity. Most likely, a reticle would be provided on the display optical axis to facilitate this operation.

The display concepts shown to the right of Figure 2 have no dynamic slew capability, i.e., the display is fixed. To view an object in high acuity, hand control must be used to slew the object to display center. This mode of operation would probably be acceptable for enroute navigation or initial cueing to the target area. Human factor opinions differ widely on acceptability of this control mode. Some opinions are that head control or even eye control could be adapted to a fixed display while other opinions conclude that it would be unacceptable for any function.

It is interesting to note that display concepts can perform all operations to the right of their locations on Figure 2 but cannot perform operations to their left. For example, the eye controlled system can be easily adapted for head control but head controlled systems cannot function with eye control because of inherent dynamic limitations. Display concepts considered to date for each control mode are discussed below:



OP77-047E-1

FIGURE 2  
MCAIR DISPLAY SYSTEMS STUDIES

## 2.1 EYE CONTROL (FULLY GIMBALED DISPLAY)

The only display concept fully adaptable to eye control is the Real Image Projection System. This approach has been studied in detail during MCAIR IRAD effort and was fabricated under Reference (3). The major disadvantage of the Real Image Projection approach is the large volume required for the display station because a sphere with a diameter of 8 to 10 feet is used as a viewing screen. A secondary problem is the large, expensive, and short-life light valve light source required to achieve adequate display brightness.

## 2.2 HEAD CONTROL (HELMET MOUNTED)

In applications where dynamics allow head pointing control of the system, much more compact and efficient direct view displays are possible. These desirable features result by directly coupling the light from the source (object) to the viewer's eye. Appendix A contains the photometric theory developed for this approach. There are two ways of implementing direct view. One employs a CRT display or solid state emitting array as a linear source and achieves distortion through non-linear optics. The other, the non-linear source approach, achieves distortion by a nonuniform arrangement of emitting or absorbing elements. These elements would probably be incorporated within the observer's visor. While this approach appears best from a weight and size standpoint it cannot be considered as current technology because non-linear arrays have not yet been produced. The application of these approaches to the non-linear requirements of the VARVS concept may be considered after they have been proven in conventional linear display systems. The holographic visor display is another method of achieving head control with a linear source. Here the distortion may be achieved in the hologram by diffraction. This approach should be considered after head-up display technology using holographic visors and linear objects are fully developed.

Therefore, the aspheric viewer is the only candidate using current technology which can be used for a head controlled system. Before discussing this system, the reasons for not selecting a fixed display with hand control will be presented.

## 2.3 HAND CONTROL (FIXED DISPLAY)

For lower dynamic situations a fixed display may be satisfactory with hand control of the sensor. Display approaches for this mode of operation are shown on the right of Figure 2. These also divide into two classes, those employing linear sources and those employing non-linear sources.

Of the linear source approaches for the fixed display configuration, all those attempting to obtain high efficiency through reflective conics were found to be not feasible. None could meet acuity, distortion, and field-of-view requirements simultaneously. The remaining two approaches, the Large Aspheric Viewer and the NLL Image Projection, are derivatives of the eye and head control approaches discussed above. In the case of the Large Aspheric Viewer, scaling of the small Direct View Display concluded that sufficient eye relief for binocular vision was impossible. The only possibility would be dual viewers, one for each eye. The technology for this approach is identical to the aspheric viewer discussed in 2.2.

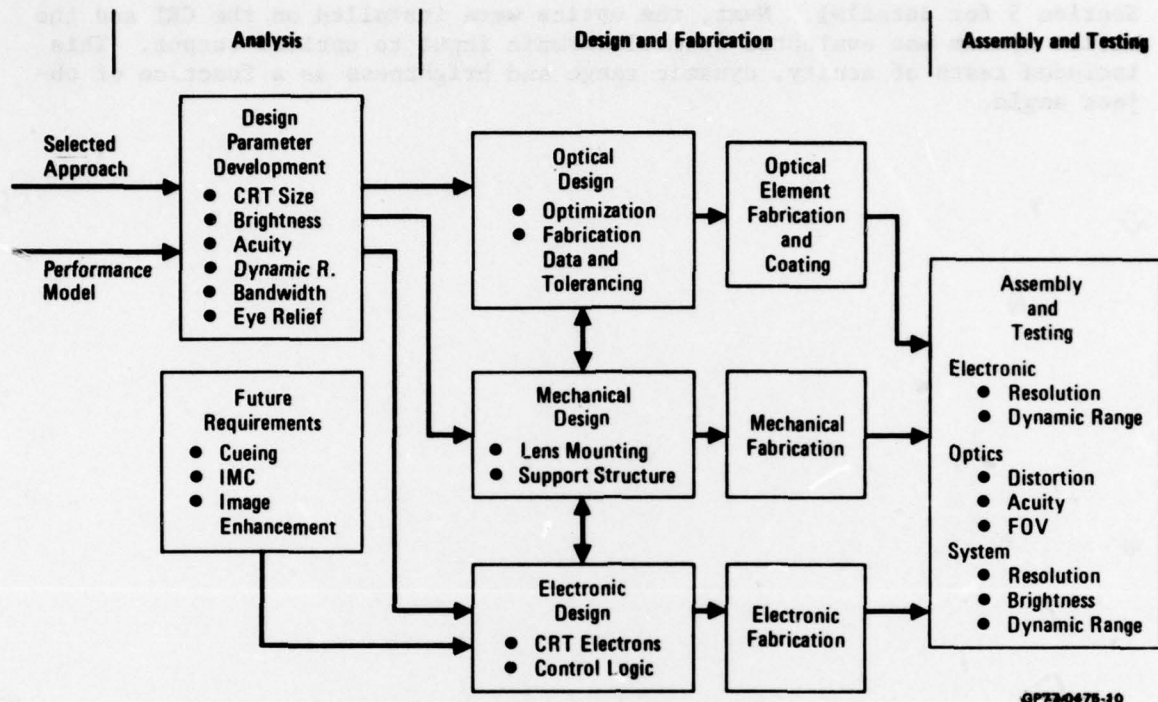
The nonlinear lens Real Image Projection approach is identical to that discussed under eye control except that the projector is fixed. This greatly reduces size, complexity, and cost because a fixed screen can be used. It can be made reasonably efficient by use of a high gain screen. It is considered the best approach for the hand-mode of operation. Its size can be reduced considerably through use of collimation optics as described in Reference (4).

The nonlinear source approach using the Direct View and Relayed CRT methods have major problems. Resolution and field-of-view cannot be achieved simultaneously. In these two methods, distortion is performed as described in Reference (2). A 5000 line CRT is required which requires high anode voltages and results in a severe X-ray hazard. In addition writing rates in the peripheral area are extremely high (416,000 inches/sec). In total then, the state-of-the-art in CRT technology is being pushed and could lead to deflection, focus, and brightness problems. The only approaches that appear to be remotely feasible for the nonlinear source are those using nonlinear arrays consisting of discrete emitters or absorbers similar to those discussed for the head controlled approach. They were ruled out for the same reasons as discussed in that section. However, the larger allowable weight and volume of the fixed display would make utilization less difficult.

#### 2.4 SELECTED SYSTEM

The display studies pointed to only two feasible display approaches, the projection approach already being fabricated under NAVY contract, Reference (3) and the Direct View Aspheric Display which was fabricated under this contract. The approach used to develop the Aspheric Direct View Variable Acuity Display is shown in Figure 3. It began with an analysis phase where design parameters were established that are not overly conservative, are practical for fabrication, and that introduce minimum degradation due to display characteristics. This was accomplished by computer modeling the entire VARVS system and then varying display parameters while observing performance in terms of minimum resolvable modulation (MRM). Also included in the analysis phase were the requirements of introducing future capabilities of displaying cues, of providing image motion compensation (IMC), and of incorporating image enchainment techniques.

In the design and fabrication phase, optical, mechanical and electronic components were designed and fabricated. The optical design consisted of adjusting the number of elements, surface profiles, and optical material types until the required distortion, acuity, and field-of-view were simultaneously achieved. Curvatures of the elements were then varied slightly while critical display parameters were monitored to determine manufacturing tolerances. The results were element drawings suitable for manufacture. Finally, grinding wheel diameters, axis locations, and tolerances were computed to assist in fabrication. Actual element fabrication was done by Franke Cooke Inc. per our specifications. Elements were coated to minimize reflections by MDEC.



GPTA-0476-10

**FIGURE 3  
APPROACH**

The mechanical design was done in parallel with optical design so that mechanical considerations could be included in the optical design. Mechanically sound methods of element mounting and spacing were developed and detailed drawings were made of the components parts. Next, assembly drawings were made and checked to assure suitable adjustment of critical components.

The mechanical design and fabrication of the support structure for the CRT and electronics were also accomplished during this phase. This necessitated that the electronic design also be done in this phase. After reviewing electronic requirements, the decision was made to purchase rather than fabricate the electronics. An arrangement was made with CONRAC Corp. to modify an existing system which utilized our CRT and meet our specifications. Very little electronic fabrication was required at MCAIR with this approach.

Assembly and test efforts were somewhat dictated by delivery of components. The CRT manufactured by Thomas Electronics was the first component that was available. It was immediately shipped to CONRAC to be incorporated into their electronics. The electronics and CRT were then returned to MCAIR where optical and electronic tests were run to determine resolution, dynamic range, and brightness. Meanwhile optical elements were shipped from Cooke as they were completed. Testing of aspheric elements was accomplished at Cooke's plant. After all elements were completed, the optics were assembled and the assembly tested end-to-end for distortion, acuity, and FOV (see



Section 5 for details). Next, the optics were installed on the CRT and the entire system was evaluated from electronic input to optical output. This included tests of acuity, dynamic range and brightness as a function of object angle.

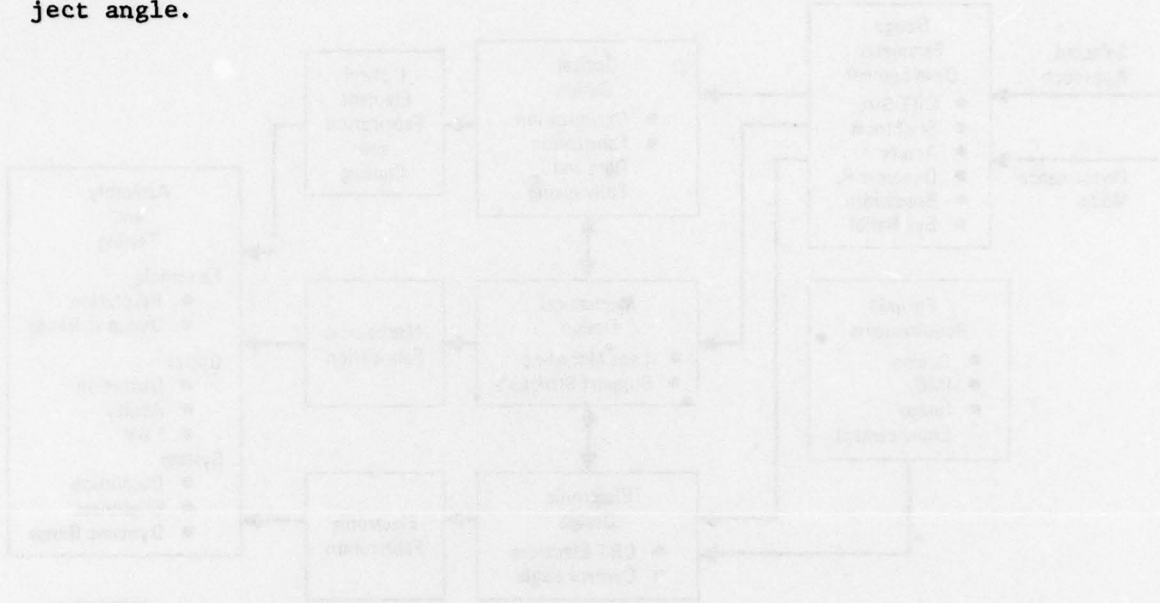


FIGURE 3  
APPENDIX

The mechanical design was done in parallel with optical design in that mechanical considerations could be factored in the optical design. Mechanical design was done in parallel with optical design and optical design was done in parallel with mechanical design. Mechanical design was done in parallel with optical design and optical design was done in parallel with mechanical design.

The mechanical design and fabrication of the support structure for the CRT and electronics was also completed during the design phase. The mechanical design was done in parallel with optical design and optical design was done in parallel with mechanical design. Mechanical design was done in parallel with optical design and optical design was done in parallel with mechanical design.

Assembly and test efforts were necessary to evaluate the system. The CRT was fabricated by Thomas Electronics and the first component was assembled. It was mechanically aligned to the CRT and the electronics. The electronics and CRT were then mounted in the support structure. The electronics and CRT were then mounted in the support structure. The electronics and CRT were then mounted in the support structure.

## Section 3

### ANALYSIS

The analytical effort established design parameters and constraints required for the actual display design. For the optical design, these are size, field-of-view, brightness, optical quality, and eye relief. For the electronics, consideration must be given to dynamic range, bandwidth, IMC and image enhancement.

#### 3.1 OPTICAL REQUIREMENTS

Size constraints for the display are based on the CRT screen size. During the early stages of design it appeared that a fiber optic faceplate would be required on the CRT. This dictated a CRT with a 2 to 3 inch diameter. In order to support possible future developments we felt that the CRT should have a resolution of about 1000 lines. These considerations, plus the fact that this display is the first of its type ever to be constructed, led us to choose a 3 inch CRT. The larger size minimizes technical risk when a fiber faceplate is fabricated, (the faceplate requires an aspheric grind on its external surface), and the larger size minimizes the risk in the remaining optical system because it is scaled directly to CRT size. After a search of available CRT's we chose a Thomas Model 3M15 which has a 2.75 inch diameter active area. A P45 phosphor was selected because of its good spectral content, efficiency, and dynamic characteristics. Our experience with the Navy system, Reference (3), indicated that a field-of-view of  $120^\circ$  is sufficient for most applications. This value was established as the minimum acceptable field-of-view.

To determine the optical parameters necessary for display design, a good systems analytic model was required. Our infrared lens design effort had convinced us that the mathematical model used by the Night Vision Laboratory (NVL) to describe the display/observer was valid and the best available. For this reason we applied the logic of the NVL model, Reference (5), to derive a visual spectrum model of the VARVS. Since the NVL model had already been converted to the VARVS in Reference (6), the only change required was the development of a sensor model that correctly handled vidicon noise. Details of this conversion are presented in Appendix B. The output of this model was Minimum Resolvable Modulation vs. linear or angular spatial frequency. At each spatial frequency this parameter is the minimum input modulation at the sensor lens that can be resolved by the observer.

The visual analytical model was operated initially to determine the effect of display brightness and optical quality. Brightness was varied from 0.01 to 100.0 footlamberts. Optical quality was varied from 5 to 80 microns equivalent optical spread function one sigma radius at the source. Equivalent source spread function (blur) was used because the design program operates with this as a parameter. To determine sensitivity of system performance to display brightness, the MRM was plotted as a function of display brightness for a fairly high on-axis angular spatial frequency, from 0 to 1 cycle/mr. The results are shown on Figure 4 for several values of display quality. Note how substantial increases of display brightness up to about 10 foot lamberts improves the performance. Beyond this level very little improvement is noted. Based on these data a minimum display brightness of 10 footlamberts

was selected as a requirement. It should be noted that this is also the CRT brightness in a direct view system (see Appendix A). The selected CRT can easily meet this requirement.

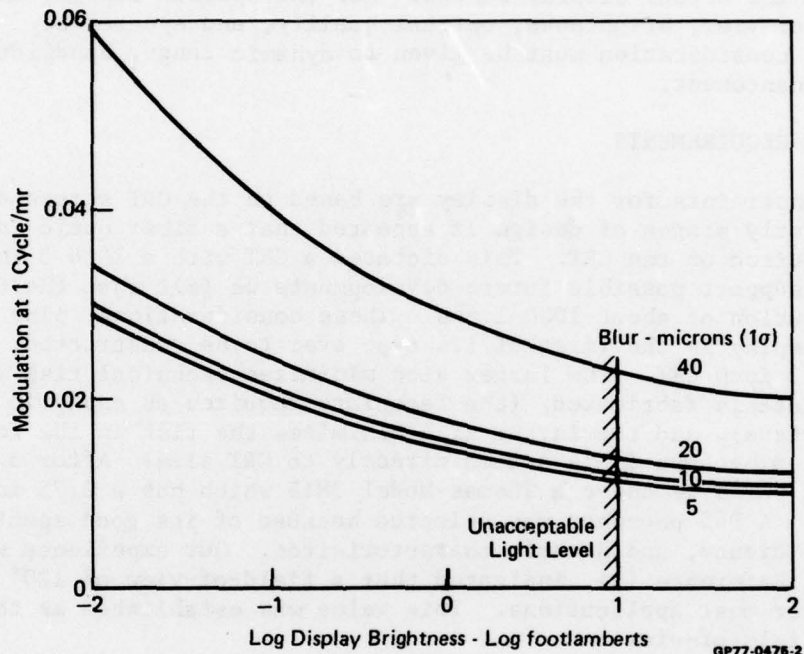


**FIGURE 4**  
**PERFORMANCE vs DISPLAY BRIGHTNESS**  
 $F_x = 1 \text{ Cycle/mr}$

Using this brightness value, the minimum resolvable modulation at the same spatial frequency (1 cycle/mr) was plotted vs display blur. The results are shown on Figure 5 for a 525 and 1023 scan line count (reasons for lower performance at 1023 lines will be discussed later). In both cases, the maximum blur that does not affect system performance significantly is about 10 microns. This value of blur was established as a display design goal. It should be noted that the basic VARVS concept is based on uniform resolution over the entire intermediate image plane. Although the 10 micron blur was calculated for an on-axis resolution, it will apply over the entire object plane CRT surface. This linear blur is related to angular blur by the focal length function,

$$\alpha = \frac{\text{linear blur}}{\text{focal length}} \quad (1)$$

Since focal length decreases as field angle increases, the allowable angular blur will increase as field angle increases.

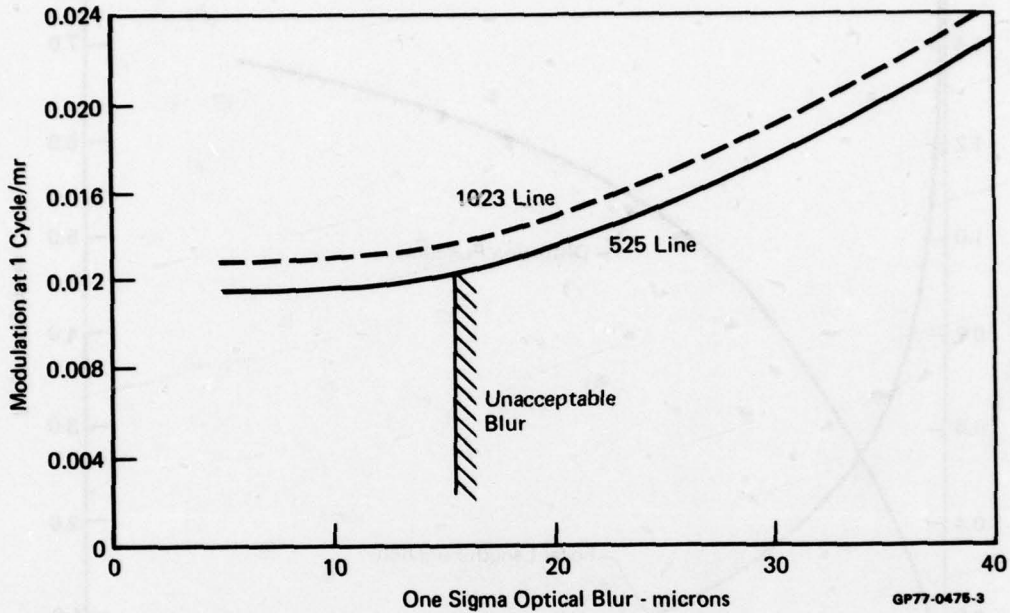


**FIGURE 5**  
**PERFORMANCE vs OPTICAL BLUR**  
 $F_x = 1 \text{ Cycle/mr}$

In order for the display to be compatible with existing sensors, it must utilize the same distortion and focal length function as the sensor. For this reason, the image height function ( $h(\theta)$ ) and focal length function ( $f(\theta)$ ) used in all previous VARVS effort were used as a design requirements for this display. The 2.75 inch maximum image diameter of the CRT dictates a 7.86 inch on-axis focal length to achieve a  $120^\circ$  field-of-view, the minimum field-of-view considered acceptable. The resulting distortion function and focal length function properly scaled to the CRT are shown in Figure 6.

The lens is designed by an iteration technique mechanized on a computer. A field angle is specified and program iterates until an image height is defined. In conventional design programs, focal length would be defined rather than image height. However, the two are related by the equation

$$f(\theta) = \frac{dh(\theta)}{d\theta} \quad (2)$$

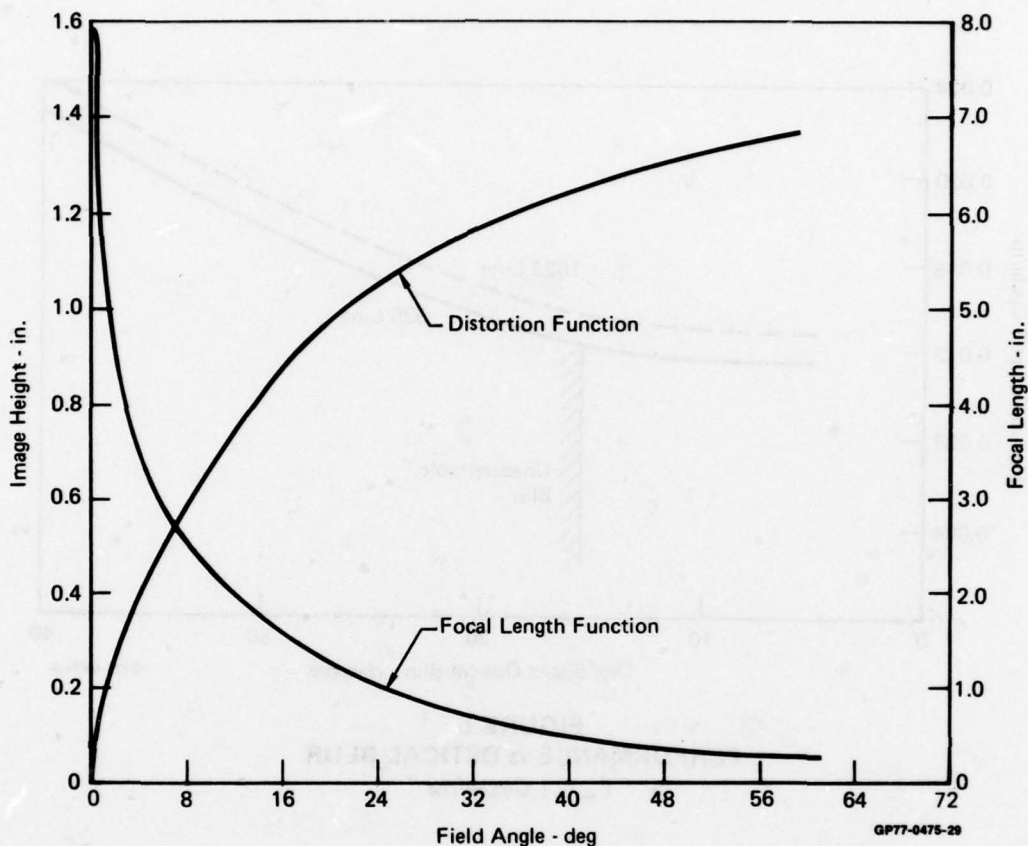


**FIGURE 6**  
**VAD DISTORTION AND FOCAL LENGTH REQUIREMENTS**

Since an exact image height may not be achieved, a tolerance must be allowed. This error in image height results in a distorted image. Based on our experience with the ONR system, we feel that the maximum allowable tolerance should be  $\pm 2$  TV lines based on a 500 line format across the maximum dimension. This tolerance is shown in Figure 7(a) as a function of field angle. This curve is the ratio of the tolerance to the maximum object height. When this tolerance is related to allowable object angular error as a function of field angle by using Equation (2), the curves of Figure 7(b) result. The allowable angular error increases as field angle increases and in the peripheral area increases quite rapidly. When viewing a stationary or slowly moving scene, this error does not cause a problem. However, if a large relative angular rate exists between camera and scene, caused by vehicle motion or sensor slewing, the angular errors can cause false detail motion in the display. To preclude this, a rate of change tolerance is required in addition to the angular error tolerance. Again our experience with ONR equipment provided data to establish such a tolerance. We had observed that

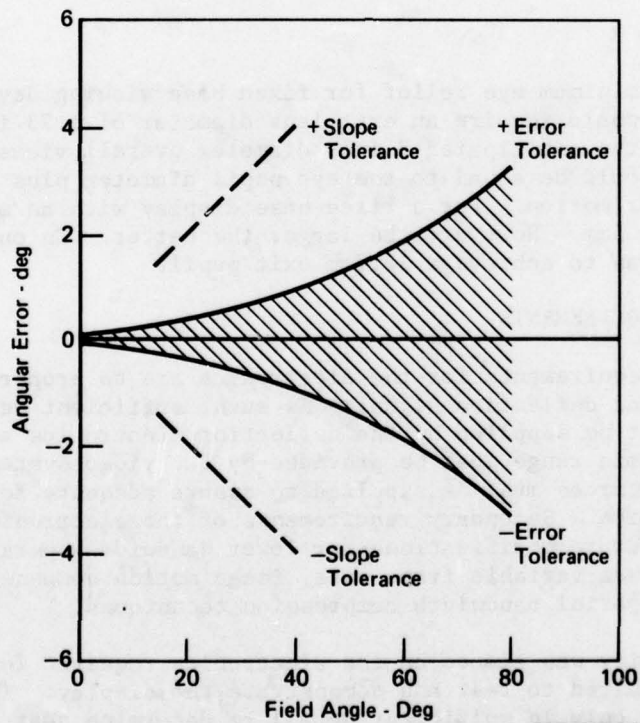
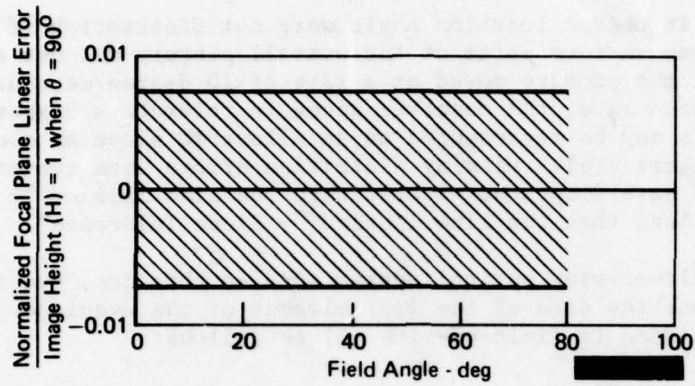


**FIGURE 7**  
**DISTORTION DESIGN TOLERANCES**

random variations in object location angle were not distracting if the rate differential between various parts of the overall picture did not exceed 1 degree/second when the picture moved at a rate of 10 degree/second. Above this 10 degree/second rate, the observer seems to tolerate a higher rate differential. This may be represented as an allowable slope as shown by the dashed lines on Figure 7(b). Display distortion errors when converted to angular terms must have slopes no greater than the line labeled "+ Slope Tolerance" and no less than the line labeled "- Slope Tolerance".

On a wide field-of-view optical system such as this one, eye relief requirements dictate the size of the last element of the eyepiece. This element size is related to field-of-view ( $\theta$ ) as follows:

$$D = 2 R \tan \theta \quad (3)$$

where  $R$  = Eye relief

$D$  = Exit lens diameter

For a  $120^\circ$  field-of-view the relationship between eye relief and diameter is

$$D = 3.46 R \quad (4)$$

The accepted minimum eye relief for fixed base viewing devices is about 0.5 inches. This would require an exit lens diameter of 1.73 inches. This is reasonable for the anticipated 3 inch diameter overall viewer optics. Exit pupil size should be equal to the eye pupil diameter plus the anticipated relative eye/viewer motion. For a fixed base display with an eye-cup, this can be as small as 5mm. However, the larger the better. In our original design, the goal was to achieve a 12.7mm exit pupil.

### 3.2 ELECTRONIC REQUIREMENTS

The primary requirements for the electronics are to properly support the CRT with a video and deflection signal. As such, sufficient deflection linearity and scan rates must be supplied by the deflection electronics and sufficient bandwidth and dynamic range must be provided by the video system. In addition, proper CRT power sources must be supplied to assure adequate focus, intensity and electron emission. Secondary requirements of the electronics are to support possible future modifications for lower bandwidth operation. These modifications include variable frame rate, image motion compensation, image enhancement, and spatial bandwidth compression techniques.

Highest priority was placed on the electronics required for CRT support since they are required to test and demonstrate the display. The other requirements were studied only in sufficient detail to determine that they could be added in the future. This approach was dictated by cost constraints encountered early in the effort. The optical design required much more time and cost than originally anticipated. Since the optics are the high risk item and the required electronics can be conventional TV equipment, we elected to purchase off-the-shelf electronics. Based on this philosophy immediate requirements

for the CRT electronics are as follows:

Raster Structure & Linearity - A 1023 line system is required for the existing Navy sensor and a 525 line system is anticipated for future sensors. Line rates should be switchable without readjustment and linearity must be better than 0.4%.

Frame Rate - Thirty frame/sec with 2/1 interlace.

Brightness - 20 footlamberts.

Resolution & Bandwidth - The display must interface with either the ONR sensor which has a 1023 line raster format or future sensors that will have a 525 line raster. Therefore, anticipated sensor bandwidths are 16 MHz and 4 MHz, respectively. These two bandwidths convert (through raster geometry) to spatial frequencies of 435 cycles/raster width and 204 cycles/raster width. Assuming these are 3 db response points, MTF theory predicts an equivalent optical spread function radius (one sigma) of Raster Width/3240 for a 1023 raster and Raster Width/1550 for a 525 raster. In order to support the 1023 line system the electronics including the CRT, should have a bandwidth better than 16 MHz and a CRT spot size of less than Raster Width/3240. Therefore, a design requirement of 20 MHz and Raster Width/4000 (1 sigma radius) was established for the electronics and CRT. For the selected 3 inch CRT, the spot size requirement is 17 microns. In more conventional terms, the 50% amplitude spot diameter should be 40 microns or 0.00157 inches.

Dynamic Range - At least 10 shades of grey on the  $\sqrt{2}$  standard.

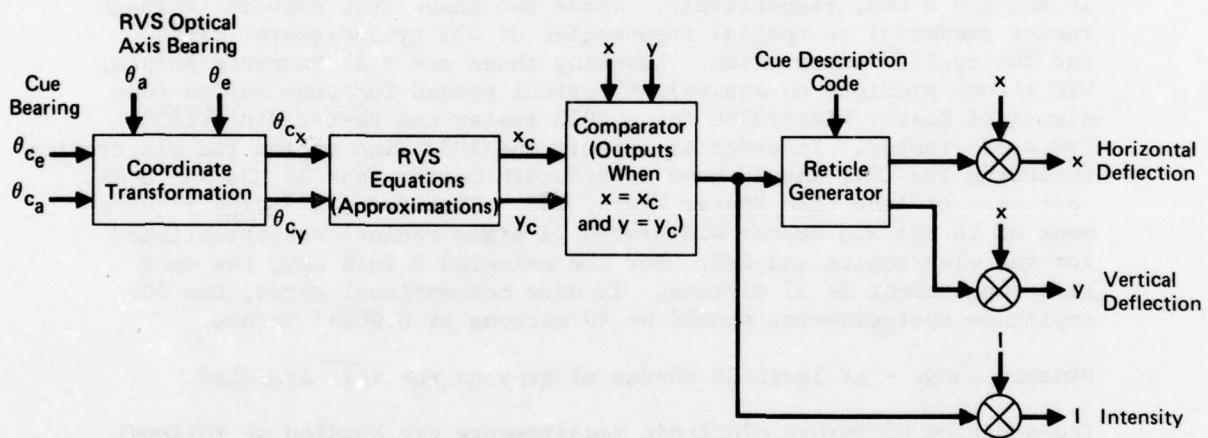
The addition of future electronic requirements are handled as follows:

Bandwidth Compression and Image Enhancement - Since the basic video of VARVS system is identical to any other TV system, any bandwidth compression or image enhancement techniques developed for a conventional TV system should operate with the VARVS system. These techniques are pure video processing techniques and can be accomplished outside of the basic display electronics. Therefore, they have no impact on our design problem.

Frame Rate Reduction, Cueing, and IMC - In order to prevent display flicker, any frame rate reduction is best performed outside of the display electronics by use of a scan converter. If a digital scan converter is utilized cues, can be injected on the input side of the scan converter as shown on Figure 8 while IMC can be mechanized as shown in Figure 9.

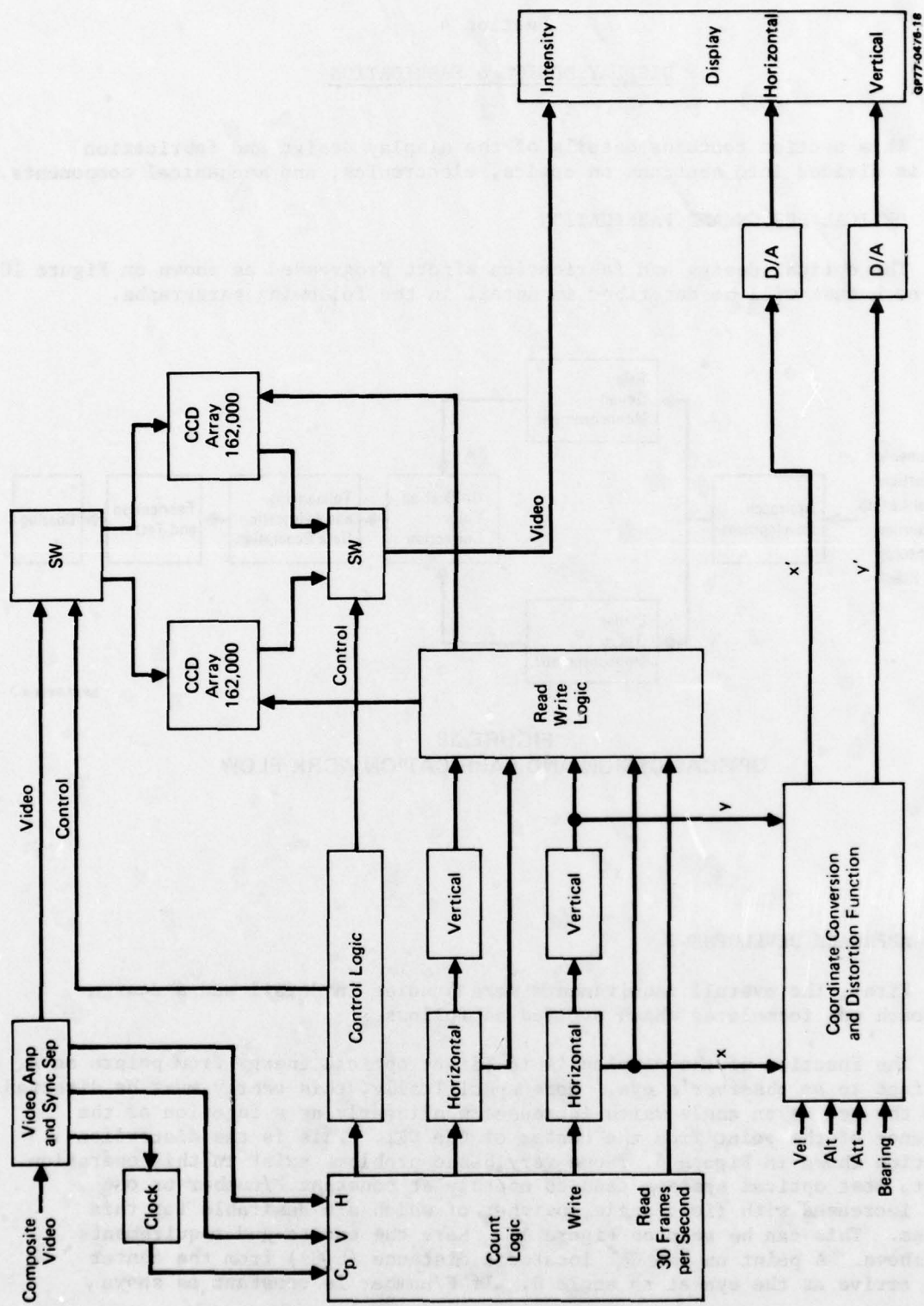
In conclusion it appears that all future electronic requirements can be implemented separately from the basic CRT electronics package. This further substantiates our choice of off-the-shelf CRT electronics.





QR77-0476-17

**FIGURE 8**  
**CUE GENERATION (OPTICAL DISTORTION CORRECTION)**



GP77-0478-18

FIGURE 9  
IMC MECHANIZATION - OPTICAL DISTORTION CORRECTION

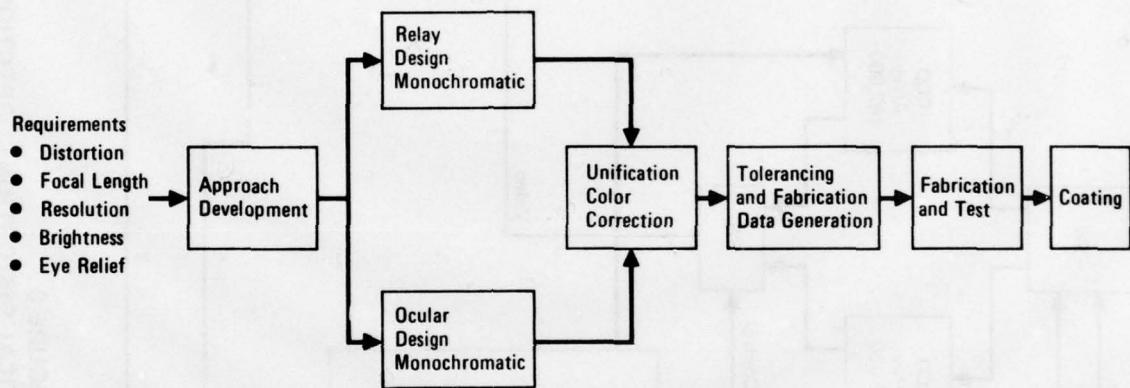
## Section 4

### DISPLAY DESIGN & FABRICATION

This section contains details of the display design and fabrication and is divided into sections on optics, electronics, and mechanical components.

#### 4.1 OPTICAL DESIGN AND FABRICATION

The optical design and fabrication effort progressed as shown on Figure 10 and each task will be described in detail in the following paragraphs.



GP77-0475-4

**FIGURE 10**  
**OPTICAL DESIGN AND FABRICATION WORK FLOW**

#### 4.2 APPROACH DEVELOPMENT

First, the overall requirements were studied in detail and a design approach was formulated which evolved as follows.

The function of the display is to direct optical energy from points on a CRT face to an observer's eye. More specifically, this energy must be directed into the eye at an angle which increases nonlinearly as a function of the distance of the point from the center of the CRT. This is the distortion function shown in Figure 6. Some very basic problems exist in this operation. First, most optical systems tend to operate at constant F/number or one that increases with field angle, neither of which are desirable for this system. This can be seen on Figure 11. Here the end-to-end requirements are shown. A point on the CRT located a distance  $(h(\theta))$  from the center must arrive at the eye at an angle  $\theta$ . If F/number is constant as shown

here, the off-axis ray has a reduced diameter ( $D(\theta)$ ) in the same proportion as the focal length has changed, viz:

$$\frac{D(\theta)}{D(0)} = \frac{f(\theta)}{f(0)} \quad (4)$$

From Figure 6 the focal length at an angle of  $60^\circ$  divided by the on-axis focal length results in a ratio of 0.035. If then, the on-axis ray bundle has the desired exit pupil diameter of 0.5 inch (from Section 3), the  $60^\circ$  ray bundle will enter the eye with a diameter.

$$D(60^\circ) = 0.035 D(0) = 0.035 \times .5 = 0.0175 \text{ inch}$$

Since this diameter is considerably smaller than the eye's pupil diameter of 0.2 inch, the eye would have to be precisely located within the pupil diameter in order to see energy from this direction. The  $60^\circ$  ray bundle could be expanded to have a diameter of 0.5 inch by scaling the focal length up. If a rather optimistic F/number of two is assumed, the focal length at an angle of  $60^\circ$  must be 1.0 inch. The on-axis focal length  $f(0)$  would be 35 inches. A 35 inch focal length would require an object size of 12 inches. The dimensions of the lens elements would also be scaled up by this factor, resulting in a minimum possible display optics size of about 13 x 40 inches. This does not meet the ultimate goal for head mounting.

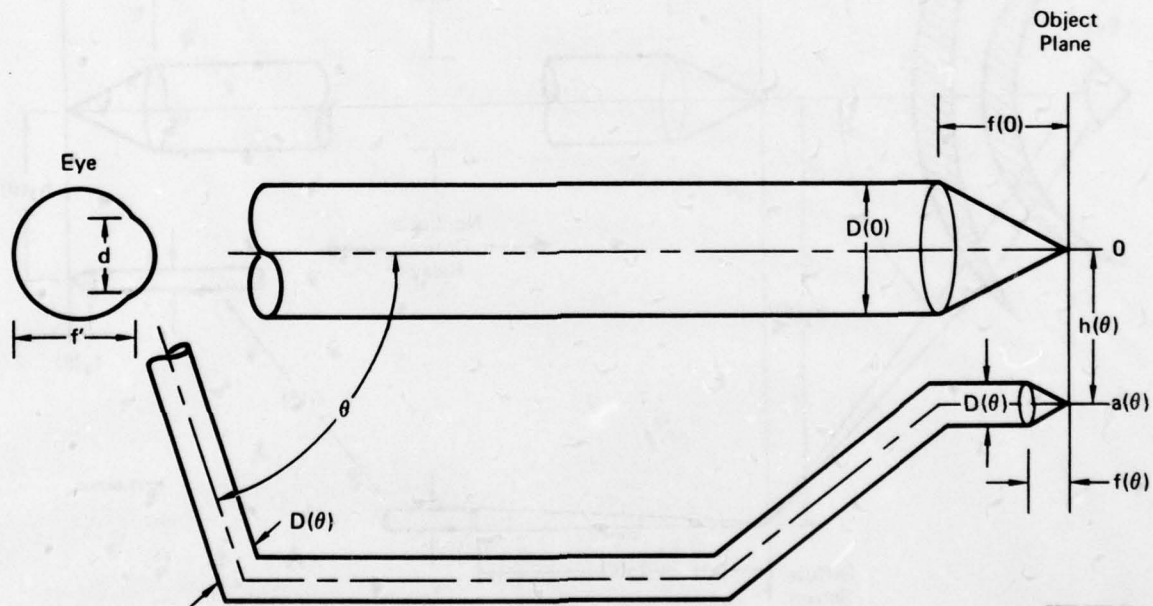


FIGURE 11  
DIRECT VIEW GEOMETRY

The only known alternate for expanding the ray bundle diameter would employ an intermediate diffuse surface as shown in Figure 12. Here, most of the required distortion is achieved in the relay. The small ray bundles in the peripheral area are expanded by the diffuse surface thereby increasing the ray bundle at the eye. Some basic relationships of this configuration are as follows:

The greatest distortion that can be generated by a wide angle eyepiece is the fish eye function; viz:

where

$$h_2(\theta) = K \sin \theta \tag{5}$$

$h_2(\theta)$  = Height on the diffuse screen

$K$  = Constant

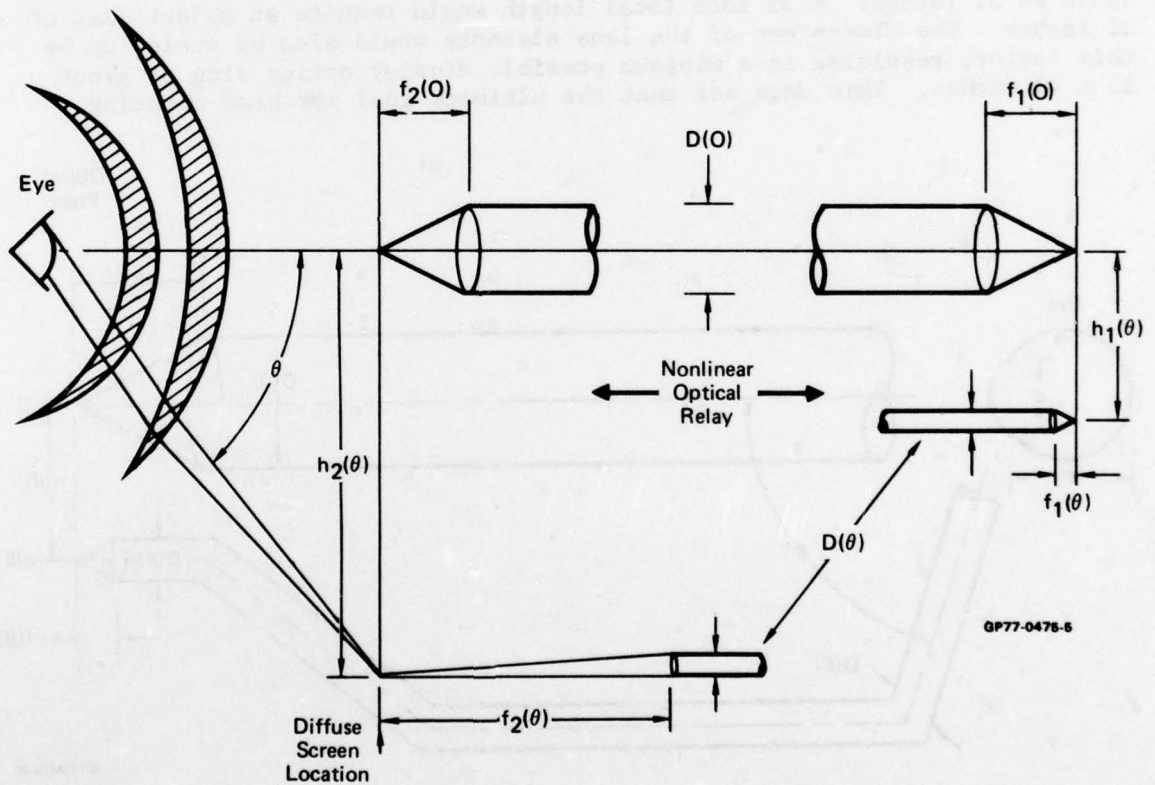


**FIGURE 12**  
**DIFFUSE SCREEN VIEWER**

Since the relay is imaging, its distortion function  $R(\theta)$  is the ratio of image height to height on the screen

$$R(\theta) = \frac{h_1(\theta)}{h_2(\theta)} \quad (6)$$

Substituting Equation (5) into (6) results in

$$R(\theta) = \frac{h_1(\theta)}{K \sin \theta} \quad (7)$$

where  $h_1(\theta)$  is the basic lens distortion function, shown in Figure 6. To maintain fairly uniform relay size, assume a maximum  $h_2(\theta)$  of 1.0 inch at a field angle of  $60^\circ$ . From Equation (5) this defines the constant (K) as

$$K = \frac{1.0}{\sin(60^\circ)} = 1.155$$

The relay function now becomes:

$$R(\theta) = \frac{h_1(\theta)}{1.155 \sin \theta} \quad (8)$$

Now if we evaluate the relay at any viewing angle, the illumination of the diffuse surface is as follows.

From geometrical optics we assume an infinitesimal emitting surface ( $dA_1$ ) at the CRT. This surface is small enough so that the focal length can be assumed constant over its area. The phosphor brightness is  $B_1$ . Then the illumination at the diffuse screen is:

$$E_2 = \frac{B_1 \omega_1 dA_1}{dA_2} \quad (9)$$

Where  $\omega_1$  is the acceptance solid angle at the phosphor and is defined by

$$\omega_1 = \frac{\pi D^2(\theta)}{4 f_1^2(\theta)} = \frac{\pi}{4 F_{NO_1}^2} \quad (10)$$

Then substituting Equation (10) into (9) results in

$$E_2(\theta) = \frac{B_1 \pi}{4 F_{NO_1}^2} \frac{dA_1}{dA_2} \quad (11)$$

The incremental areas are related to the focal lengths by

$$\frac{dA_1}{dA_2} = \frac{f_1^2(\theta)}{f_2^2(\theta)} \quad (12)$$

Substituting Equation (12) into (11)

$$E_2(\theta) = \frac{B_1 \pi}{4F_{NO_1}^2} \frac{f_1^2(\theta)}{f_2^2(\theta)} \quad (13)$$

Since the focal length is the derivative of image height with respect to angle, viz:

$$f(\theta) = \frac{dh(\theta)}{d\theta} \quad (14)$$

We may differentiate Equation (5) and write

$$f_2(\theta) = \frac{dh_2(\theta)}{d\theta} = K \cos \theta \quad (15)$$

Then substituting into Equation (13)

$$E_2(\theta) = \frac{B_1 \pi}{4F_{NO_1}^2} \frac{f_1^2(\theta)}{K^2 \cos^2 \theta} \quad (16)$$

This illumination converts to a brightness as follows:

$$B_2 = r \frac{E_2}{\omega_2} \quad (17)$$

where  $\omega_2$  is the reemission ray cone angle and  $r$  is the transmission efficiency. If the surface is perfectly diffuse,  $r = 1.0$  and  $\omega = \pi$ . Then, Equation (16) substituted in (17)

$$B_2 = B_1 \frac{f_1^2(\theta)}{4F_{NO_1}^2 K^2 \cos^2 \theta} \quad (18)$$

Now then the brightness at an angle of  $60^\circ$  will be determined. The focal length taken from Figure 6 is 0.277. Assume a very optimistic collection F/number of 2.0 at the phosphor. Equation (18) gives the brightness at the eye in terms of brightness of the CRT phosphor:

$$B_2 = \frac{B_1 (.277)^2}{4(4)(1.155)^2 (.5)^2} = 0.014388 B_1 \quad (19)$$

Then for an eye brightness ( $B_2$ ) of 10 ft lamberts, the CRT brightness is

$$B_1 = \frac{10}{.01438} = 695 \text{ footlamberts}$$

This optimistic value is considerably beyond the 50 foot lambert capability of the selected CRT if resolution is to be maintained. Our lens work has shown that a more probable F/number would be 8 or greater. Even at F/8.0 the required CRT brightness for 10 footlamberts observed brightness would be nearly 10,000 footlamberts. These first order calculations show that a diffuse intermediate imaging surface cannot be tolerated in the direct view display. This leaves only one alternative which is to accept a smaller than desired exit pupil.

At this point an experiment was set up in the laboratory to access the effects of a small exit pupil. This experiment is shown in Figure 13. Collimated point sources with variable apertures were arranged to form a pupil as shown in the figure. The pupil sizes were varied from the desired 0.5 inch down to 0.005 inch. As the pupil size was reduced, the requirement for more precise eye location was noted until the pupil size was roughly equal to the eye's iris diameter. Below this, no additional discomfort was noted, even for the smallest pupil size. It was concluded that a small pupil could be tolerated with the use of an eye cup to assist in maintaining eye position. With this point settled, viewer optical design was continued.

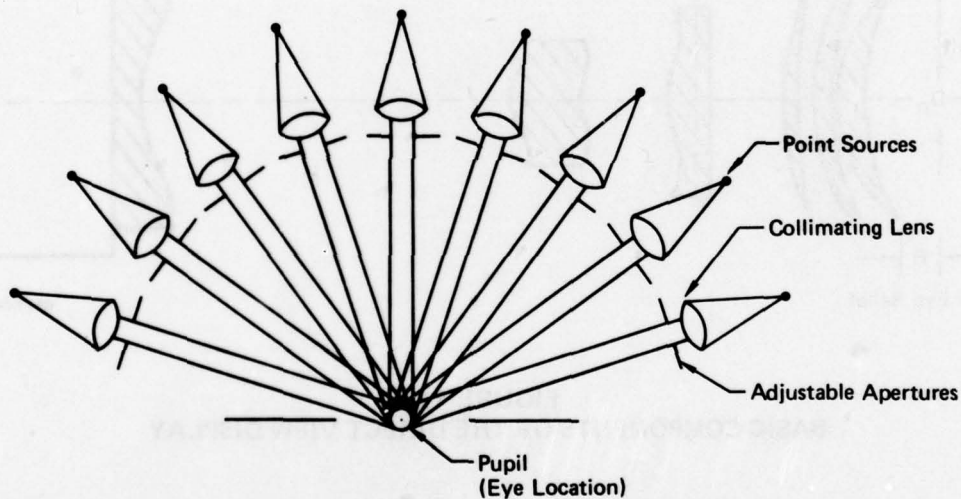


FIGURE 13  
EFFECT OF SMALL PUPIL TEST SETUP

At this point it was clear that the relay/ocular approach, less the diffuse imaging surface, was the only way of achieving the required distortion. This is based on the fact that it is difficult enough to design a wide angle ocular with conventional optics let alone aspherical optics. The maximum distortion that can be achieved safely with wide angle spherical optics is described by Equation (5), (The Fish Eye Function). The



remainder of the required distortion must be allocated to the relay as stated in Equation (7). The basic design configuration was therefore that of Figure 12, less the diffuse surface. Essential components of this design are shown on Figure 14. The CRT field lens directs the optical energy output of the phosphor into the relay group. The relay group creates the required relay optical distortion  $R(\theta)$  and assures a flat field at the image location. Here the aspheric field lens redirects the optical energy into the ocular to properly locate the pupil, at the desired eye relief distance (0.5 inch) from the last element.

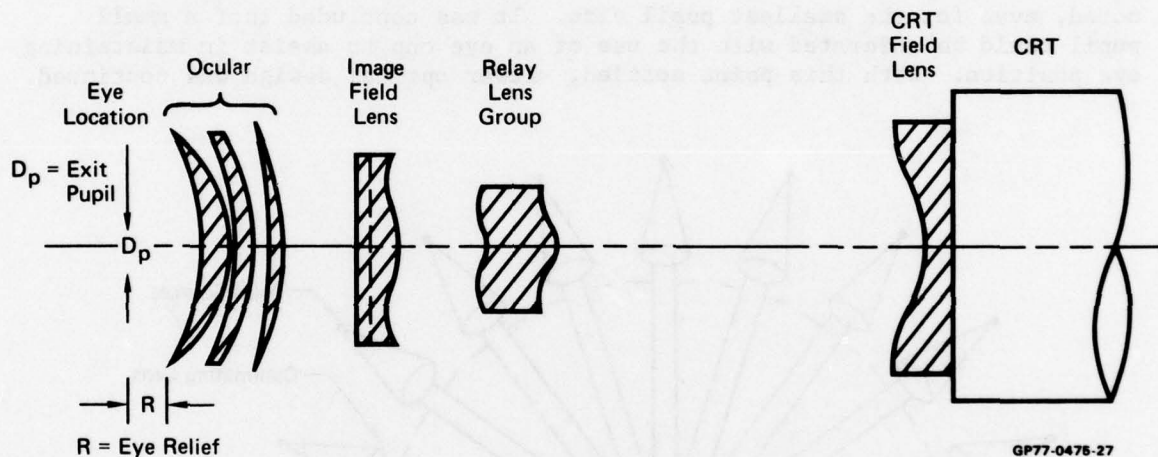


FIGURE 14  
BASIC COMPONENTS OF THE DIRECT VIEW DISPLAY

#### Ocular Design

The ocular was designed for a distortion obeying the equation

$$h_2(\theta) = K \sin \theta \quad (20)$$

with  $K = 1.2992$  inch.

The greatest field angle achievable from the ocular while maintaining 0.5 inch eye relief was found to be  $120^\circ$ . This makes an image height requirement of 2.25 inch for the relay. With these inputs, the ocular design was relatively routine.

### Relay Design

Most effort was spent on relay design. The design distortion is:

$$R(\theta) = \frac{h(\theta)}{1.2992 \sin \theta} \quad (21)$$

where  $h(\theta)$  is defined on Figure 6.

Initially, we attempted to achieve this distortion in a four inch object-to-image distance. This compact approach was found to make surfaces critically sensitive to tolerances and required a fiber optic faceplate to adequately control CRT energy output. The critical tolerance problem was eliminated along with the fiber optic faceplate by increasing object-to-image distance to 12 inches.

### Unification and Color Correction

The ocular was mated to the relay and the system achromatized for wavelengths of 480.0, 546.1, and 643.8 nm. Adequate color correction was achieved by use of one spline interface and several spherical doublets. The final configuration is shown on Figure 15. Predicted performance from ray trace data is shown on Figure 16. The theoretical blur is shown on Figure 16(a). Distortion error is shown on Figure 16(b). Note that the resolution (blur) is well within tolerance while distortion is slightly out of tolerance at several points. When further optimization runs failed to bring these distortions in tolerance, we terminated the effort and finalized the design.

It should be noted that these data are blur and distortion in the radial direction only. Data is presented this way because both design and measurement experience to date indicate this direction is most difficult to achieve. In all theoretical ray trace efforts and actual measurement on the visual lens, once radial resolution and distortion are achieved, circumferential performance is always acceptable. The reason for this lies in the rotational symmetry of the lens, the larger blur tolerance in the circumferential direction (Reference 4), and the fact that the aspheric elements are essentially spherical in this direction. The final computer data is shown in Appendix C.

### Tolerancing and Fabrication Data Generation

In an attempt to relieve manufacturing tolerances, the optical design was optimized in its final stages using actual glass melt optical parameters. Tolerances were established by computing allowable optical error and then statistically allocating this tolerance equally to each element by the RMS method. For fabrication of the aspheric (spline) elements, surface profile data was converted to grinding wheel axis locations and wear tolerances. These data plus nominal measurement and tolerance data were sent to the fabricator.

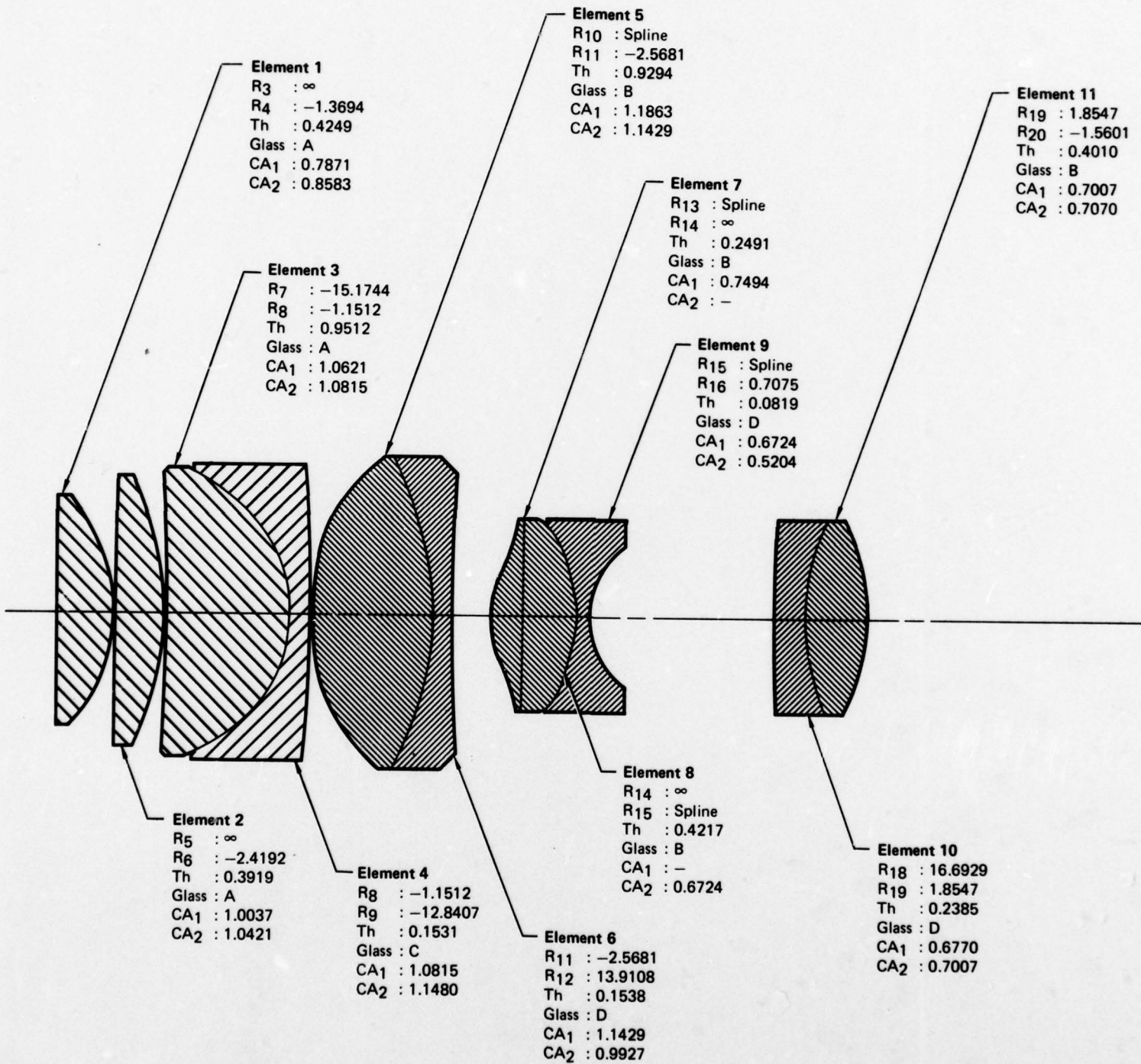


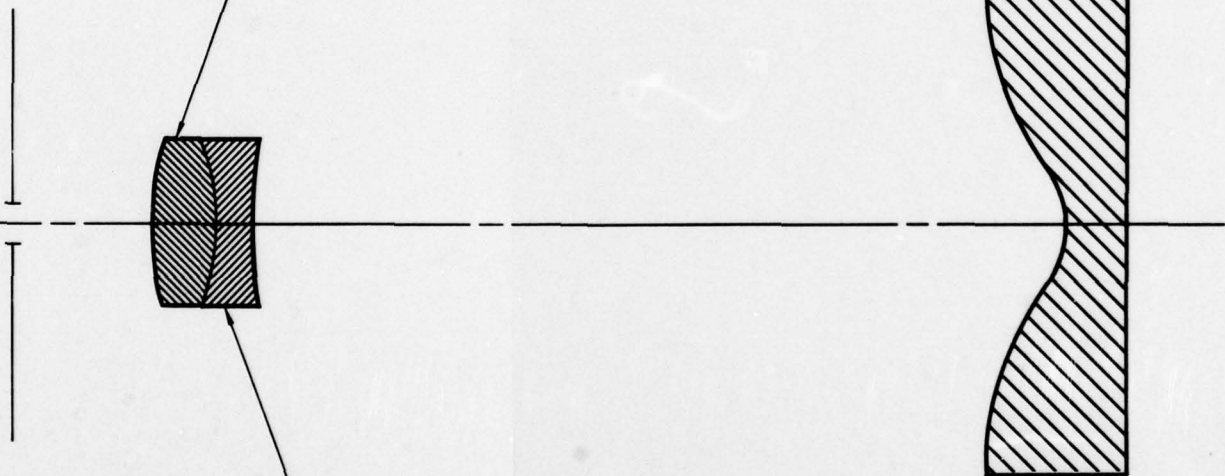
FIGURE 15  
OPTICAL ELEMENTS OF VAD

GP77-0475-37

**Element 11**  
 R19 : 1.8547  
 R20 : -1.5601  
 Th : 0.4010  
 Glass : B  
 CA<sub>1</sub> : 0.7007  
 CA<sub>2</sub> : 0.7070

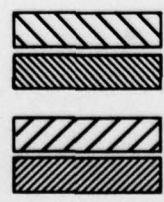
**Element 12**  
 R22 : 1.9872  
 R23 : -1.4772  
 Th : 0.3885  
 Glass : B  
 CA<sub>1</sub> : 0.3118  
 CA<sub>2</sub> : 0.3365

**Element 14**  
 R25 : Spline  
 R26 : ∞  
 Th : 0.3465  
 Glass : A  
 CA<sub>1</sub> : 1.2398  
 CA<sub>2</sub> : 1.3594



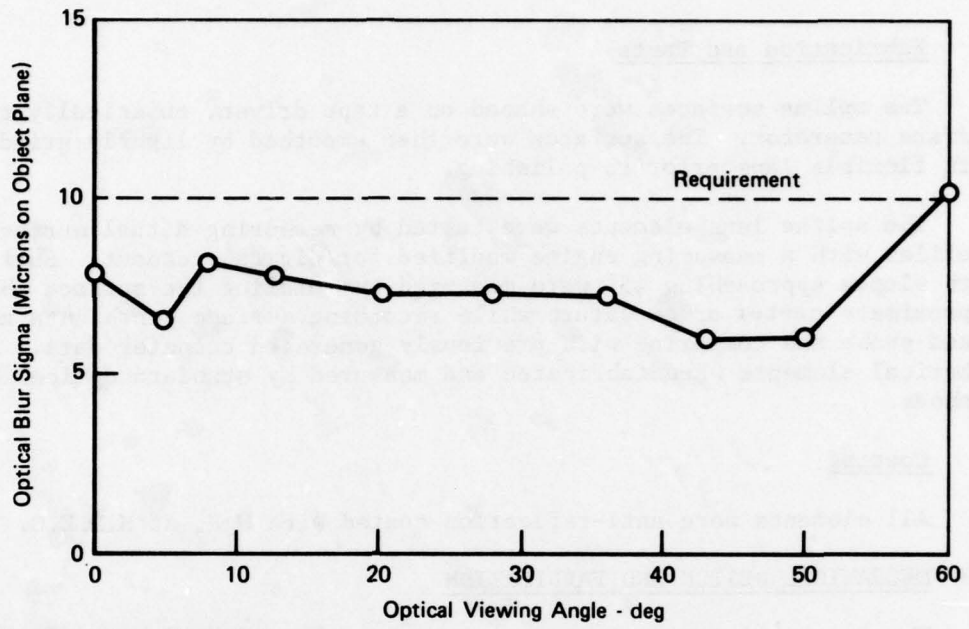
**Element 13**  
 R23 : -1.4772  
 R24 : 3.1733  
 Th : 0.2214  
 Glass : D  
 CA<sub>1</sub> : 0.3365  
 CA<sub>2</sub> : 0.3578

**Materials:**  
**Crowns**  
 A: LaK N14  
 B: SK16  
**Flints**  
 C: SF8  
 D: F2

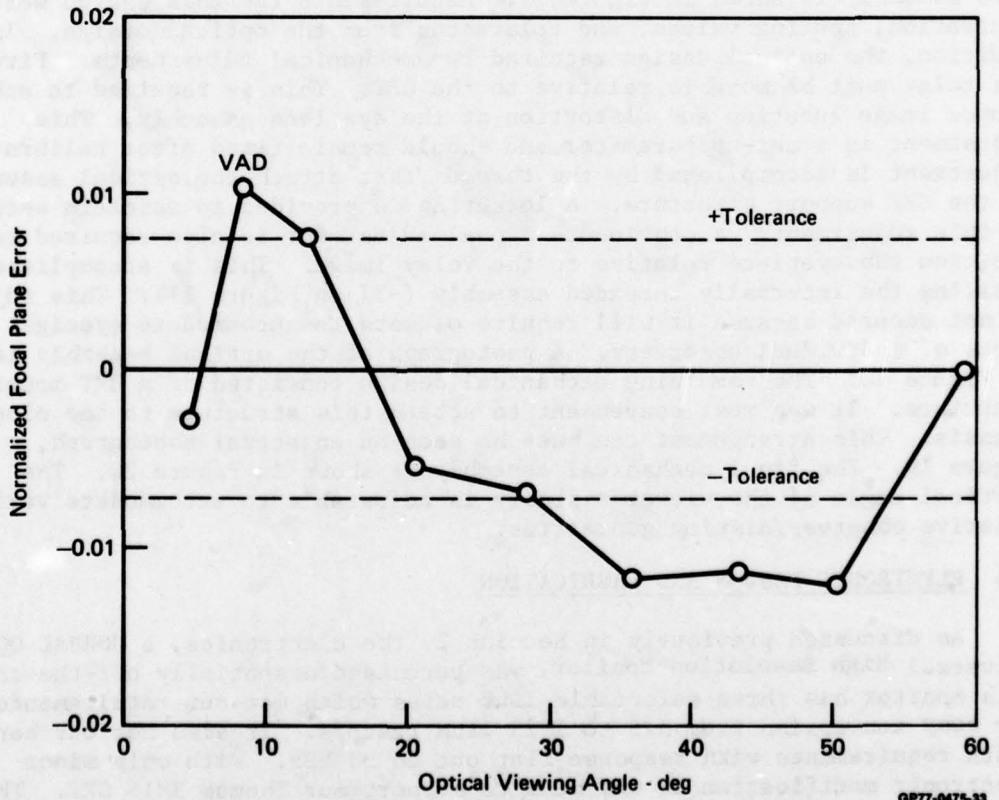


2

(a) Optical Quality



(b) Distortion Error from Theoretical



QP77-0475-33

**FIGURE 16**  
**PREDICTED PERFORMANCE FROM DESIGN RAYTRACE**

### Fabrication and Tests

The spline surfaces were shaped on a tape driven, numerically controlled surface generator. The surfaces were then smoothed by lightly grinding with flexible laps prior to polishing.

The spline lens elements were tested by measuring actual surface profiles with a measuring engine modified for digital readout. Surfaces with slopes approaching  $45^\circ$  were measured by rotating the surface about the approximate center of curvature while recording surface depth data under a fixed probe and comparing with previously generated computer data. All spherical elements were fabricated and measured by standard optical shop methods.

### Coating

All elements were anti-reflection coated with  $MgF_2$  at M.D.E.C.

## 4.3 MECHANICAL DESIGN AND FABRICATION

The lens mounting structure was the primary mechanical design effort. This assembly is shown in Figure 17. Requirements for this design were centration, spacing values, and tolerances from the optical design. In addition, the optical design required two mechanical adjustments. First, the relay must be movable relative to the CRT. This is required to achieve proper image location and distortion at the eye lens assembly. This adjustment is a set-up parameter and should remain fixed after calibration. Adjustment is accomplished by the threads that attach the optical assembly to the CRT support structure. A lock-ring is provided to maintain security of this adjustment. A continuous manual adjustment is also required to position the eyepiece relative to the relay image. This is accomplished by rotating the internally threaded assembly (-37 on Figure 17). This adjustment is not secured because it will require offsets to accommodate eyesight focus of individual observers. A photograph of the optical assembly is shown in Figure 18. The remaining mechanical design consisted of a CRT mounting structure. It was most convenient to attach this structure to the electronic chassis. This arrangement can best be seen on an actual photograph, Figure 19. The final mechanical assembly is shown in Figure 20. The vertical angle of the viewer assembly is adjustable to accommodate various relative observer/display geometries.

## 4.4 ELECTRONIC DESIGN AND FABRICATION

As discussed previously in Section 2, the electronics, a CONRAC QQA Universal High Resolution Monitor, was purchased essentially off-the-shelf. This monitor has three selectable line rates which met our requirements for easy conversion from 525 to 1023 line rasters. It also met our bandwidth requirements with response flat out to 30 MHz. With only minor electronic modification it was made to support our Thomas 3M15 CRT. These modifications and verification tests were done by CONRAC using our CRT which was shipped to them for that effort.

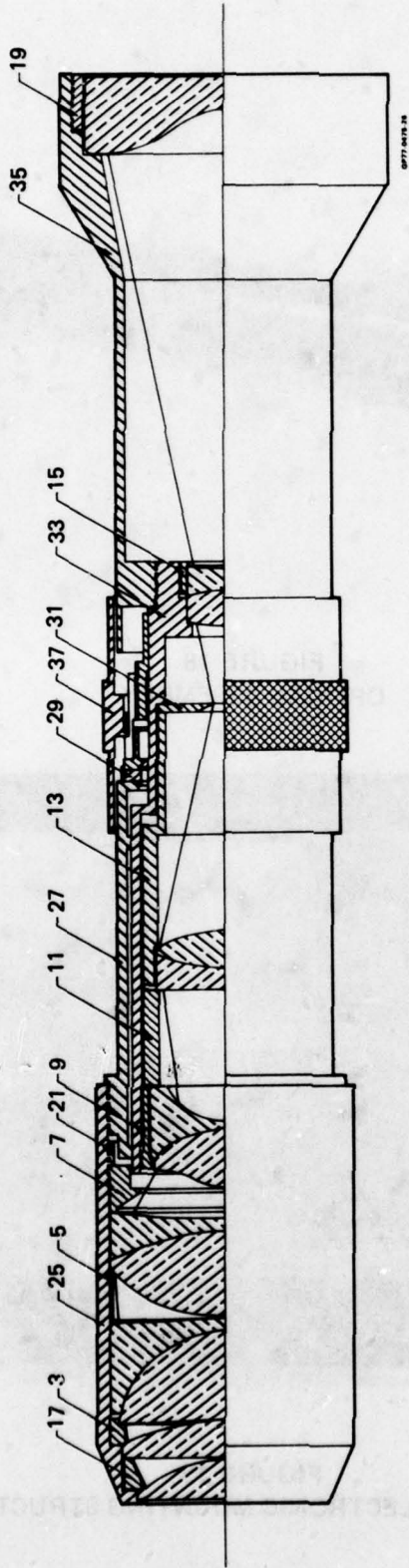
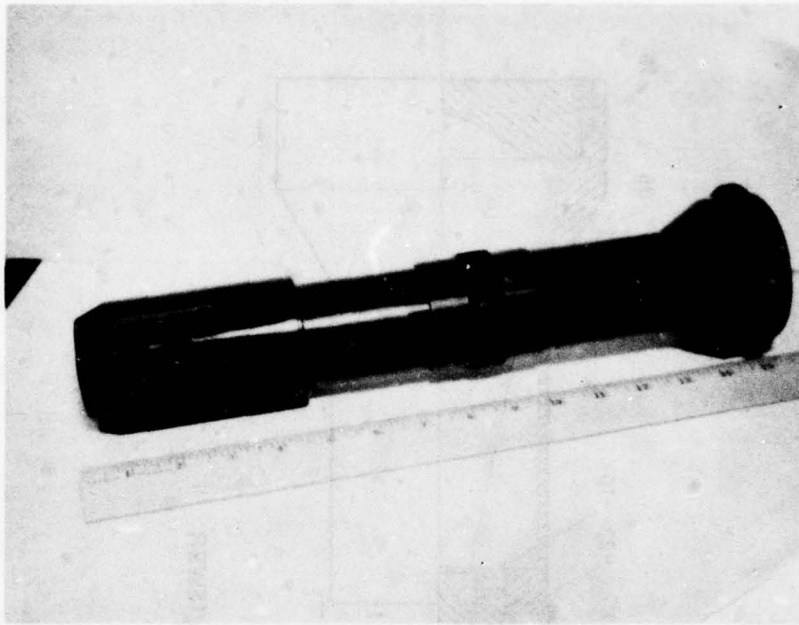
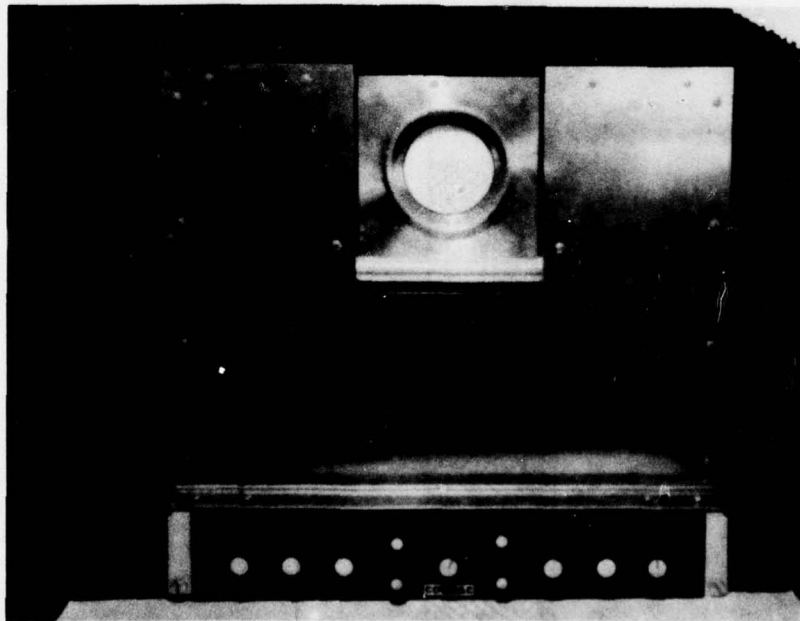


FIGURE 17 -  
VARIABLE ACUITY ASPHERIC VIEWER

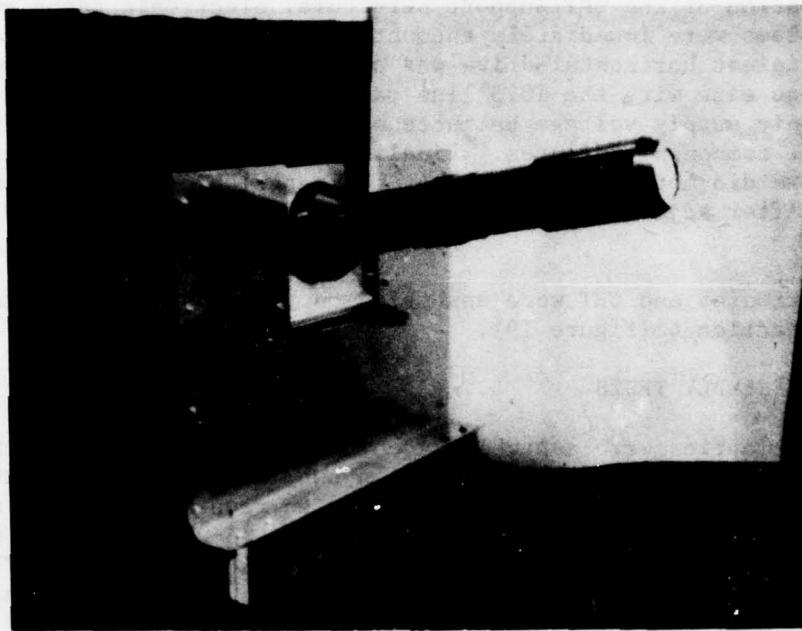


**FIGURE 18**  
**OPTICAL ASSEMBLY**



**FIGURE 19**  
**CRT AND ELECTRONIC MOUNTING STRUCTURE**





4-11-62

**FIGURE 20**  
**FINAL MECHANICAL ASSEMBLY**

## Section 5

### ASSEMBLY AND TEST OF VIEWER

In this section the assembly and test of the viewer are described. The section is divided into two parts, the first on the electronics and the second on the optics.

#### 5.1 ELECTRONICS

Because of the optical fabrication problems discussed in Section 4, the electronic assembly was the first item available for assembly and test. After installation of the CRT support structure, electronic tests were initiated. Problems were immediately encountered with the deflection electronics. First, insufficient horizontal drive was available to achieve the required 2.75 inch image size with the 1023 line raster. CONRAC recommended that the drive electronic supply voltage be increased. This corrected the drive but caused several component failures. Finally, it was established that the deflection yoke did not have the correct characteristics. CONRAC supplied a new yoke. After adjustment, the electronic performance was found to be satisfactory.

The electronics and CRT were assembled on the supporting bracket as described in Section 4 (Figure 19).

#### 5.2 OPTICAL ASSEMBLY TESTS

The viewer optics were assembled according to the drawings of Section 4. Several photographs of this assembly were shown in Figures 18 and 20. Tests were run on this assembly to see how well design requirements were met. This was performed by the apparatus of Figure 21. A microscope is mounted on a nodal slide which is centered on the exit pupil of the VAD. The microscope is supplied with a filar eyepiece to make accurate incremental angular measurements. A micrometer slide is located at the object plane of the VAD which translates a resolution target in a plane parallel to the axis of nodal slide rotation and normal to the optical axis. Initially, a reference point on the resolution target is made to translate through the optical axis of the display. With the nodal slide set at zero degrees, the target reference mark is positioned until it lies on the crosshair of the filar eyepiece. The grid of the eyepiece is now at a central position. The target location is then recorded and designated as the optical axis position.

The resolution target is then moved with the micrometer to determine the maximum resolution occurring when the target is on the crosshair. This resolution is the threshold spatial frequency for the contrast of the target being used. It will be used to compute the optical blur below in the paragraph labeled "Optical Quality". Next, the nodal slide is rotated a fixed angular increment (usually 5°) and the target is translated until the reference mark again lies on the crosshairs. The lateral position of the target slide from the zero degree location is the image height for this viewing angle. After recording this value the threshold resolution is measured as

discussed before. The nodal slide is then rotated to the next angle and image height and threshold resolution are measured as before. This procedure is repeated until the entire field-of-view is covered. Results are as follows:

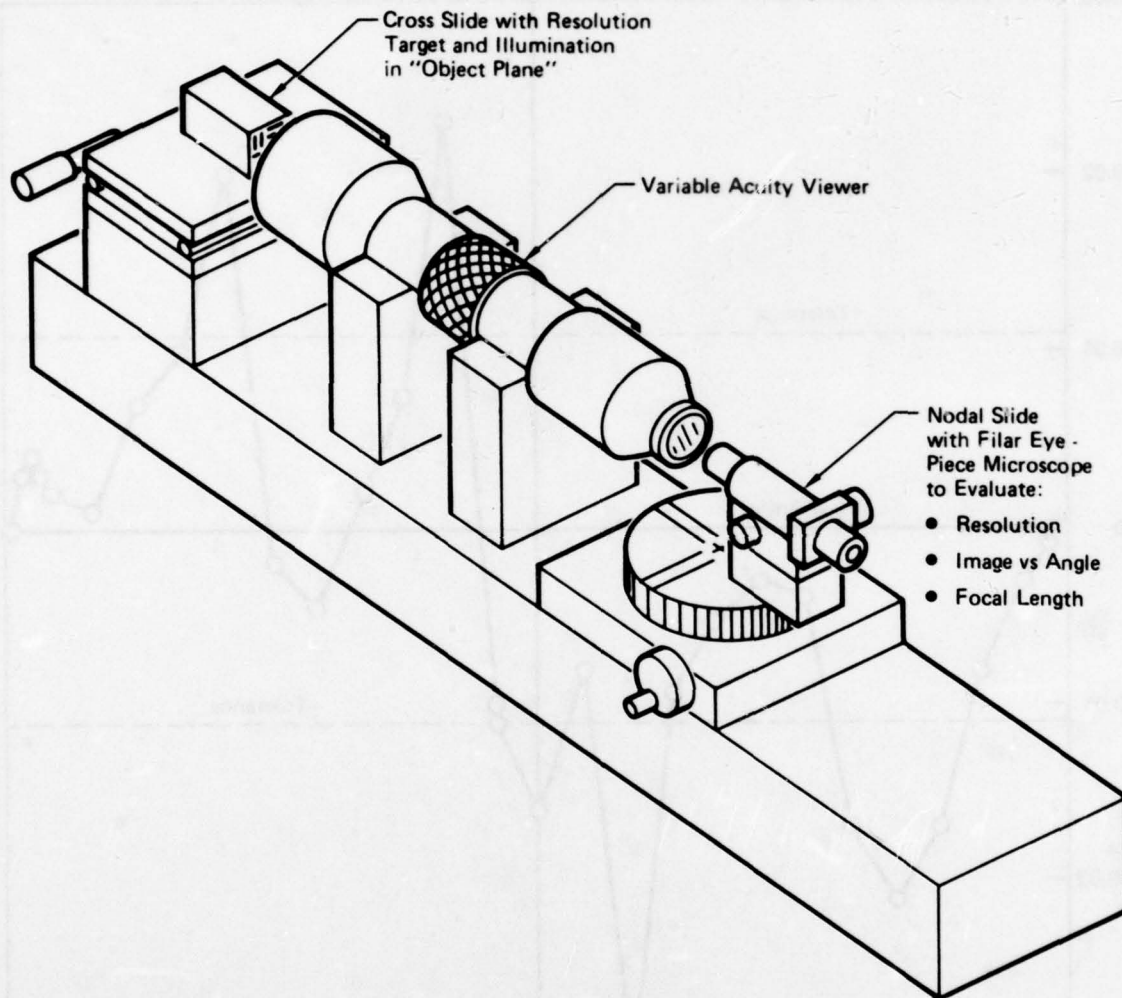
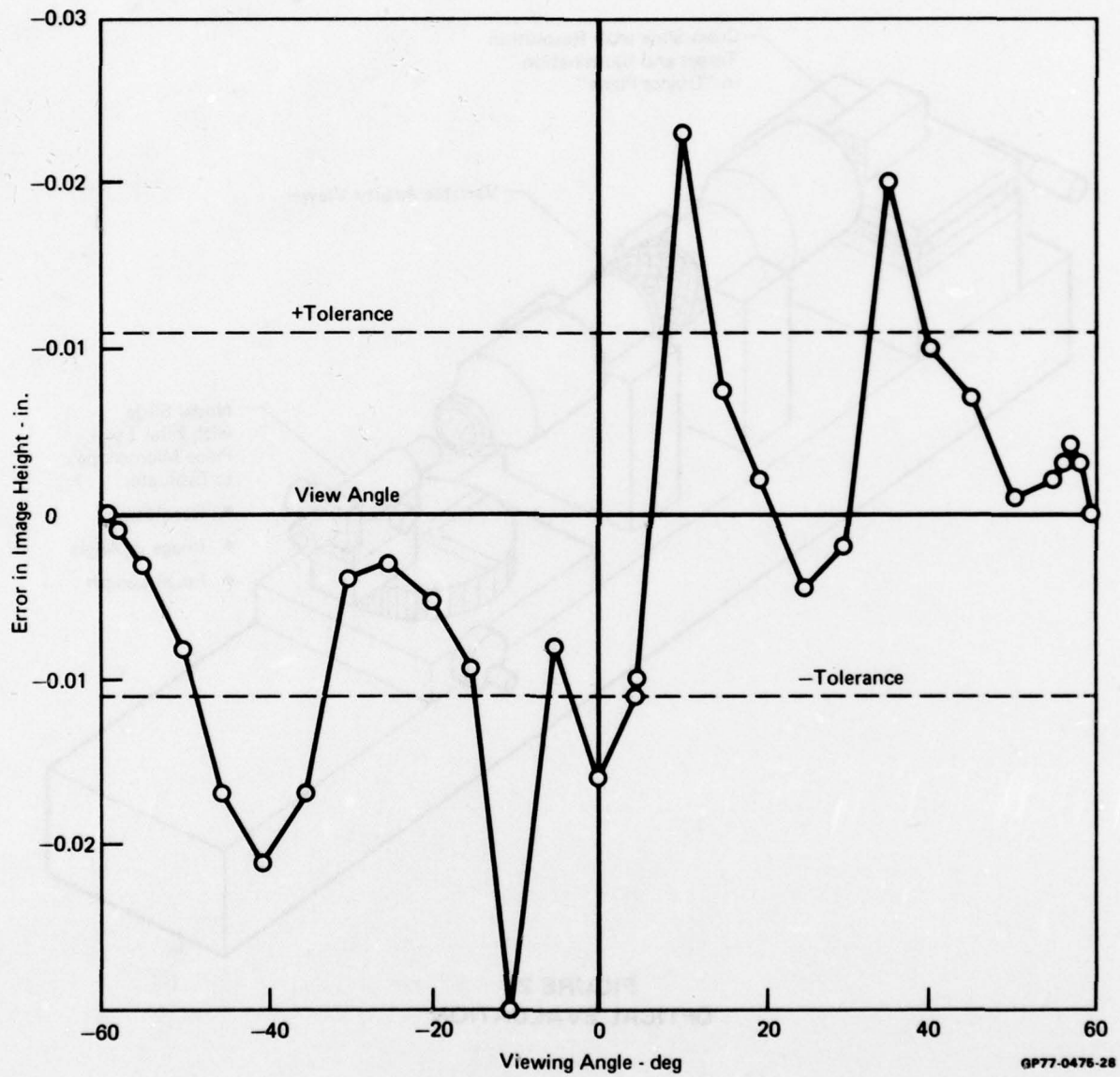


FIGURE 21  
OPTICAL EVALUATION

#### Distortion Function

The measured error in distortion is plotted on Figure 22. While the measured distortion is seen to fall outside of the tolerance band in several regions, it is still quite good (within 1%). It should be noted that the design also predicted that some points would be out of tolerance (Figure 16(b)). By comparison to the measured data, the errors are seen to be of

similar magnitude but not always correlated with viewing angle. In general, this indicates that all optical elements have correctly fabricated slopes, curvatures and centration.



**FIGURE 22**  
**MEASURED IMAGE HEIGHT ACCURACY**

### Optical Quality

The resolution values measured for each viewing angle were converted to optical blur by assuming a gaussian MTF as follows:

$$\tau(s) = e^{-2\pi^2 \sigma^2 s^2} \quad (22)$$

Solving for sigma:

$$\sigma = \frac{1}{s\pi} \sqrt{-\frac{\ln\tau(s)}{2}} \quad (23)$$

Since the power of the viewing microscope was adjusted for maximum observed resolution the value of  $\tau(s)$  is the viewers minimum threshold - about 0.002.\* With this threshold value Equation (23) becomes

$$\sigma = \frac{.542}{s} \quad (24)$$

Using this equation the measured resolution was converted to the sigma blur radius and is plotted in Figure 23. At small viewing angles, this blur is four times worse than the desired requirement of 10 microns. Since the distortion function agrees so well with the prediction, this must be due to poor element surface quality; more specifically, that of the severe aspherics because no method has yet been devised to satisfactorily test the quality of these surfaces. The only testing conducted on these elements was surface profile testing which would only assure proper distortion, not optical quality, exactly the problem noted here.

In general, we feel that the large blur on-axis is most serious. The large blur occurring at 50° would probably not be noticeable because angular resolution is very low in this region anyway. (Later, it is shown that the quality is much better at this point when a CRT source is used.)

At this point the seriousness of the 40 micron blur sigma was reassessed. Returning to our original requirement which was to design a display system that introduced no system degradation we find that the 10 micron blur would assure 95% modulation at the highest anticipated spatial frequency. This may not be a realistic requirement when the degradation of bandwidth and CRT spot size are considered. For example, for a CRT to also have a 10 micron blur sigma, it must have a spot size of about 0.0004 inch. This equates to a resolution of about 1200 TV lines/inch or 3300 TV lines for the 2.75 inch raster size. This is a very special and expensive CRT which may have X-ray radiation problems and limited brightness. Even if this spot size were possible, the system bandwidth imposes a degradation equivalent to a 54 micron blur for a 525 line raster (see Section 3). The impact of the 40 micron optical blur on system performance will be assessed in Section 6.

\* It should be noted that only 10% difference occurs in sigma if the threshold modulation varies from 0.001 to 0.01.

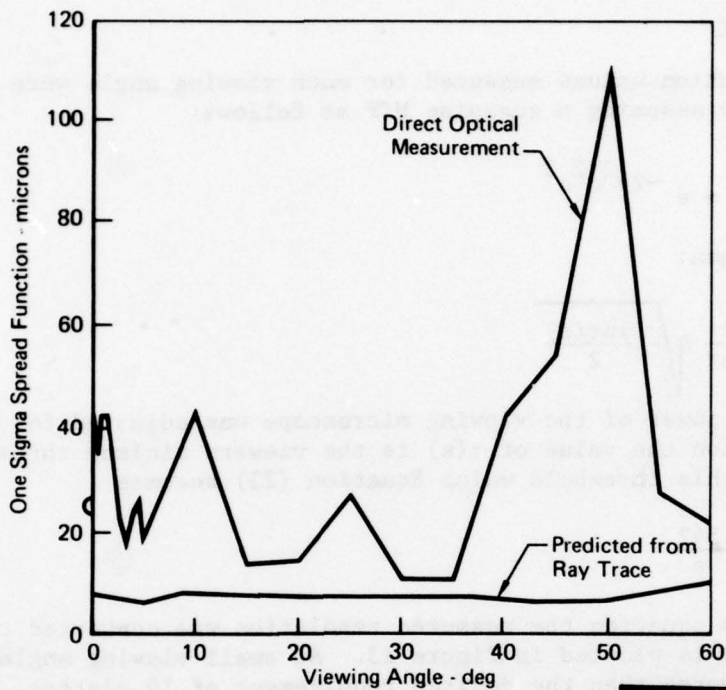


**FIGURE 23**  
**MEASURED OPTICAL BLUR**

Systems Tests

The entire display was tested as a system using the apparatus of Figure 24. First a transparent scale was placed across the CRT face precisely along a diagonal as show in Figure 25 and parallel to the scan direction. The high resolution TV camera is oriented so that the threshold resolution could be read at the display center. The camera was then rotated about an axis perpendicular to the scan direction until the threshold target appeared at 0.25 inch from display center along a diagonal. After recording this threshold resolution, the camera is again rotated to measure resolution at another 0.25 inch step on the CRT. This procedure is repeated until the entire diagonal has been covered in 0.25 inch steps. Next, the optics was attached to the CRT and the above procedure repeated but threshold resolution was measured by viewing through the display optics. The results of both of the above tests are shown on Figure 26.

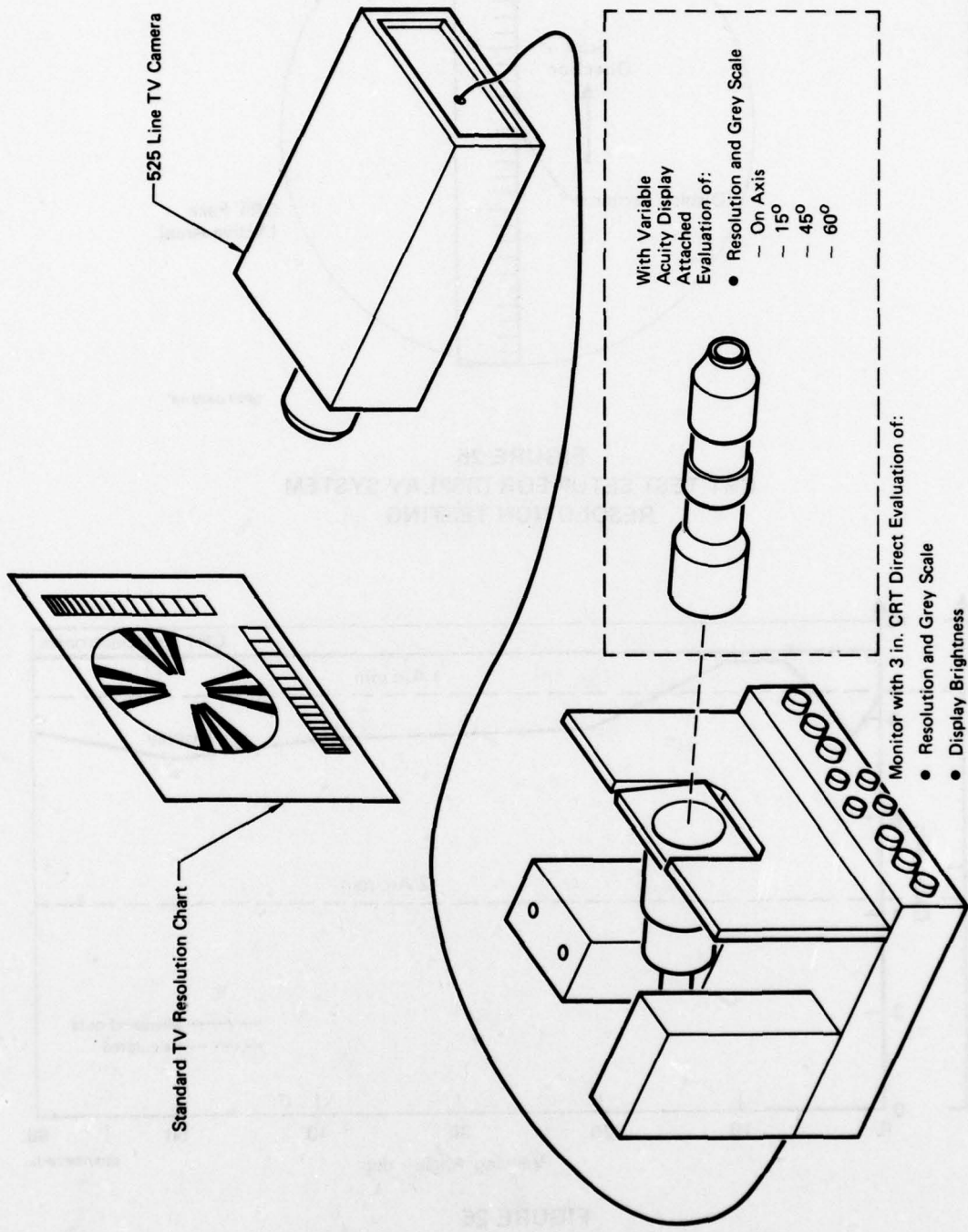
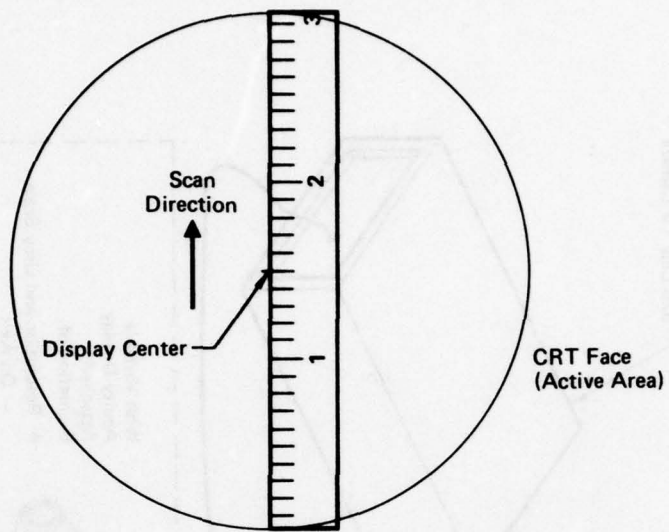
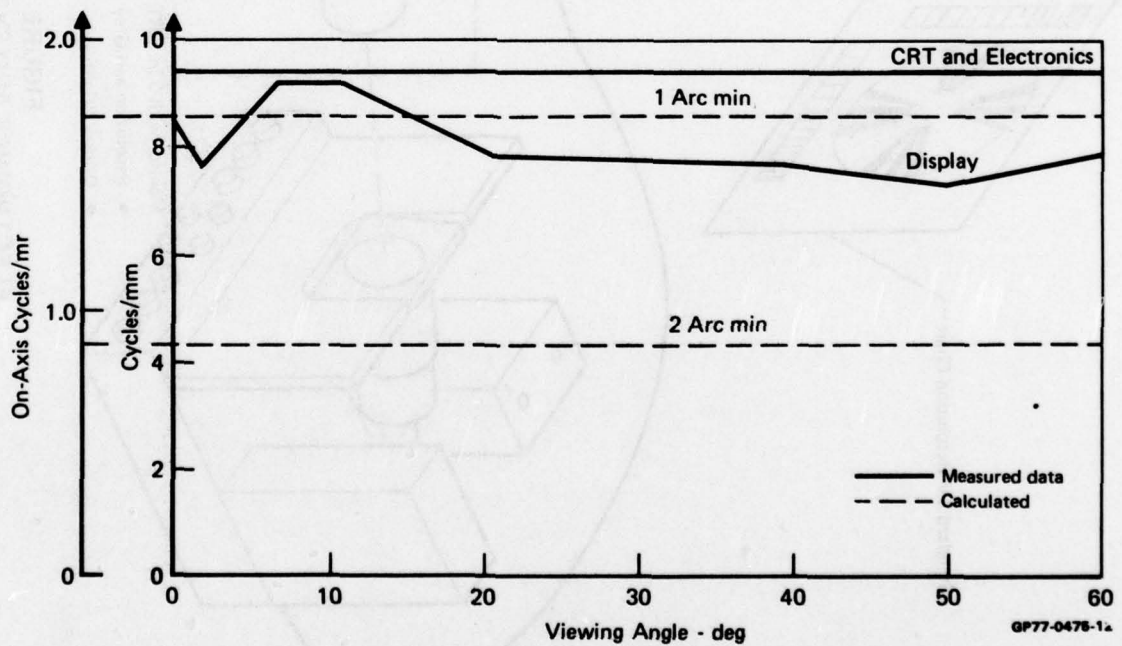


**FIGURE 24**  
**ELECTRONICS AND SYSTEM TEST SETUP**



GP77-0476-11

**FIGURE 25**  
**CRT TEST SETUP FOR DISPLAY SYSTEM**  
**RESOLUTION TESTING**



GP77-0476-12

**FIGURE 26**  
**MEASURED VIEWER PERFORMANCE LIMIT**  
 High Contrast Target = 400/l  
 Brightness = 50 footlamberts



The CRT and Electronics produced a constant threshold resolution along the diagonal of 9.2 cycles/mm. By the method of Equation (23) this converts to a gaussian spread function having a sigma of 59 microns. If the CRT has a spread function of 33 microns, the specified value, the electronics has an equivalent spread of

$$\sigma_e = \sqrt{59^2 - 33^2} = 49 \text{ microns}$$

This sigma may be converted into an equivalent bandwidth by using the MTF for a gaussian function, via:

$$\text{MTF} = \exp - (2\mu^2\sigma^2 \left(\frac{T}{\text{FR} \cdot \text{N} \cdot \text{D}} f\right)^2) \quad (25)$$

where     FR = frame rate  
           N = number of scan lines  
           D = CRT diameter  
           f = spatial frequency  
           T = active scan line time factor

The bandwidth is the value of f at the 3 db down response point where the MTF is equal to 0.707. For a 30 frame per second, 525 line, CRT diameter of 2.8 inches, and 0.89 line factor, the bandwidth is 3.5 MHz. Since the display has a bandwidth of greater than 20 MHz, this is primarily the camera bandwidth.

When the optics are included, the threshold resolution is the lower solid curve of Figure 26. These data indicate an overall worst case system spread function sigma of 74 microns which occurs at a field angle of about 5°. The on-axis spread function for this test is somewhat better, 64 microns. To visualize the angular display acuity of these data, the spatial frequency scale of Figure 26 was converted to on-axis angular spatial frequency using the on-axis focal length of 7.86 inch. This scale is on the left of Figure 26. Also noted on this scale is the classical human static and dynamic resolution of 1 and 2 minutes of arc. This shows that the display is capable of supporting static human acuity on-axis. This was noted during tests where magnification was found to be necessary in order to measure the limiting on-axis resolution.

In order to correlate these data with the previous optical tests, the measured 59 micron CRT plus system electronics spread function was removed from the measured system spread function at each test point. The results are the one sigma radius optical spread function at each measurement angle. These data are plotted on Figure 27 along with the same data obtained by direct optical measurements. For reference the performance predicted from the original ray trace data is also shown on this figure. These data show comparable optical performance for the assembly for both test methods, in general in the 40 micron range. Several salient differences are noted, however. The poor performance noted in optical tests at the 50° viewing angle definitely does not appear in the systems tests. Similar performance improvements are noted in the 10° area and on-axis. Conversely, system per-

formance improvements data indicates worse performance in the 20° to 40° area. While some of this discrepancy may be due to lack of continuous test data, the primary reason for the difference is believed to be due to the difference in spectral and geometrical emission of the CRT used in the systems test and the resolution target used in the optical tests. Since the measured data represents the final display configuration, it should be accepted as more representative of the actual display performance.

Other tests run on the assembled display were brightness and dynamic range. The threshold resolution was found to remain constant up to a brightness of 50 foot-lamberts, above this level degradation in resolution was noted. The display brightness does not vary noticeably over the entire 120° field-of-view.

Dynamic range was determined using the apparatus of Figure 24. A standard shade of grey pattern was shifted throughout the display field-of-view by rotating the camera. A uniform dynamic range of 10 shades of grey ( $\sqrt{2}$ ) was noted.

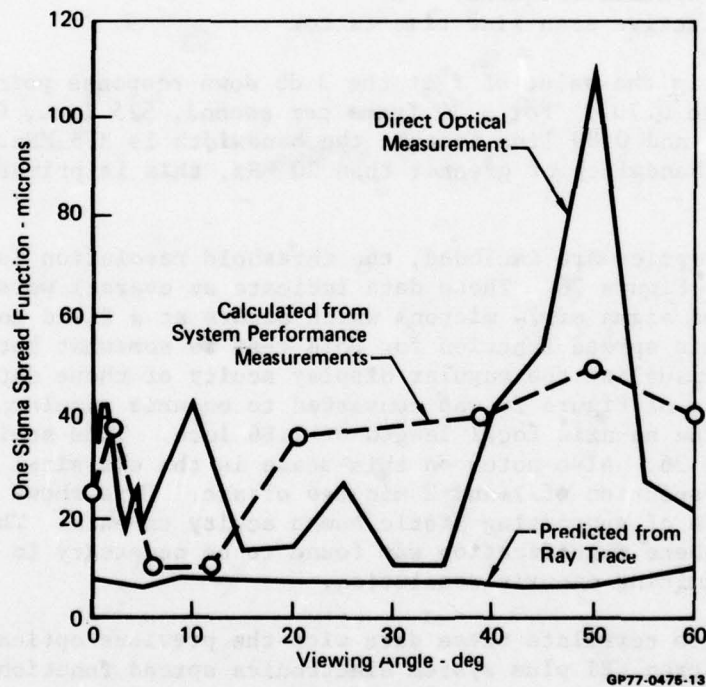


**FIGURE 27**  
**DISPLAY OPTICAL PERFORMANCE COMPARISONS**

## Section 6

### CONCLUSIONS AND VARVS SYSTEM PERFORMANCE PREDICTIONS

The variable acuity display met all requirements except for the resolution requirements at low contrast, specifically:

1. The optical system that was designed for a 10 micron one sigma spread function demonstrated about 43 microns during tests. The reason for this appears to be poor surface quality on the spline elements.
2. The CRT/electronics appears to have an optical equivalent of a 33 micron spread function compared to design goals of about 20 microns.

To study the impact on system performance, minimum resolvable modulations (MRM) was run for several hypothetical and actual display configurations, all operating with the ONR sensor (stopped down for minimum blur) at 525 and 1023 line rasters with sensor bandwidths of 4 and 16 MHz, respectively. These data are shown on Figure 28. Two spatial frequency scales are provided on this figure, one which shows MRM as a function of angular spatial frequency for on-axis viewing (highest resolution) and another which shows MRM as a function of linear spatial frequency at the CRT face, which remains constant for all fields-of-view. The latter scale can be used to compute resolution at any viewing angle by dividing by focal length at that angle (Figure 6).

A perfect display would produce the performance shown by the 10 micron curve. If the optics had the theoretical 10 micron quality but were operated with the CRT and electronics, the 34 micron performance characteristics would apply. In the third case, the actual measured optical performance is combined with the CRT limitation to predict performance of the completed display. While the display induced system degradation is significant, the 52 micron display resulting from this study appears to be very adequate to support human dynamic acuity. This can be seen more clearly on Figure 29 which is the lower values of MRM of Figure 28. Human dynamic resolution can be obtained with a (.014) system input contrast ratio. To provide more detail pertaining to Figures 28 and 29, the contributing MTF's are plotted on Figures 30, 31 and 32 for the three display qualities. For a fixed scan line rate, the effects of lower display quality are easily seen by this lower display MTF. In Figure 30 for the design goal system, the display performance is not a factor. Here the eye and response are the dominant factors. If the display optical quality met the design goals and the existing CRT and electronics were used, the MTF's would be described in Figure 31. All are the same as Figure 30 except for the display which now produces a degradation comparable to the vidicon but less than the eye. The MTF's for the final system (Figure 31) show display degradation exceeding the eye degradation at the higher spatial frequencies.

Now some discussion is in order concerning raster line rate. Note that the only change in MTF's for the two line rates is in the MTF of the system electronics. There is no change in vidicon MTF because it is a silicon array type and its response is defined by the mosaic structure of its photocathode.

A reversal of performance vs line rate is seen on the MRM curves (Figures 28 and 29) compared to the MTF curves. This is a result of the manner in which the NVL computes performance (Appendix B). In this model the electronics MTF results in more signal to the display at the higher line rate. The wide bandwidth of the electronics however, allows more noise to reach the display. In our case, the noise increased at a greater rate than signal, hence a lower performance is predicted at the higher line rate.

To complete the comparison, the total MTF of the three systems are plotted on Figure 33 for a 525 line rate. Note that there is very little difference in all three, except at higher spatial frequencies. This was also seen in the MRM curve with the amplified scales on Figure 29.

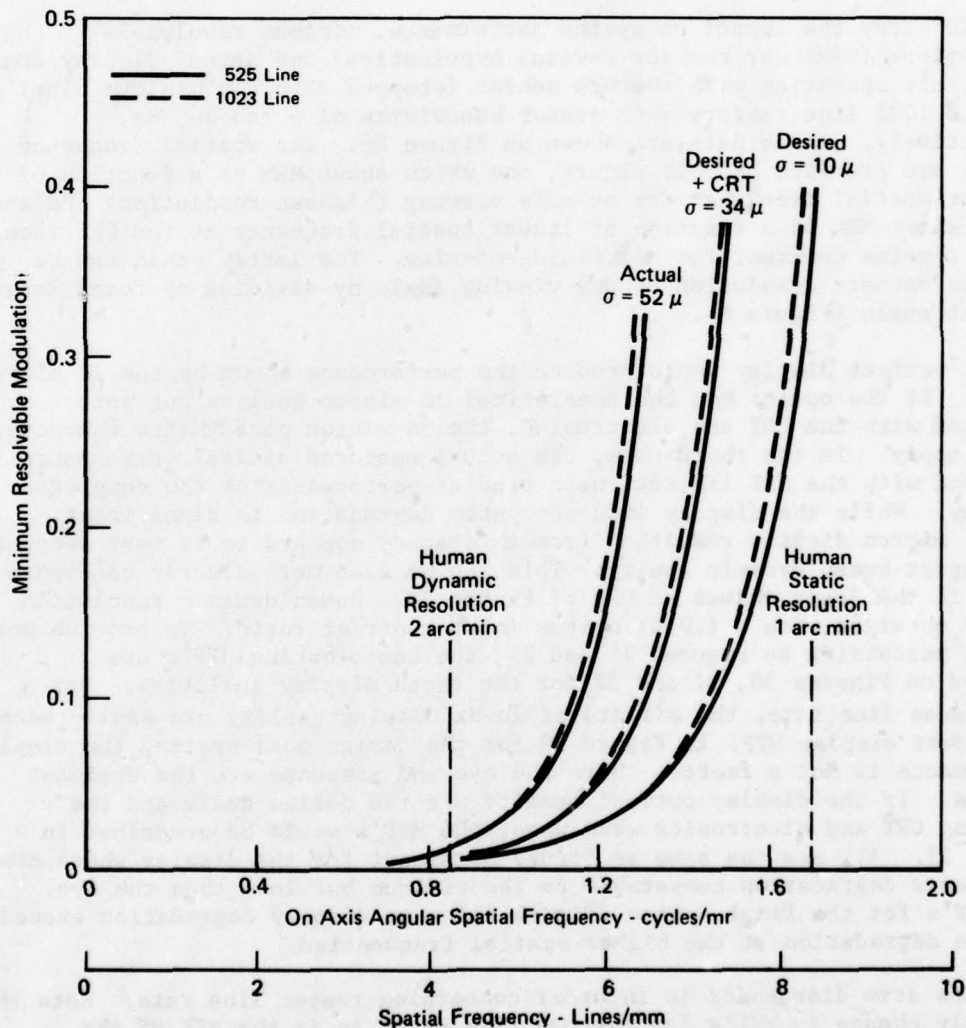


**FIGURE 28**  
**VARIABLE ACUITY DISPLAY SYSTEM PERFORMANCE WITH ONR CAMERA**  
 Brightness - 10 footlamberts

GP77-0476-14

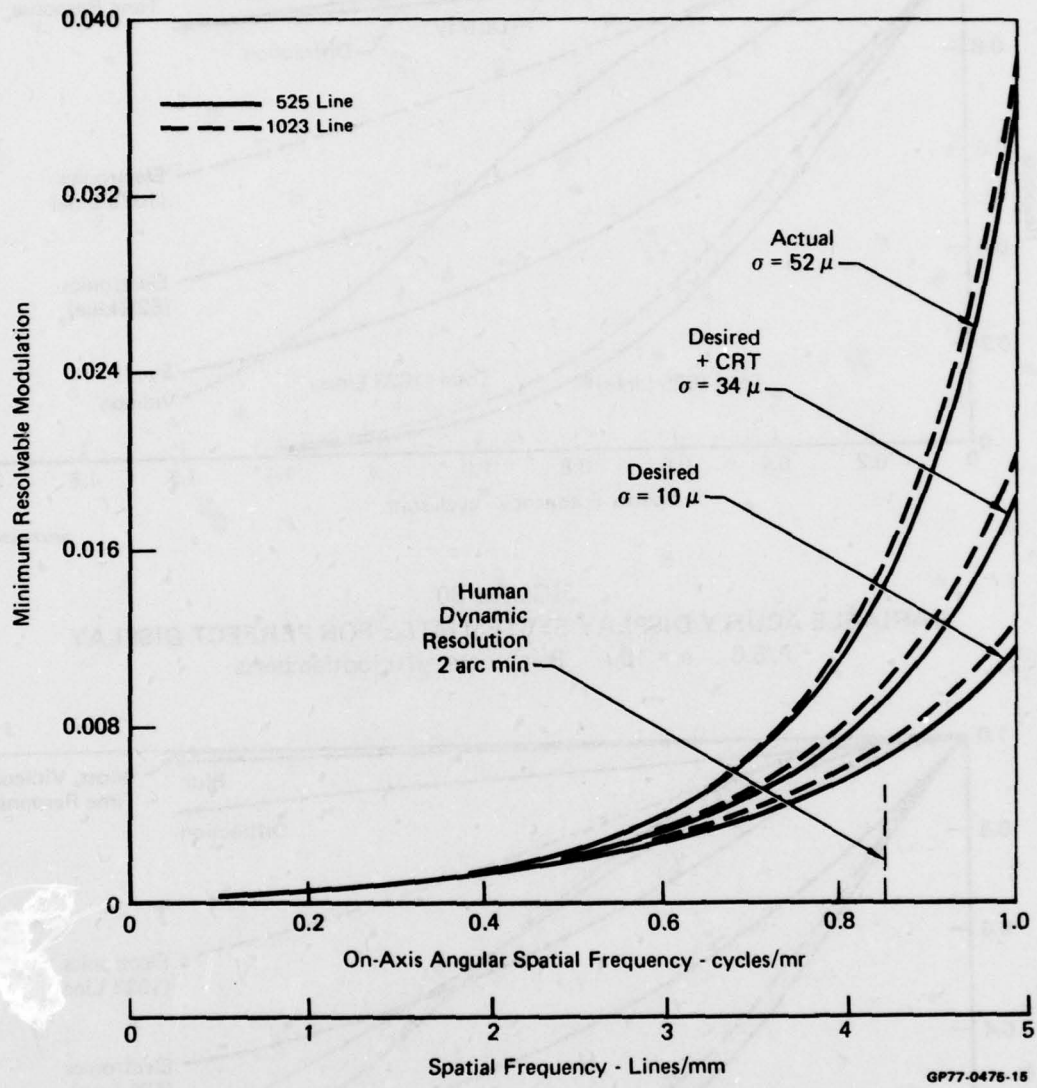
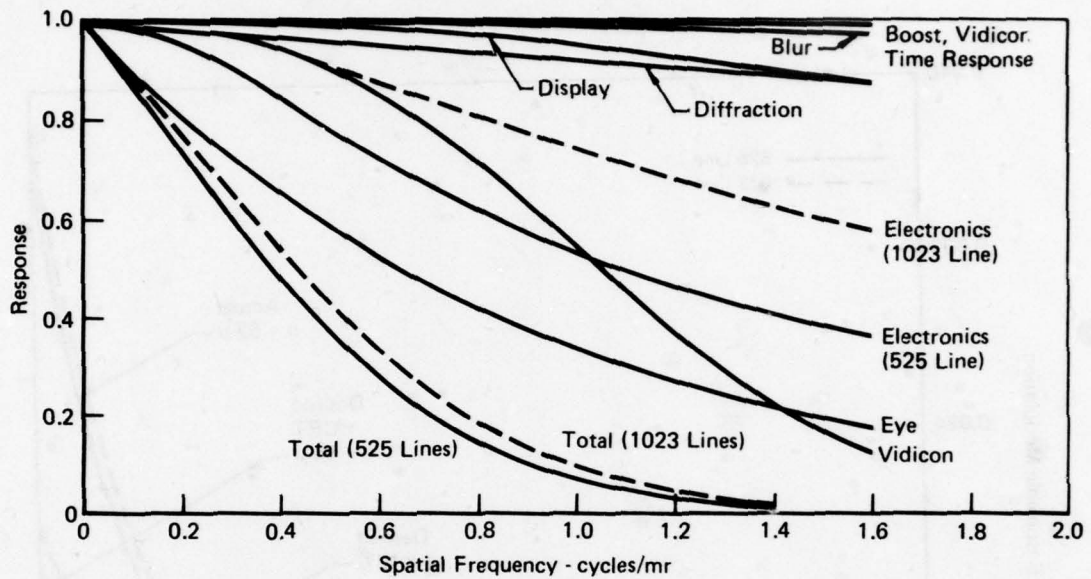
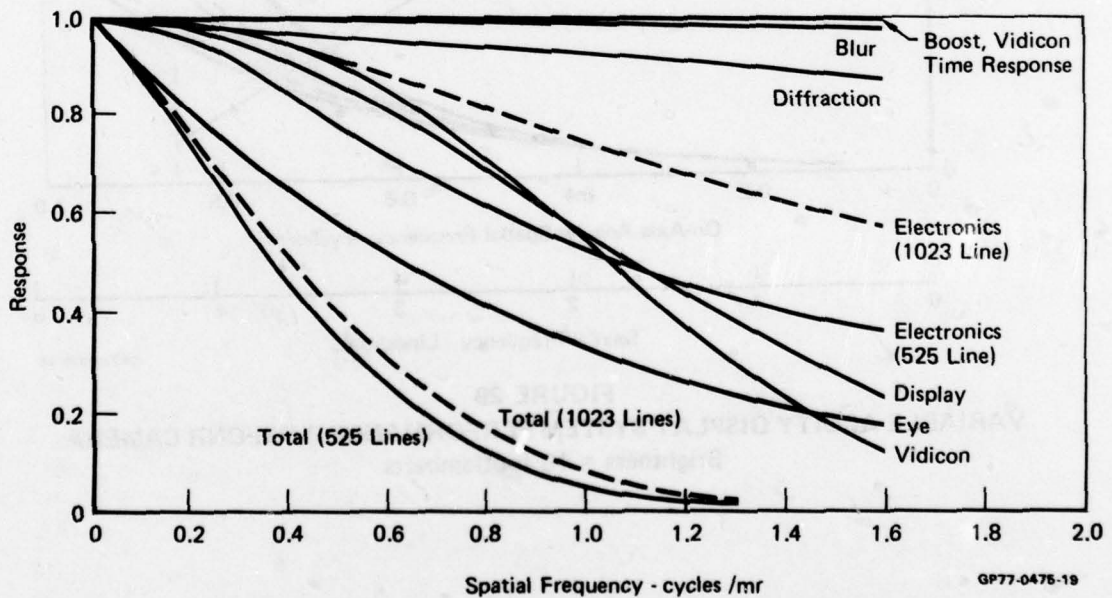


**FIGURE 29**  
**VARIABLE ACUITY DISPLAY SYSTEM PERFORMANCE WITH ONR CAMERA**  
 Brightness = 10 footlamberts



GP77-0476-20

**FIGURE 30**  
**VARIABLE ACUITY DISPLAY SYSTEM MTF's FOR PERFECT DISPLAY**  
 F/5.6  $\sigma = 10\mu$  Brightness = 10 footlamberts



GP77-0476-19

**FIGURE 31**  
**VARIABLE ACUITY DISPLAY SYSTEM MTF's FOR DESIGN GOAL OPTICS AND EXISTING CRT AND ELECTRONICS**  
 F/5.6  $\sigma = 34\mu$  Brightness - 10 footlamberts

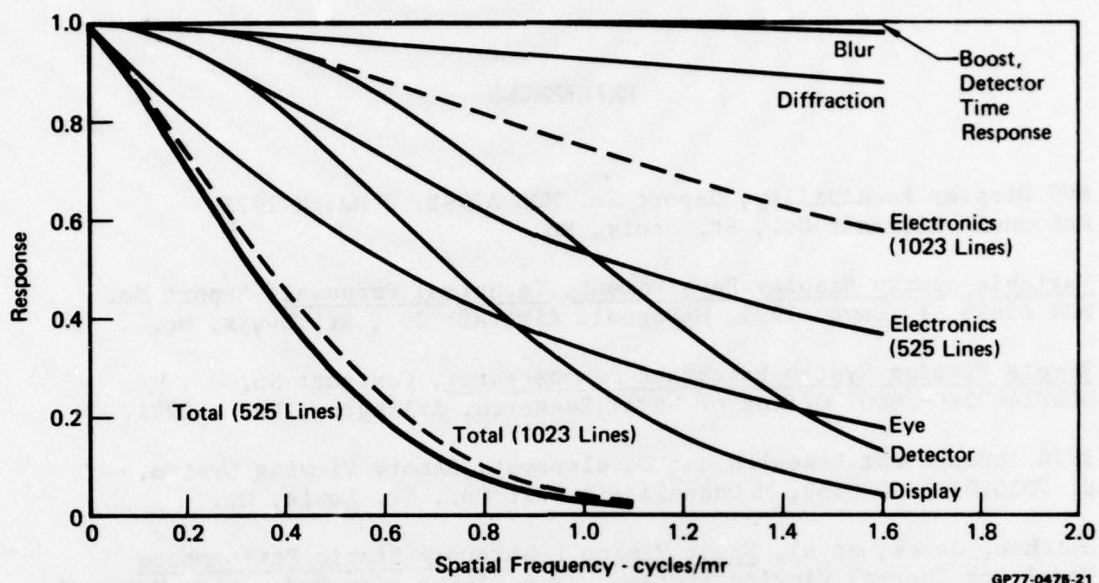


**FIGURE 32**  
**VARIABLE ACUITY DISPLAY SYSTEM MTF's FOR COMPLETED DISPLAY**  
 F/5.6  $\sigma = 54\mu$  Brightness = 10 footlamberts

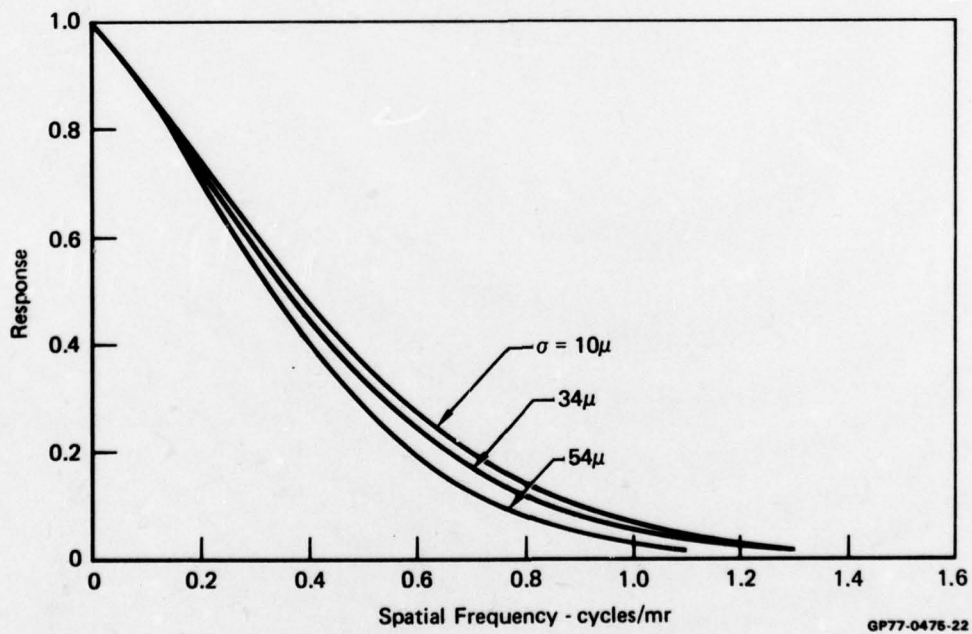


**FIGURE 33**  
**VARIABLE ACUITY DISPLAY SYSTEM TOTAL MTF's**  
 F/5.6 Brightness = 10 footlamberts

#### REFERENCES

1. RVS Display Feasibility, Report No. MDC A3992, 3 March 1975, McDonnell Aircraft Co., St. Louis, Mo.
2. Variable Acuity Display Development, Technical Proposal, Report No. MDC A3663, 17 Sept. 1975, McDonnell Aircraft Co., St. Louis, Mo.
3. Remote Viewing System Baseboard Demonstrator, Contract No. N00014-75-C-0660, Office of Naval Research, Arlington, Va. 22217
4. 1976 Independent Research and Development, Remote Viewing System, p. 7056.01 - 7056.59, McDonnell Aircraft Co., St. Louis, Mo.
5. Ratches, James, et al, Night Vision Laboratory Static Performance Model For Thermal Viewing Systems, Army Electronics Cmd., Fort Monmouth, N.J., Report No. 7043, April 1975.
6. Fisher, R.W., et al, Foveal Lens Feasibility Study, 8 to 14 Micron Spectral Region Final Report, to be published May 1977, Contract No. N00014-76-C-0699, Office of Naval Research, Arlington, Va. 22217

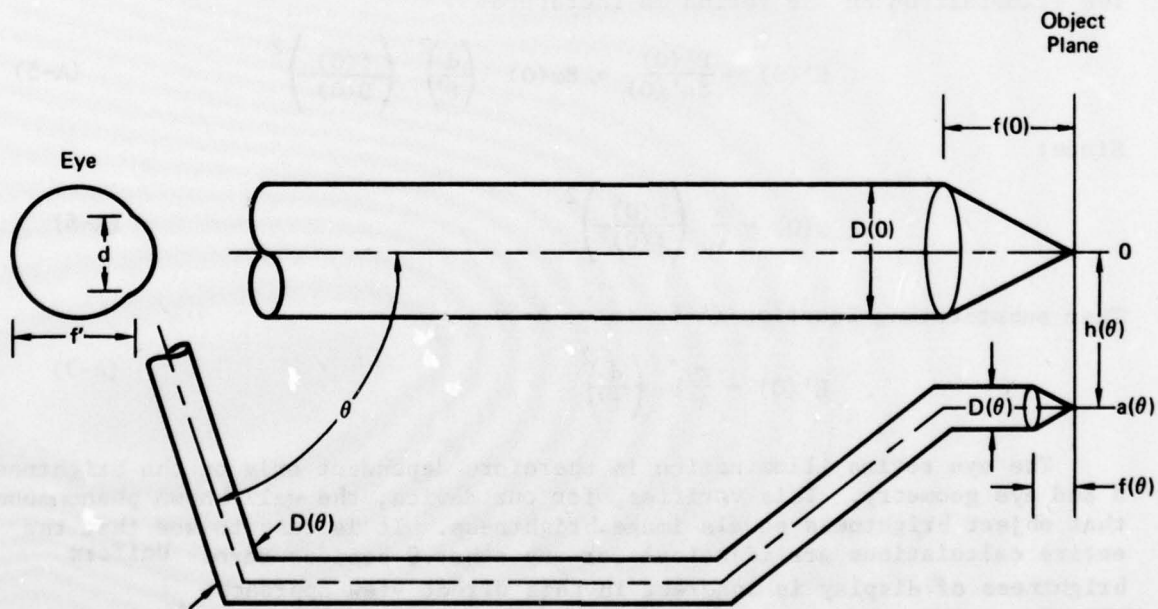


Appendix A

DIRECT VIEW PHOTOMETRIC ANALYSIS

Some general calculations are possible for direct viewing that can assist us in establishing feasibility of various approaches. For this purpose the layout of Figure A-1 is postulated. For direct view, light emitted from the object plane (CRT Phosphor) at some point  $a$ , a distance  $h(\theta)$  from the optical axis, must enter the eye as a collimated bundle at angle  $\theta$ . The variation of function  $h(\theta)$  with  $\theta$  must be identical to the variation of the camera lens. In addition, to accommodate some head motion, the collimated bundle received by the eye should be larger than the eye iris aperture. Exactly how much larger is dependent on details of the optics utilized. For example, if an eyepiece is used, 0.3 to 0.5 inch may be required, while a free head system would require at least one inch.

Certain brightness relationships are inherent to the direct view display and will now be discussed. Figure A-1 will aid in this discussion. In this figure the object plane is a CRT phosphor screen. A generalized distortion function must exist, i.e.,  $h(\theta)$  versus  $\theta$  which is identical to that of the nonlinear lens.



GP77-0475-16

**FIGURE A-1  
DIRECT VIEW GEOMETRY**

If the solid angle ( $\omega(0)$ ) emission from point 0 is large enough to fill the aperture diameter  $D(0)$ , the flux into  $D(0)$  from element of area  $dA$  with brightness (B) is:

$$F(0) = B \omega(0) dA \quad (A-1)$$

For area  $dA$  this is the flux contained in the bundle received at the eye with diameter  $D$ . The illumination of the eye pupil is:

$$E(0) = \frac{F(0)}{\frac{\pi}{4} D(0)^2} \quad (A-2)$$

This actual flux entering the eye iris of diameter (d) is:

$$F'(0) = \frac{E(0) \pi d^2}{4} = F(0) \left( \frac{d}{D(0)} \right)^2 \quad (A-3)$$

This flux is spread over an area on the retina:

$$da'(0) = dA \left( \frac{f'}{f(0)} \right)^2 \quad (A-4)$$

The illumination on the retina is therefore:

$$E'(0) = \frac{F'(0)}{da'(0)} = B \omega(0) \left( \frac{d}{f'} \right)^2 \left( \frac{f(0)}{D(0)} \right)^2 \quad (A-5)$$

Since:

$$\omega(0) = \frac{\pi}{4} \left( \frac{D(0)}{f(0)} \right)^2 \quad (A-6)$$

Then substituting Equation (A-6) into (A-5)

$$E'(0) = \frac{\pi}{4} b \left( \frac{d}{f'} \right)^2 \quad (A-7)$$

The eye retina illumination is therefore dependent only on the brightness B and eye geometry. This verifies, for our device, the well known phenomenon that object brightness equals image brightness. It is easy to see that the entire calculations are identical for any other  $\theta$  besides zero. Uniform brightness of display is inherent in this direct view approach.

## Appendix B

### APPLICATION OF THE NIGHT VISION LABORATORY (NVL) THERMAL VIEWING SYSTEM STATIC PERFORMANCE MODEL TO THE RVS

It was suggested that the NVL Thermal Viewing System Static Performance Model, Reference (B-1) be used to evaluate the performance of the Remote Viewing System (RVS). However, repeated attempts to convert the RCS parameters directly to the NVL model have led to the following problem. The radial distortion function of the foveal lens does not lend itself to an MTF analysis as a function of object field angular spatial frequency as called for in the NVL model. All parameters can be converted successfully except for the scan velocity term because a linear raster scan on the lens image plane will create a variable angular velocity and variable direction scan in the object field. This is depicted in Figure B-1. Extreme complexity results when attempts are made to convert spatial into temporal frequency. This is illustrated by the rotation of the  $f_x$  bar pattern in the lens image plane shown in Figure B-1. Given enough time<sup>x</sup>, an analysis could be made in a manner compatible with the NVL model. However, the analysis is much simpler if performed, not in object field angular frequency (cycles/milliradian) but in spatial frequency terms (cycles/millimeter). For our purpose of optimizing the RVS lens, it is simpler to work in terms of spatial frequency on the foveal lens focal plane.

This simplicity arises because seven of the nine MTF's are independent of object field angle at this foveal lens focal plane location, and the scan velocity is unidirectional and uniform at this location, thereby making easy conversion from spatial to temporal parameters. The only non-linear conversions necessary are simple geometrical ones which translate from focal plane to object field and display space. The advantages of working in the spatial frequency terms will become clear as the analysis is developed. In the following development, the NVL model approach will be used precisely but will be applied in the foveal lens focal plane as a function of linear spatial frequency (cy/mm). Parameters will be covered in the same order as they are in the NVL Report Reference B-1, which describes the model in detail.

#### B.1 MTF's

Optical MTF The optical MTF's consist of a diffraction MTF and a Gaussian MTF.

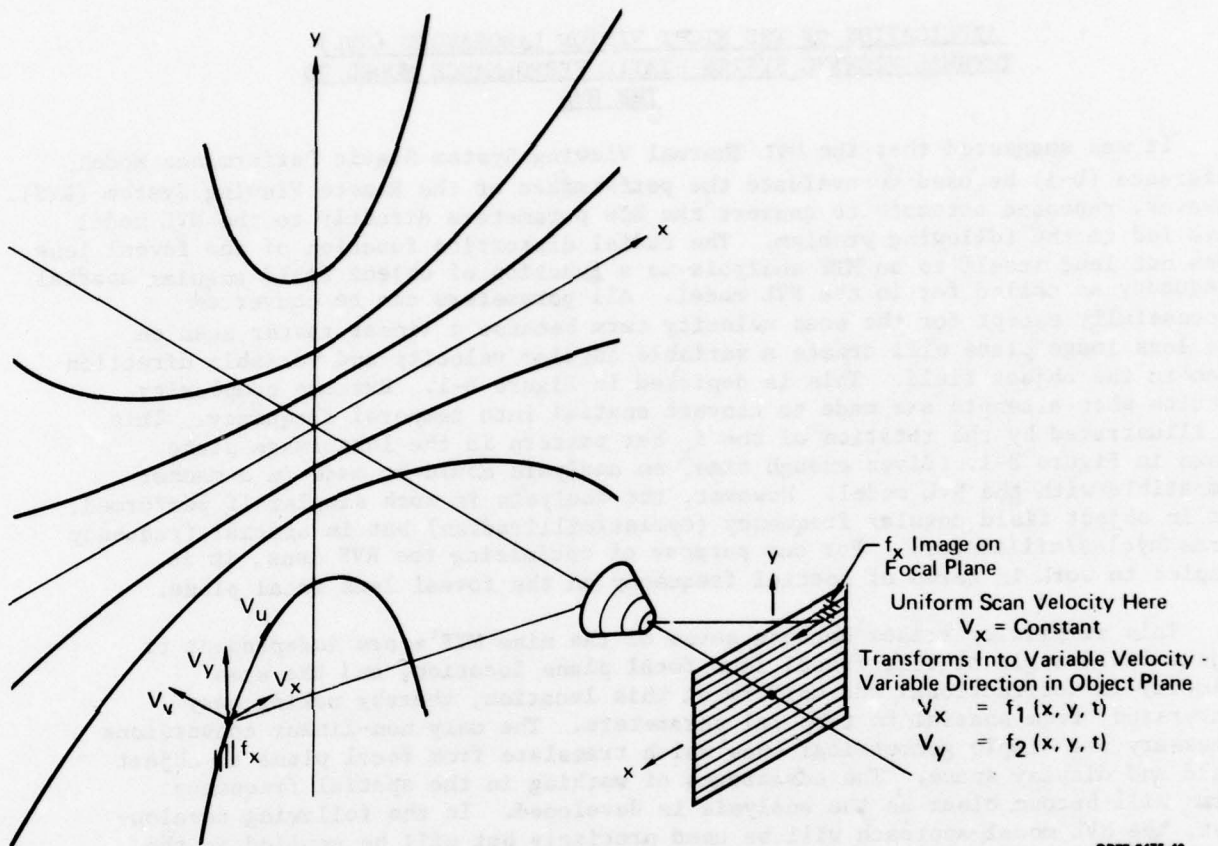
(a) Diffraction In angular terms, the diffraction MTF is referenced as Equations (9) and (10) of the NVL report:

$$H_{\text{opt}}(f_x, \theta) = \frac{2}{\pi} [\cos^{-1} A - A(1 - A^2)^{1/2}] \quad (\text{B-1})$$

$$\text{where } A = \lambda F_{\#} f_x / L(\theta) \quad (\text{B-2})$$

where  $L(\theta)$  is the equivalent focal length which changes over a 50/1 range as object field angle  $\theta$  changes. The angle  $\theta$  is the absolute angle between the point of interest and the lens optical axis. At the foveal lens image plane

$$S_x = \frac{f}{L(\theta)} \quad (\text{B-3})$$



GP77-0475-40

FIGURE B-1  
SCAN DISTORTION INTRODUCED BY FOVEAL LENS

where  $S_x$  is the image plane spatial frequency and  $f_x$  is its object field angular equivalent measured along the scan line projection in the object field ( $\mu$  direction on Figure B-1). Solving for  $f_x$  in Equation (B-3) and substituting this for  $f_x$  in Equation (B-2).

$$A = \lambda F_{\#} S_x \quad (B-4)$$

Since the F/number of our lens is constant, the diffraction MTF is no longer a function of object field angle. Thus we may write  $H_{opt}(S_x)$  which indicates that the MTF is a function of the independent variable  $S_x$  only. Note, however, that conversion to object field angular spatial frequency is very simple because focal length is constant over small angular increments and may be determined from

$$f_{\mu} = S_x L(\theta) \quad (B-5)$$

where  $\mu$  is along the scan line projection in the object field

likewise

$$f_w = S_y L(\theta) \quad (B-6)$$

where  $w$  is normal to the scan direction in the object field

(b) Blur - A similar simplicity exists here. The MTF equation with the angular term  $b$  of Equation (11) of Reference(B-1) replaced with its equivalent is:

$$H_{blur}(f_x, \theta) = \exp \left[ - \frac{2\pi^2 \sigma^2}{L(\theta)^2} f_x^2 \right] \quad (B-7)$$

The foveal lens inherently has a constant spatial blur over its entire focal plane, so that the sigma ( $\sigma$ ) of Equation(B-7) is a constant. Substituting Equation(B-5) into (B-7) we see the blur MTF simplifies to

$$H_{blur}(S_x) = \exp \left[ - 2\pi^2 \sigma^2 S_x^2 \right] \quad (B-8)$$

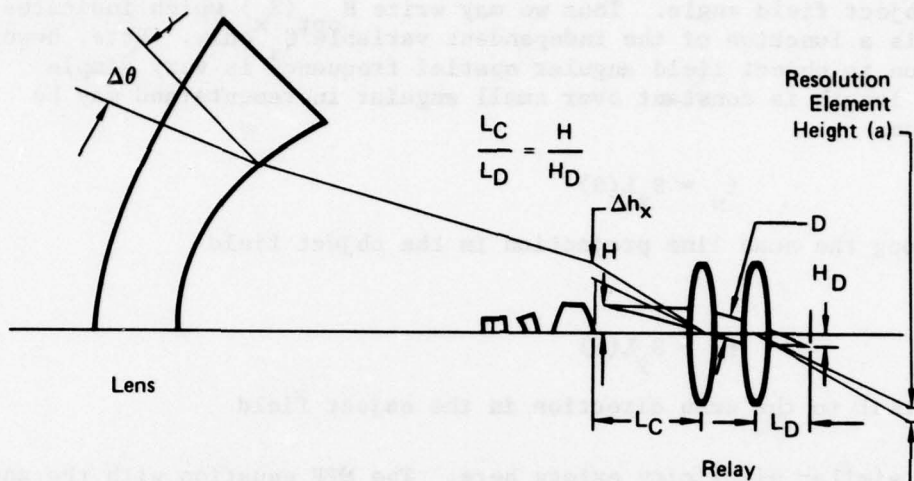
Thus this MTF like the diffraction MTF, is no longer a function of object field angle because the focal length variable has been removed.

Detection MTF - The spatial filter MTF of the detector is defined as:

$$H_{Det}(f_x, \theta) = \frac{\text{Sin}(\pi f_x \Delta x)}{\pi f_x \Delta x} \triangleq \text{Sinc}(f_x \Delta x) \quad (B-9)$$

It is also complex in our system because the angular projection of the detector into the object field ( $\Delta\theta$ ) in this equation varies with absolute object field angle ( $\theta$ ). Since the detector height is still uniform at the lens focal plane, shown in Figure(B-2) as  $\Delta h$ , Equation(B-9) can be restated as:

$$H_{Det}(S_x) = \frac{\text{Sin}(\pi S_x \Delta h_x)}{\pi S_x \Delta h_x} \quad (B-10)$$



GP77-0475-32

**FIGURE B-2**  
**OPTICAL RELAY PARAMETERS**

Again the MTF becomes independent of object field angle. Note from Figure(B-2) that the detector height ( $\Delta h_x$ ) is a function of detector size ( $a$ ), detector system focal length ( $L_D$ ), and relay focal length ( $L_C$ ), viz:

$$\Delta h_x \approx a_x \frac{L_C}{L_D} \quad (B-11)$$

If the detector characteristics are known, the focal lengths are a function of detector size ( $\Delta h$ ) projected onto the image plane as shown in Figure (B-2). Detector size  $\Delta h$  can be computed directly from either the on-axis resolution required, the number of scan lines required across the vertical FOV, or bandwidth/response restrictions and frame rate requirements. The focal lengths,  $L_C$  and  $L_D$ , are then selected to make the detector dimension appear as the required  $\Delta h$  at the foveal lens focal plane. The detector MTF becomes:

$$H_{\text{Det}}(S_x) = \text{Sinc} \frac{S_x a_x L_C}{L_D} \quad (B-15)$$

Again this MTF is independent of object field angle.

Detector Electronics MTF - It is in the MTF, the detector electrical response, that we get into real trouble trying to work in object field angular space. For a conventional linear optical system, a linear detector scan velocity converts into a scaled but linear angular scan in the object field. This is not true in our system as was shown in Figure B-1. A linear scan in the x direction on the image plane results in angular velocities in both  $\theta_x$  and  $\theta_y$  directions in the angular object field. Both of these angular components are nonlinear functions of both x and y position on the image plane. Thus, converting from spatial frequency to temporal frequency becomes very complex. All of this can be avoided by working in linear spatial plane terms. If the scanner has an angular scan velocity  $\beta$ , then the linear motion of the instantaneous FOV on the foveal lens image is

$$V_x = \beta L_C \quad (B-16)$$

The conversion to temporal frequency (f) is therefore

$$f = V_x S_x \quad (B-17)$$

This is a constant conversion and not a function of time. Therefore, all electronic MTF's of the NVL model are valid. These are

$$H'_{\text{Det}}(f)$$

$$H_{\text{Elect}}(f)$$

$$H_B(f)$$

Display - The RVS display is the inverse of the foveal lens, which results in a conventional linear raster generated on the CRT. The CRT has a constant spot size and the expansion optics has a constant blur at the object focal plane. Again this MTF, if derived in the linear spatial plane, will not be a function of object angle. If the optical blur and CRT spot size are combined and assumed to have a Gaussian MTF, a composite sigma ( $\sigma_d$ ) results and the MTF is:

$$H_{\text{Disp}}(S_x) = \exp [-2\pi^2 (r\sigma_d)^2 S_x^2] \quad (B-18)$$

where r is the physical ratio of format sizes; viz

$$r = \frac{H_{\text{LENS IMAGE}}}{H_{\text{DISPLAY CRT}}} \quad (B-19)$$

By contrast, if this were accomplished in the object angular plane, the MTF would be much more complex, viz

$$H_{\text{Disp}}(f_x, \theta, M) = \exp \left[ - \frac{2\pi^2 (r\sigma_d)^2 f_x^2}{L(\theta)^2 M^2} \right] \quad (\text{B-20})$$

where M is any system angular magnification from object field to the viewer. Again the simplicity is obvious.

Stabilization and Eyeball - The remaining two MTF's are the only two that are not simplified by working in linear spatial rather than angular terms. First, stabilization tends to be angular input to the system. Using the MTF from the NVL report:

$$H_{\text{Los}}(f_x) = \exp(-P f_x^2) \quad (\text{B-21})$$

Converting to the foveal lens image plane results in

$$H_{\text{Los}}(S_x, \theta) = \exp[-P S_x^2 L(\theta)^2] \quad (\text{B-22})$$

Similarly, the eye views the display in angular terms. The NVL MTF is

$$H_{\text{Eye}}(f_x) = \exp \left[ - \frac{\Gamma f_x}{M} \right] \quad (\text{B-23})$$

Equation(B-23) must be converted to the foveal lens image plane

$$H_{\text{Eye}}(S_x, \theta) = \exp \left[ - \frac{\Gamma S_x L(\theta)}{M} \right] \quad (\text{B-24})$$

In conclusion, seven MTF's have been simplified at the expense of two that have been made slightly more complex by the conversion to linear spatial frequency.

## B.2 NOISE EQUIVALENT MODULATION (NEM)

For visual spectrum applications noise equivalent modulation must replace NEAT in the NVL model. In the visual model, the primary noise source is the detector which is a silicon vidicon. Its NEM was extracted from data of Reference (B-2). These data show vidicon S/N as a function of faceplate illumination for a specific bandwidth. The basic function is approximately

$$\frac{\text{peak-to-peak signal}}{\text{noise (rms)}} = 100 E \quad (\text{B-21})$$



where E is faceplate illumination in LUX. The noise equivalent signal is (signal input that just equal noise)

$$NEM = \frac{\text{noise}}{\text{signal}} = \frac{1}{100E} \quad (B-22)$$

assuming that the noise is proportional to the square root of the bandwidth ( $\Delta f$ ) of  $4(10^8)$  Hz. For data given:

$$NEM = \frac{\Delta f}{100E \sqrt{4 \times 10^6}} = 5 \times 10^{-6} \frac{\sqrt{\Delta f}}{E} \quad (E \text{ in LUX}) \quad (B-23)$$

For E in footcandles:

$$NEM = \frac{4.64 \times 10^{-7} \sqrt{\Delta f}}{E} \quad (E \text{ in Foot-Candles}) \quad (B-24)$$

The faceplate illumination can be calculated from system geometry as follows:

$$E_f = \frac{B T_a T_o}{4 F_{no}^2} \quad (B-25)$$

Where

B=Scene brightness in footlamberts

$T_a$  = Atmospheric transmission

$T_o$  = Optical transmission within sensor

$F_{no}$  = The equivalent F/number or F/number actually supplying the vidicon. This is the lens F/number modified by the relay and from basic geometrical optical theory is:

$$F_{noe} = F_{no} \frac{L_D}{L_c} \quad (B-26)$$

If the sensor employs an automatic light level control which operates on vidicon target current, E will be accurately maintained. Therefore, Equation (B-24) applies as written for the level of E which is preset. For the silicon vidicon under study, best performance is obtained when the level is about 0.1 lumens/ft<sup>2</sup>. Equation (B-23) then becomes:

$$NEM = 4.64 \times 10^{-6} \sqrt{\Delta f} \quad (B-27)$$

### B.3 MRM CALCULATIONS

The following MRM equation modifications are required so that the computation may be performed in linear spatial frequency terms. First, in the NVL MRT equation,  $\Delta y$  must be replaced by the apparent detector size at the foveal lens image plane, i.e., it must be the  $\Delta h$  defined on Figure B-2. As previously demonstrated in Equation (B-11).

$$\Delta h_y = a_y \frac{L_C}{L_D} \quad (B-28)$$

Also, in the MRM equation, it is best to compute the Q integral in terms of temporal frequency. This eliminates the velocity term in the MRT equation and makes the Q integral easier to compute. The Q integral is therefore

$$Q(f, \theta) = \int_0^{\infty} \frac{S(f)}{S(f_0)} H_N^2(f) H_w\left(\frac{f}{v_x}\right)^2 H_{Eye}\left(\frac{f}{v_x}\right) df \quad (B-29)$$

Of these terms, only  $H_w$ , the transfer function for a rectangular bar of width w, has not been defined. This transfer function is in linear rather than angular dimensions, i.e.,

$$H_w\left(\frac{f_x}{v_x}\right) = \text{Sinc } w\left(\frac{f_x}{v_x}\right) = \text{Sinc } \left(WS_x\right) \quad (B-30)$$

where

$$w \triangleq \frac{1}{2S_x} \quad (B-31)$$

The MRM equation written to show the dependency of two variables is

$$\text{MRM}(S_x, \theta) = \frac{\text{SNR} \pi^2 \text{NEM}}{4\sqrt{14} \text{MTF}_{\text{TOTAL}}(S_x, \theta)} \left[ \frac{\Delta h_y S_x Q(f, \theta)}{\Delta f_N F_R t_e \eta_{\text{OVSC}}} \right]^{1/2} \quad (B-32)$$

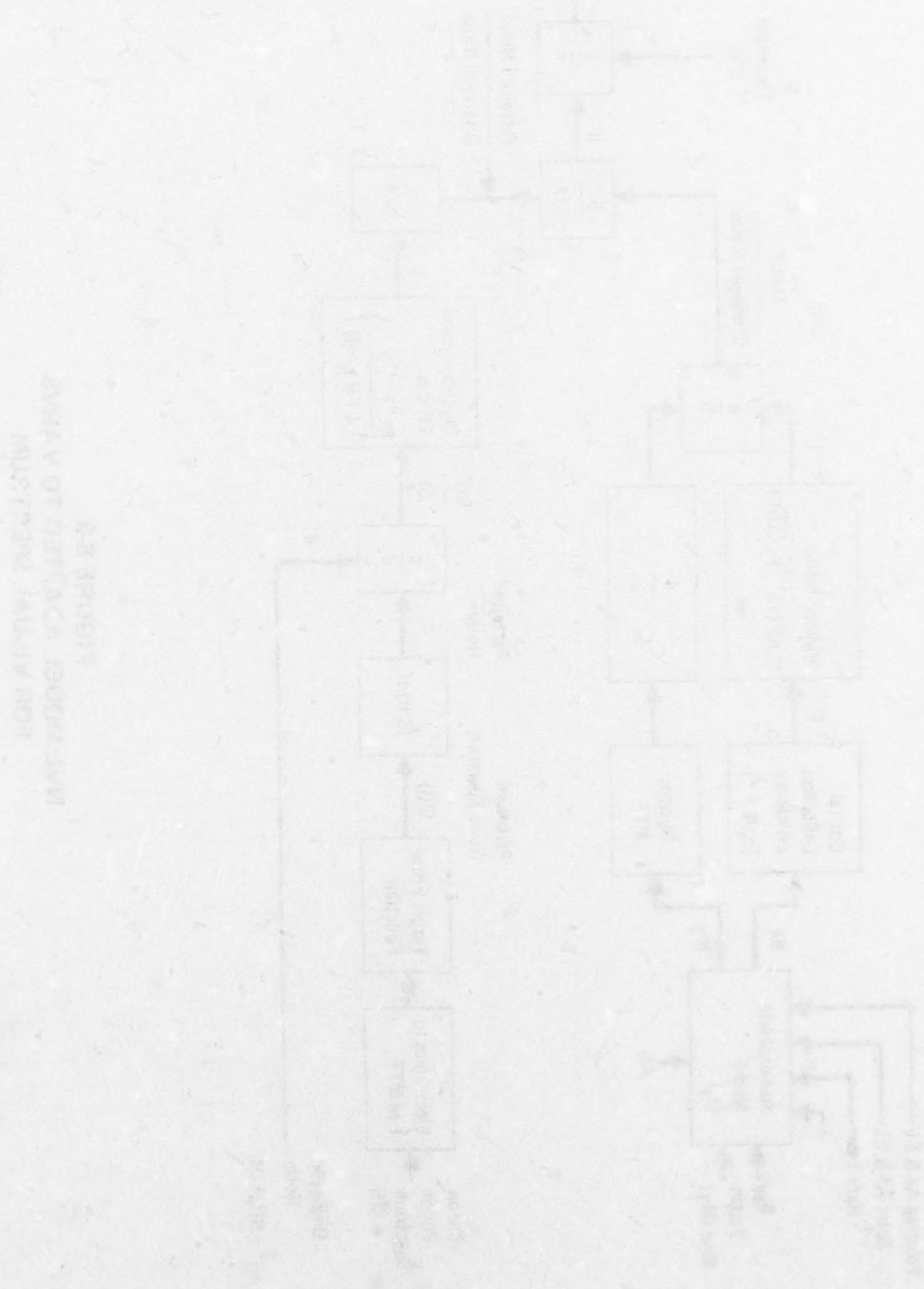
This equation results in an MRT very weakly dependent on  $\theta$ . To obtain the MRM for any field angle  $\theta$ , we convert the spatial frequency term  $S_x$  into an angular frequency term by using Equation(B-9) containing the focal length function:

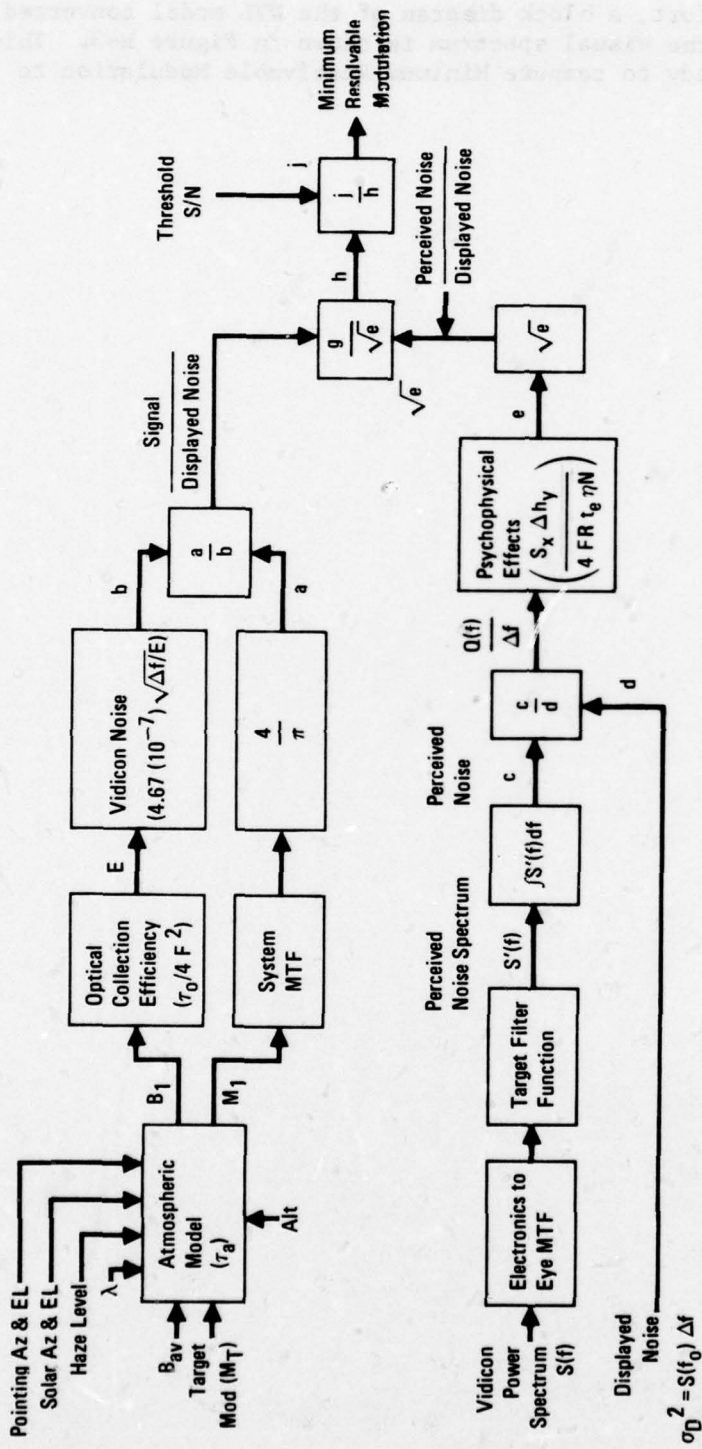
$$f_\mu = S_x L(\theta)$$

Note this will be the angular spatial frequency in the scan direction (target bars normal to the scan direction). It could be related to  $f_x$  and  $f_y$  but this does not appear to be required at this point.

#### B.4 CONCLUSIONS

To conclude this effort, a block diagram of the NVL model converted to the VARVS Concept in the visual spectrum is shown in Figure B-3. This model was used in the study to compute Minimum Resolvable Modulation to predict performance.





GP77-0476-7

FIGURE B-3  
NVL MODEL ADAPTED TO VARVS  
FOR VISUAL SPECTRUM

Appendix C

COMPUTER DESIGN DATA

This appendix contains the results of the computer runs which were used to design the VAD.

LINE	UPDATE	IOV	VIEWER	NR	MS	MT	NPASS	M3	M	NHOLD	NLOOP	NFT	NINC	NM3	M1	M2	M3	M4	M5	M6	M7	MOR	1	4
01	0	0	0	0	0	0	0	0	0	0	0	0	0	0	0	0	0	0	0	0	0	0	0	0
02	0	0	0	0	0	0	0	0	0	0	0	0	0	0	0	0	0	0	0	0	0	0	0	0
03	0	0	0	0	0	0	0	0	0	0	0	0	0	0	0	0	0	0	0	0	0	0	0	0
04	0	0	0	0	0	0	0	0	0	0	0	0	0	0	0	0	0	0	0	0	0	0	0	0
05	0	0	0	0	0	0	0	0	0	0	0	0	0	0	0	0	0	0	0	0	0	0	0	0
06	0	0	0	0	0	0	0	0	0	0	0	0	0	0	0	0	0	0	0	0	0	0	0	0
07	0	0	0	0	0	0	0	0	0	0	0	0	0	0	0	0	0	0	0	0	0	0	0	0
08	0	0	0	0	0	0	0	0	0	0	0	0	0	0	0	0	0	0	0	0	0	0	0	0
09	0	0	0	0	0	0	0	0	0	0	0	0	0	0	0	0	0	0	0	0	0	0	0	0
10	0	0	0	0	0	0	0	0	0	0	0	0	0	0	0	0	0	0	0	0	0	0	0	0
11	0	0	0	0	0	0	0	0	0	0	0	0	0	0	0	0	0	0	0	0	0	0	0	0
12	0	0	0	0	0	0	0	0	0	0	0	0	0	0	0	0	0	0	0	0	0	0	0	0
13	0	0	0	0	0	0	0	0	0	0	0	0	0	0	0	0	0	0	0	0	0	0	0	0
14	0	0	0	0	0	0	0	0	0	0	0	0	0	0	0	0	0	0	0	0	0	0	0	0
15	0	0	0	0	0	0	0	0	0	0	0	0	0	0	0	0	0	0	0	0	0	0	0	0
16	0	0	0	0	0	0	0	0	0	0	0	0	0	0	0	0	0	0	0	0	0	0	0	0
17	0	0	0	0	0	0	0	0	0	0	0	0	0	0	0	0	0	0	0	0	0	0	0	0
18	0	0	0	0	0	0	0	0	0	0	0	0	0	0	0	0	0	0	0	0	0	0	0	0
19	0	0	0	0	0	0	0	0	0	0	0	0	0	0	0	0	0	0	0	0	0	0	0	0
20	0	0	0	0	0	0	0	0	0	0	0	0	0	0	0	0	0	0	0	0	0	0	0	0











3	.00000	.10039	.01591														
4	.03849	.10962	.04168														
5	.00000	.12821	.02009														
6	.03009	.13317	.02721														
7	.00475	.13579	.03001														
8	.09654	.13835	.10955														
9	.00938	.14698	.07108														
10	.06267	.15204	.02181														
11	.03453	.14668	.05878														
12	.00456	.12742	.08210														
13	.02554	.08538	.00635														
14	.00000	0.00000	.02852														
15	.02548	.08496	.06426														
16	.02831	.06578	.15538														
17	.00000	0.00000	.00176														
18	.00176	.08468	.04633														
19	.01760	.08772	.01206														
20	.02169	.09053	.33418														
21	.00000	.01501	.11057														
22	.00315	.03993	.04162														
23	.00497	.04309	.03591														
24	.00259	.04581	.56816														
25	.06111	.15875	.10548														
26	.00000	.17406	.02227														
27	.00000	.17967	.03201														
28	.00000	.18477	.01176														
29	1.30293	.33512	7.73006	0E-08													
30	.84	3	112	6	-3	1											
31	3	-198	4	-2	-34	61	0	5	-16								
32	-20	21	4	-2	-32	92	27	2	-19								
33	-24	3	-3	-2	-32	92	27	2	-19								
34	13	-13	4	-1	-13	98	46	-0	-19								
35	41	17	4	-1	-18	116	48	-0	-26								
36	120	36	4	-1	-18	116	48	-0	-26								
37	116	-42	72	305	-18	-0	25	-53	-48	3	13						
38	53	3	11	3	24	-352	-17	-1	-18	133	35	0	-31				
39	137	18	3	7	-272	-15	-1	-25	61	37	0	-23					
40	80	23	-35	6	-159	-10	-3	-64	-51	-3	6	-46					
41	63	11	4	-18	98	152	-25	-0	-3	-159	-35	3	-23				
42	147	13	-18	-18	-26	-54	-34										
43	49	23	-29	-22	-251	-35	-8										
44	260	4	7	-22	-281	-35	-8										
45	159	11	9	-14	-332	-38	-10										
46	165	7	9	-14	-332	-38	-10										
47	74	93	-38	-18	-322	-54	-34										
48	268	-33	-1	-29	-281	-35	-8										
49	82	10	14	9	-77	-18	-10										
50	103	-5	-14	-9	-77	-18	-10										
51	461	-354	-213	-2	-51	-153	-10										
52	20	8	2	8	13	20	28										
53	82	8	2	8	13	20	28										
54	89	10	10	10	13	20	28										
55	89	-17	-7	5	97	-37	8										
56	0	0	0	0	0	0	0										
57	0.00000	0.00000	0.00000	0.00000	0.00000	0.00000	0.00000										
58	0.00000	0.00000	0.00000	0.00000	0.00000	0.00000	0.00000										
59	0.00000	0.00000	0.00000	0.00000	0.00000	0.00000	0.00000										
60	0.00000	0.00000	0.00000	0.00000	0.00000	0.00000	0.00000										
61	0.00000	0.00000	0.00000	0.00000	0.00000	0.00000	0.00000										
62	0.00000	0.00000	0.00000	0.00000	0.00000	0.00000	0.00000										
63	0.00000	0.00000	0.00000	0.00000	0.00000	0.00000	0.00000										
64	0.00000	0.00000	0.00000	0.00000	0.00000	0.00000	0.00000										
65	0.00000	0.00000	0.00000	0.00000	0.00000	0.00000	0.00000										
66	1	1-10	2603.2617	0.	0.	0.	0.	0.									

1	21	- .8092	1.0000000	0.0000000	.0270648				
2	2	2603.2617	0.						
2	6	.4945	1.0000000	0.0000000	.0270648				
3	3	0.4210.5263	0.						
3	1	.4249	1.6995200	54.8900000	-.0003152				
4	3	-1.3694	0.						
4	1	.0250	1.0000000	0.0000000	.0270648				
5	3	0.0000	0.						
5	1	.3919	1.6995200	54.8900000	-.0003152				
6	3	-2.4192	0.						
6	1	.0147	1.0000000	0.0000000	.0270648				
7	3	-15.1745	0.						
7	1	.9512	1.6995200	54.8900000	-.0003152				
8	3	-1.1512	0.						
8	1	.1531	1.6944300	30.8700000	.0992492				
9	3	-12.8403	0.						
9	1	.0143	1.0000000	0.0000000	.0270648				
10	3	30.9004	3.1332E-02	3.7168E-04	1.6158E-05	4.4842E-07	1.1337E-08		
10	10	.9294	1.6229400	60.2200000	-.0002974				
11	3	-2.5680	1.6480E-02						
11	1	.1338	1.6233800	36.1200000	.1007334				
12	3	13.9104	0.						
12	1	.3211	1.0000000	0.0000000	.0270648				
13	3	.5368	2.4506E-01	7.7662E-04	1.3746E-05	1.5156E-07	5.7386E-10		
13	10	.2491	1.6231900	60.1900000	-.0002638				
14	3	0.0000	2.0856E-02						
14	1	.4217	1.6231900	60.1900000	-.0002638				
15	3	-.2711	-2.0730E-01	-5.9470E-04	-1.2371E-05	-6.7379E-07	-1.3878E-08		
15	10	.0819	1.6233800	36.1200000	.1007334				
16	3	1.7075	1.2900E-02						
16	1	1.4345	1.0000000	0.0000000	.0270648				
17	3	0.0000	0.						
17	1	0.0000	1.0000000	0.0000000	.0270648				
18	3	16.6927	0.						
18	1	.2385	1.6233800	36.1200000	.1007334				
19	3	1.8547	0.						
19	1	.4010	1.6228300	60.3300000	-.0005563				
20	3	-1.5601	0.						
20	1	2.4405	1.0000000	0.0000000	.0270648				
21	3	0.0000	0.						
21	1	.8389	1.0000000	0.0000000	.0270648				
22	3	1.9872	0.						
22	1	.3885	1.6232800	60.1000000	-.0000515				

23 I -1.4772 0.6231600 36.2200000 .1003142  
 24 I 3.1733 0.0000000 0.0000000 .0270648  
 25 I 4.9347 1.0000000 0.0000000 .0270648  
 26 I -3.3086-1.9231E-01-1.1840E-03-1.6132E-05-1.6361E-07-1.2695E-10  
 27 I 3.4666 1.6695200 54.8900000 -.0003152  
 28 I 0.0000 3.1468E-02 0.0000000 .0270648  
 29 I 1.739 1.0000000 0.0000000 .0270648  
 30 I 0.0000 0.0000 0.0000000 .1286331  
 31 I .2500 1.5507200 41.8900000 .1286331  
 32 I 0.0000 0.0000 0.0000000 .1286331  
 33 I .0919 1.5507200 41.8900000 .1286331  
 34 I -0.9936 1.5507200 41.8900000 .1286331  
 35 I 0.0000 0.0000 0.0000000 0.0000000  
 36 I .0000 0.0000 0.0000004 0.0000000  
 Q514.PP2,PP2 -1.80979 7.86902  
 SURFACE TO ONE SPACE EQUALS -67.40782 7.86902

HEIGHT  
 00  
 01  
 02  
 03  
 04  
 05  
 06  
 07  
 08  
 09  
 10  
 11  
 12  
 13  
 14  
 15  
 16  
 17  
 18  
 19  
 20  
 21  
 22  
 23  
 24  
 25  
 26  
 27  
 28  
 29  
 30  
 31  
 32  
 33  
 34  
 35  
 36  
 37  
 38  
 39  
 40  
 41  
 42  
 43  
 44  
 45  
 46  
 47  
 48  
 49  
 50  
 51  
 52  
 53  
 54  
 55  
 56  
 57  
 58  
 59  
 60  
 61  
 62  
 63  
 64  
 65  
 66  
 67  
 68  
 69  
 70  
 71  
 72  
 73  
 74  
 75  
 76  
 77  
 78  
 79  
 80  
 81  
 82  
 83  
 84  
 85  
 86  
 87  
 88  
 89  
 90  
 91  
 92  
 93  
 94  
 95  
 96  
 97  
 98  
 99  
 00

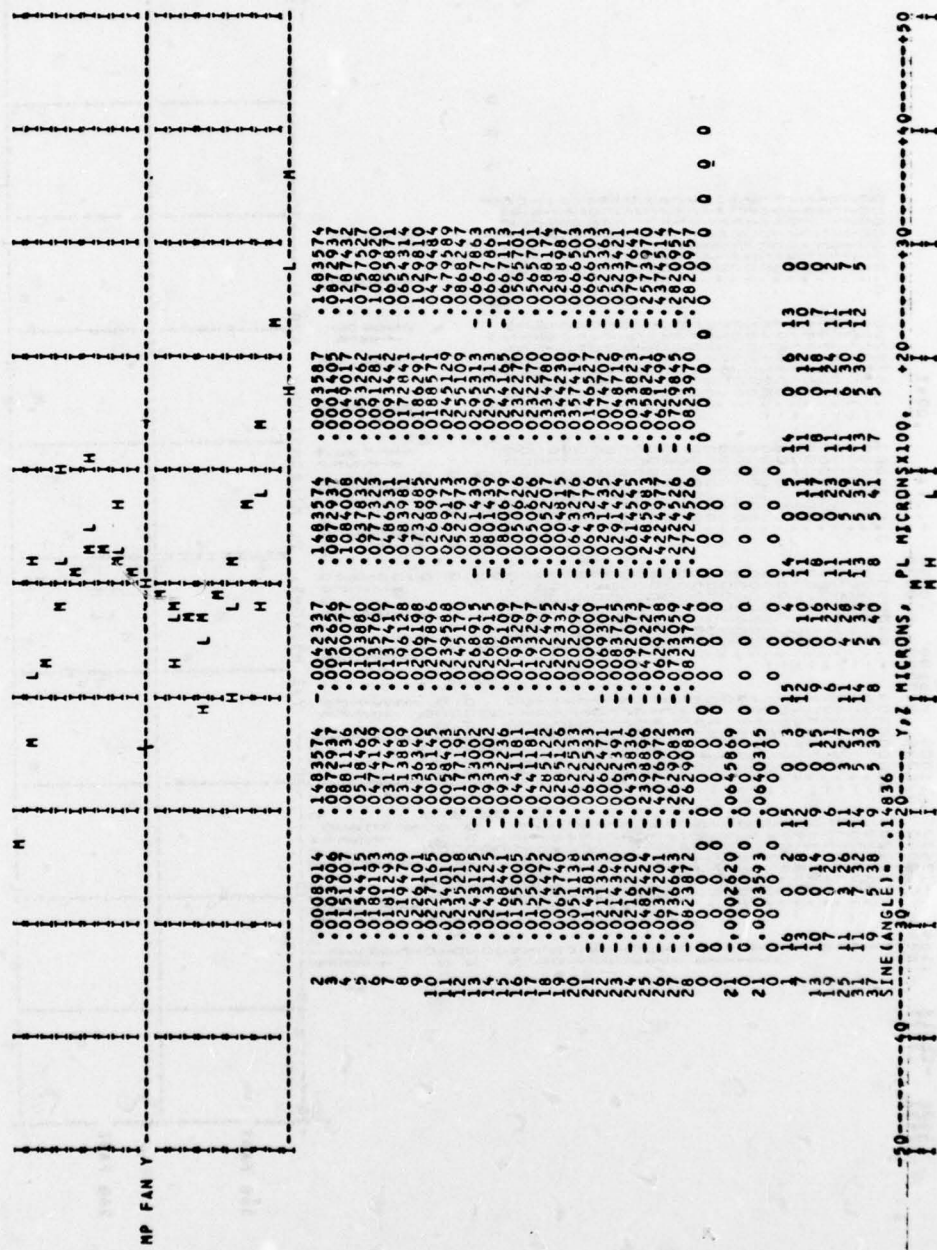






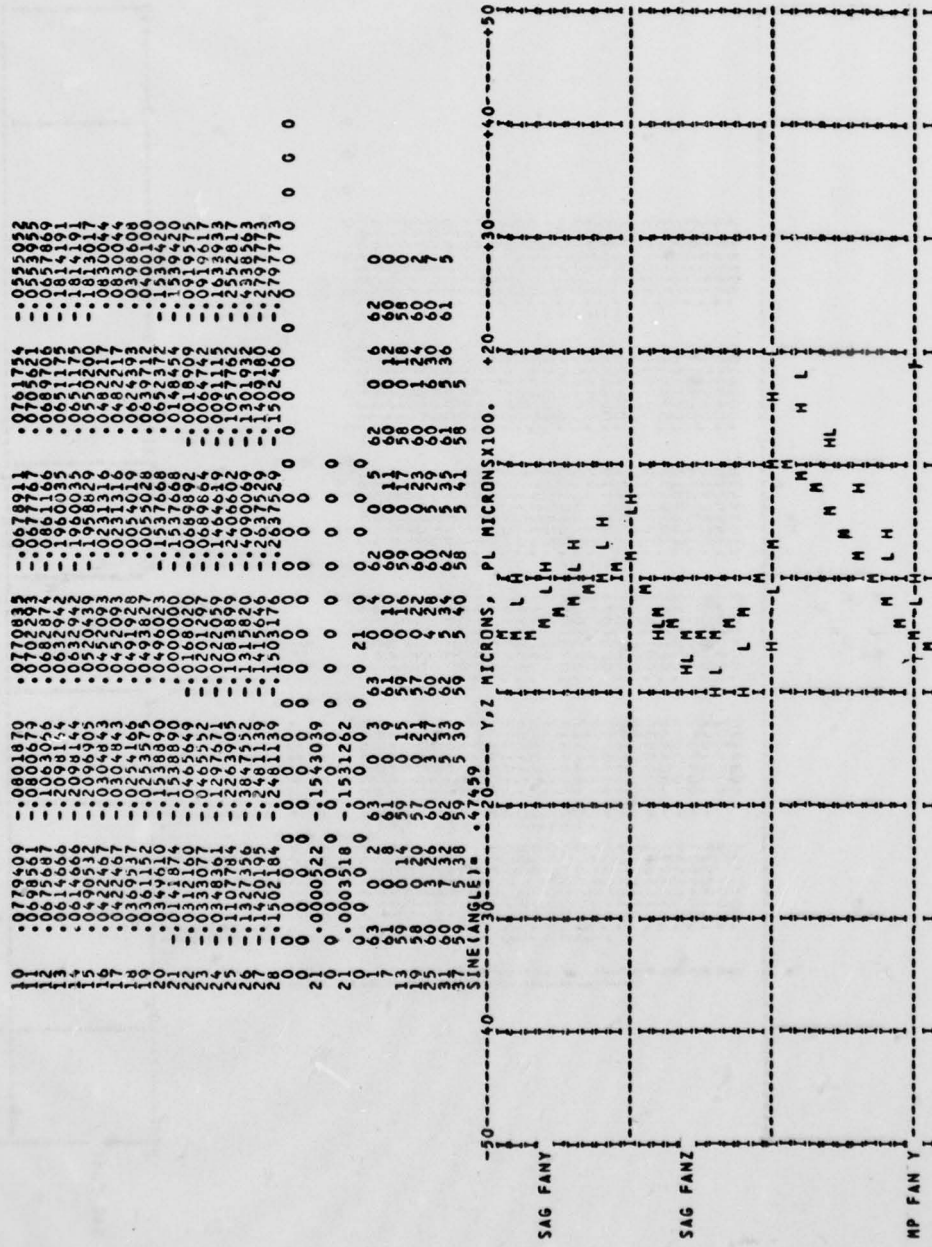


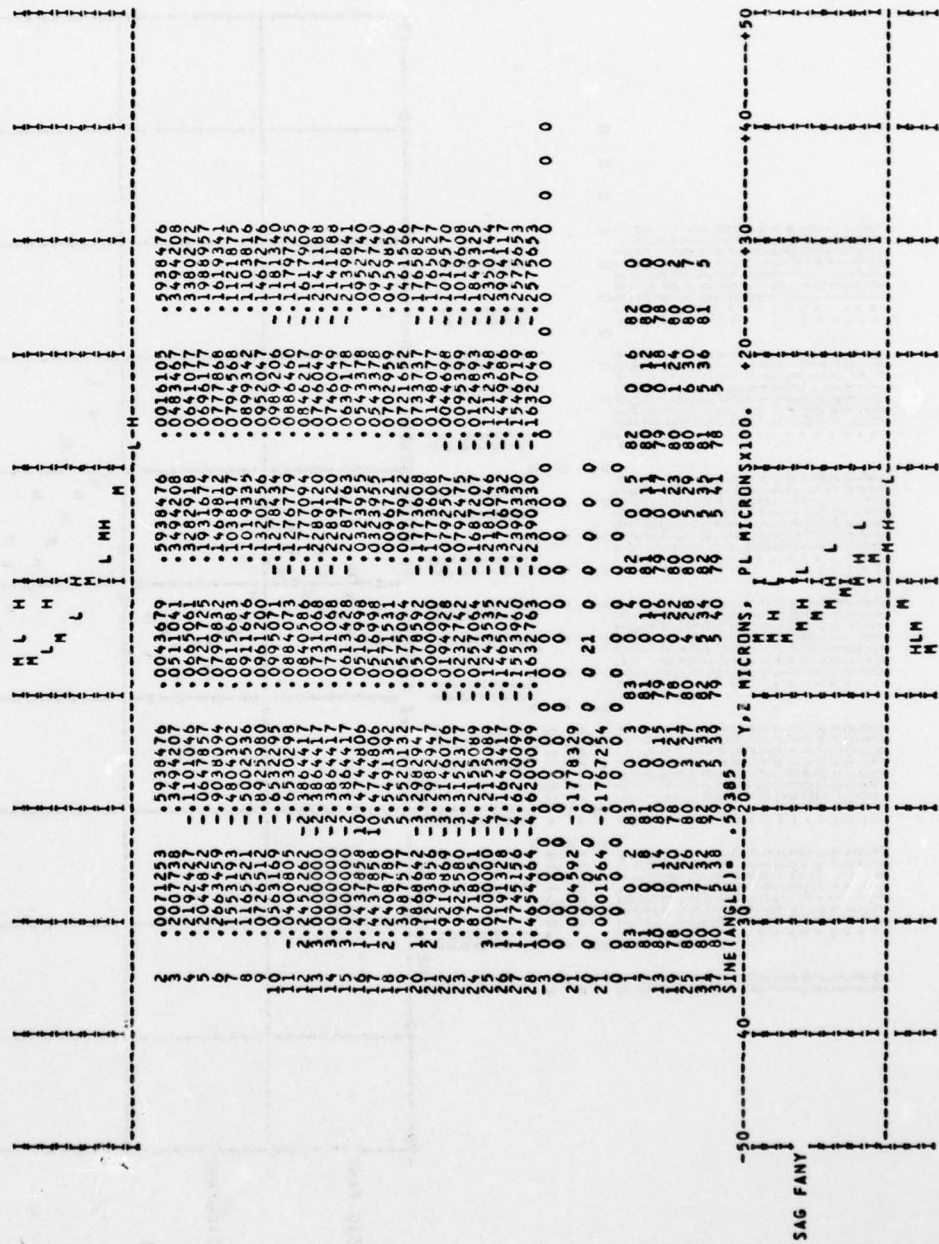




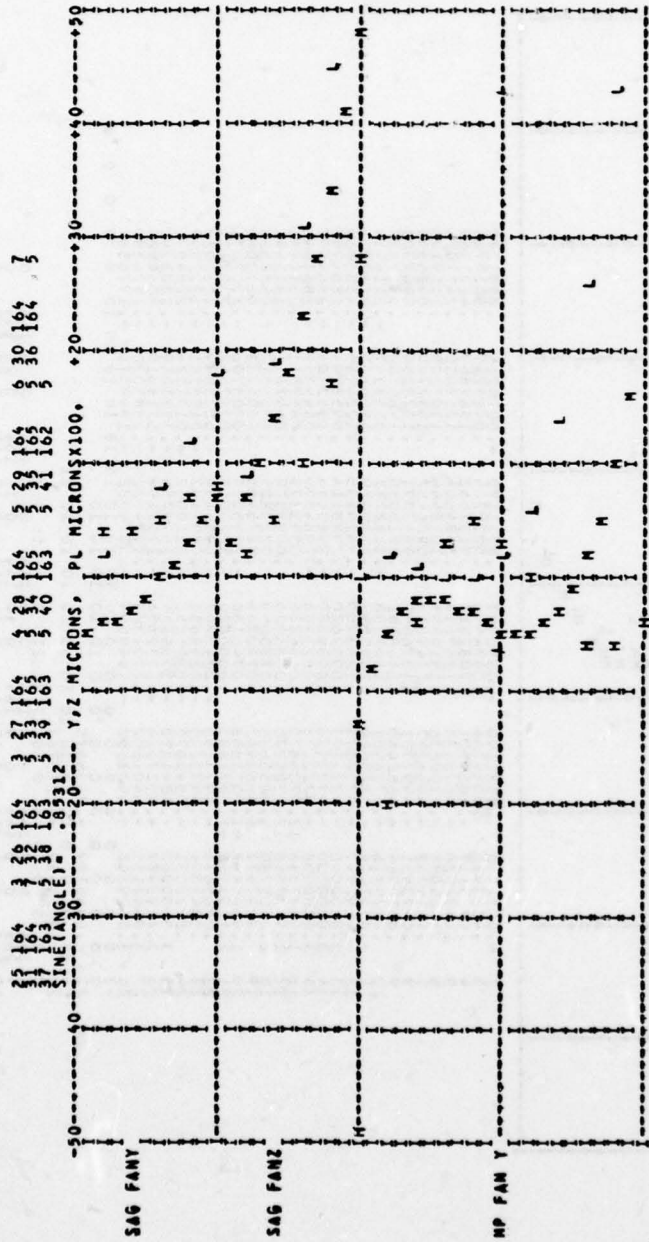






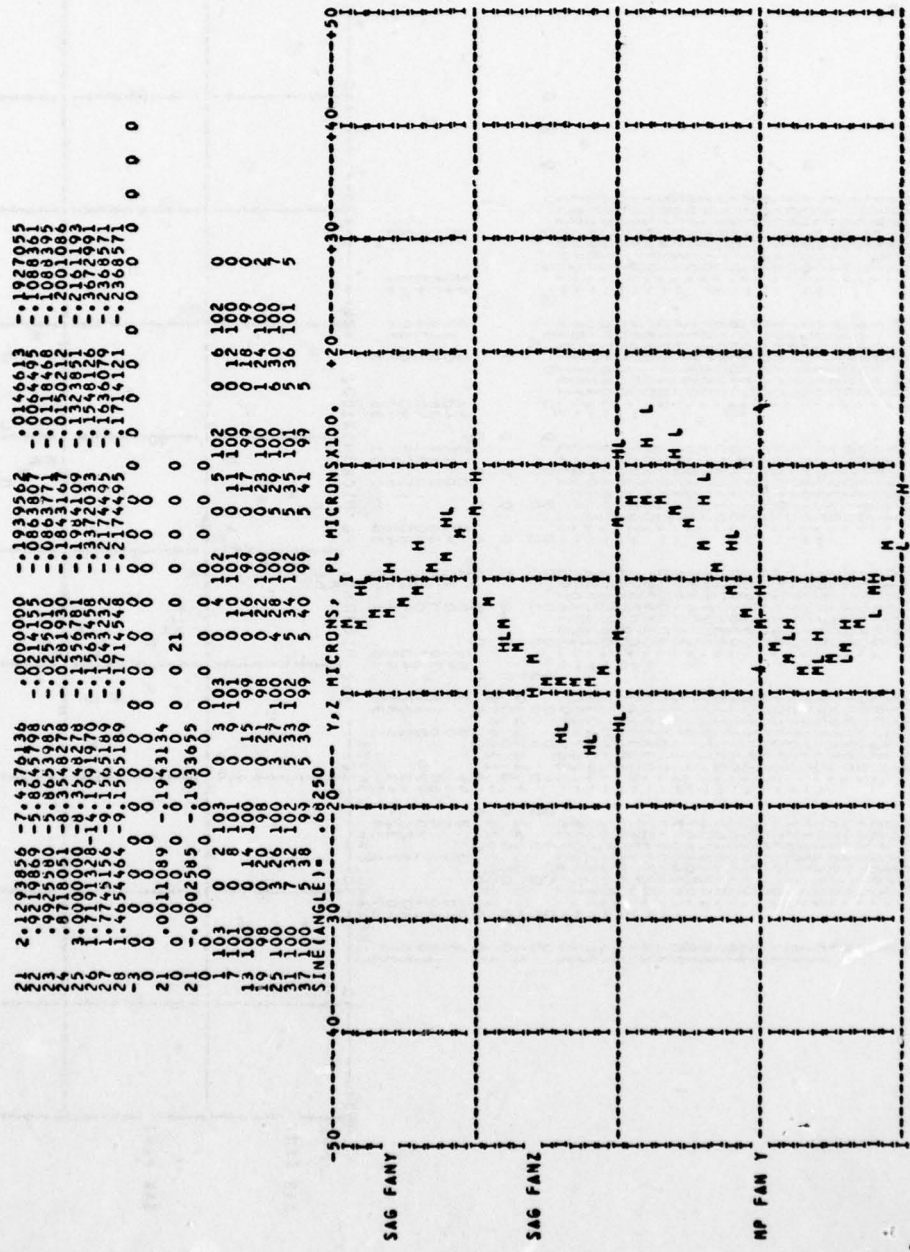




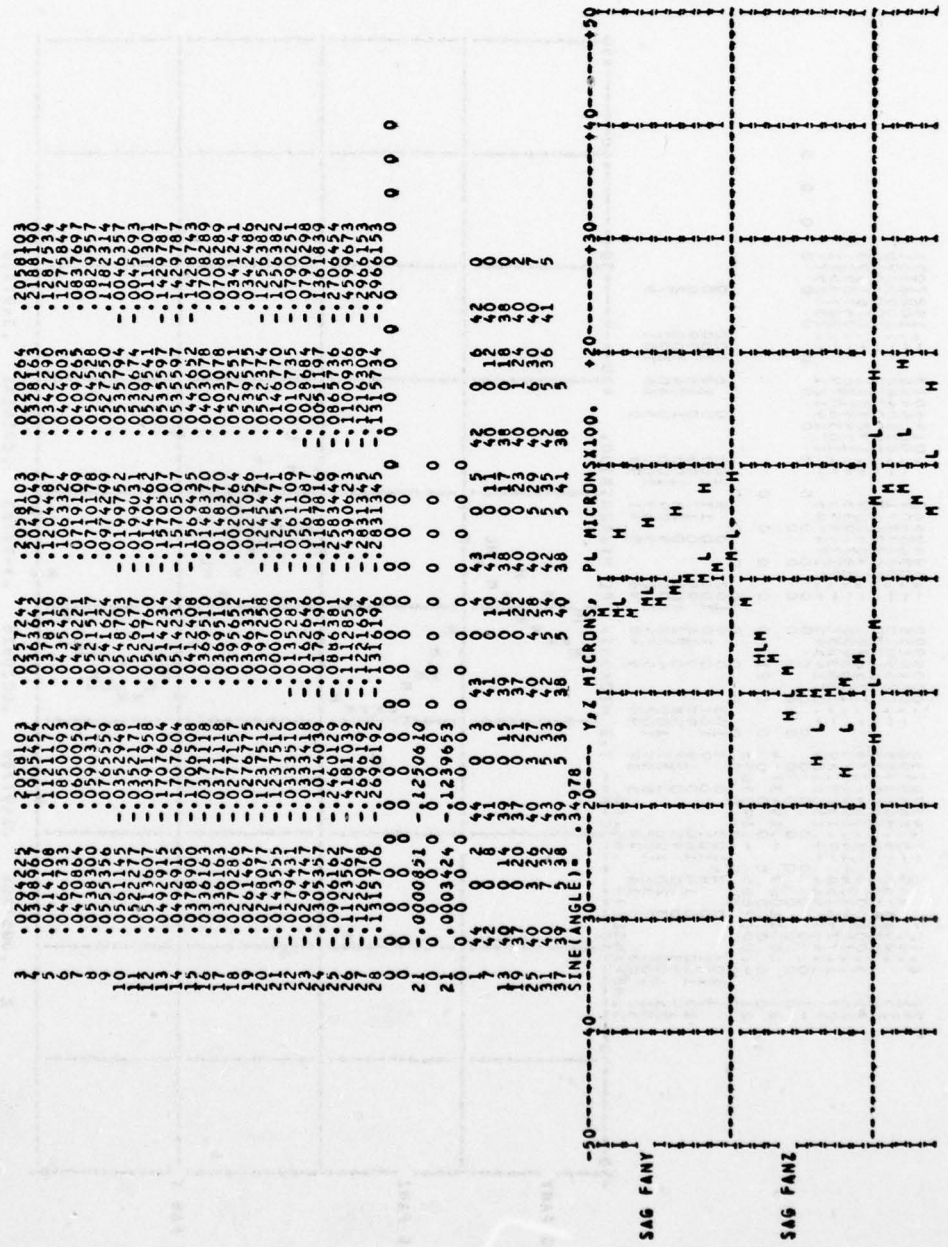


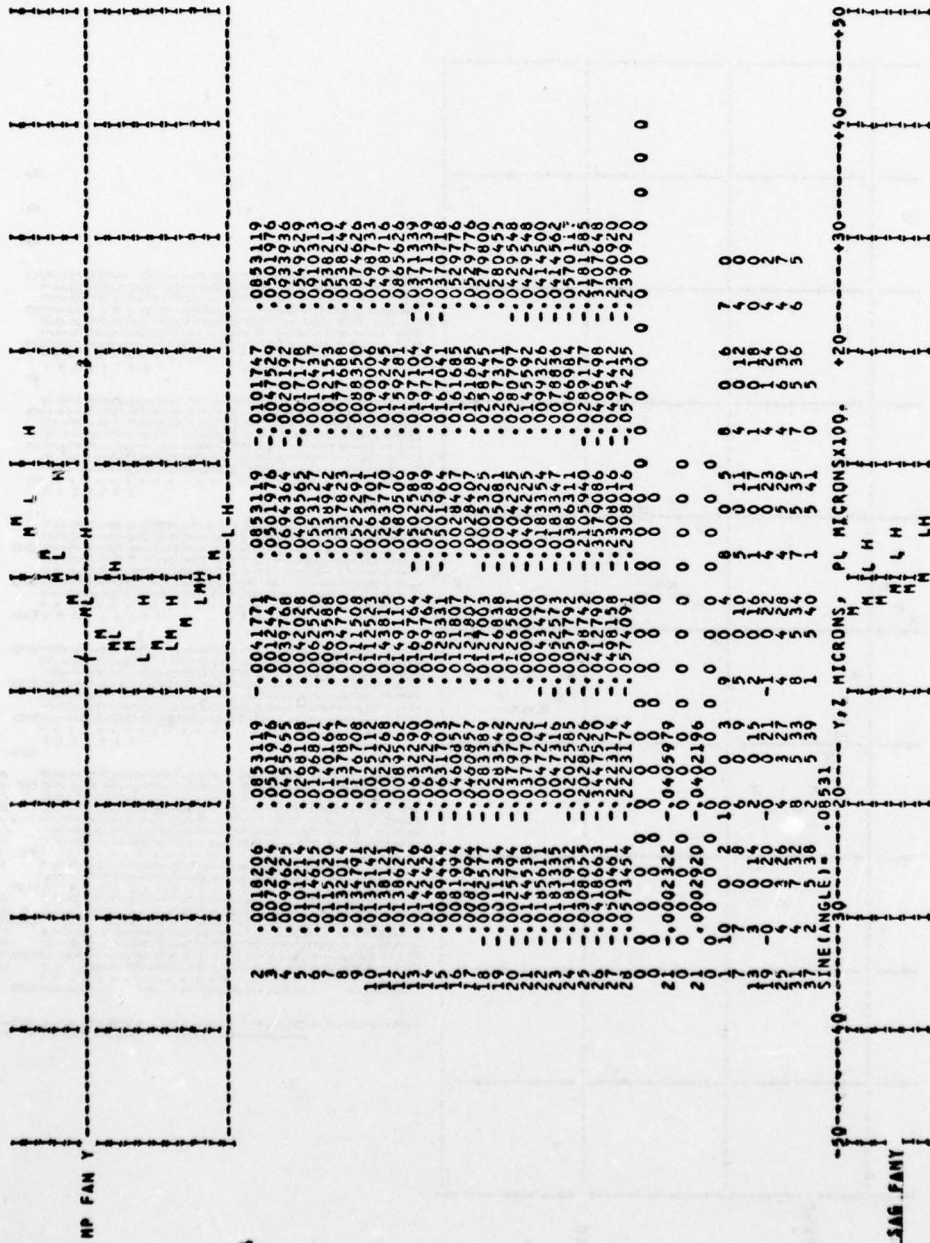
0	10	20	30	40	50
0	0	0	0	0	0
10	0	0	0	0	0
20	0	0	0	0	0
30	0	0	0	0	0
40	0	0	0	0	0
50	0	0	0	0	0



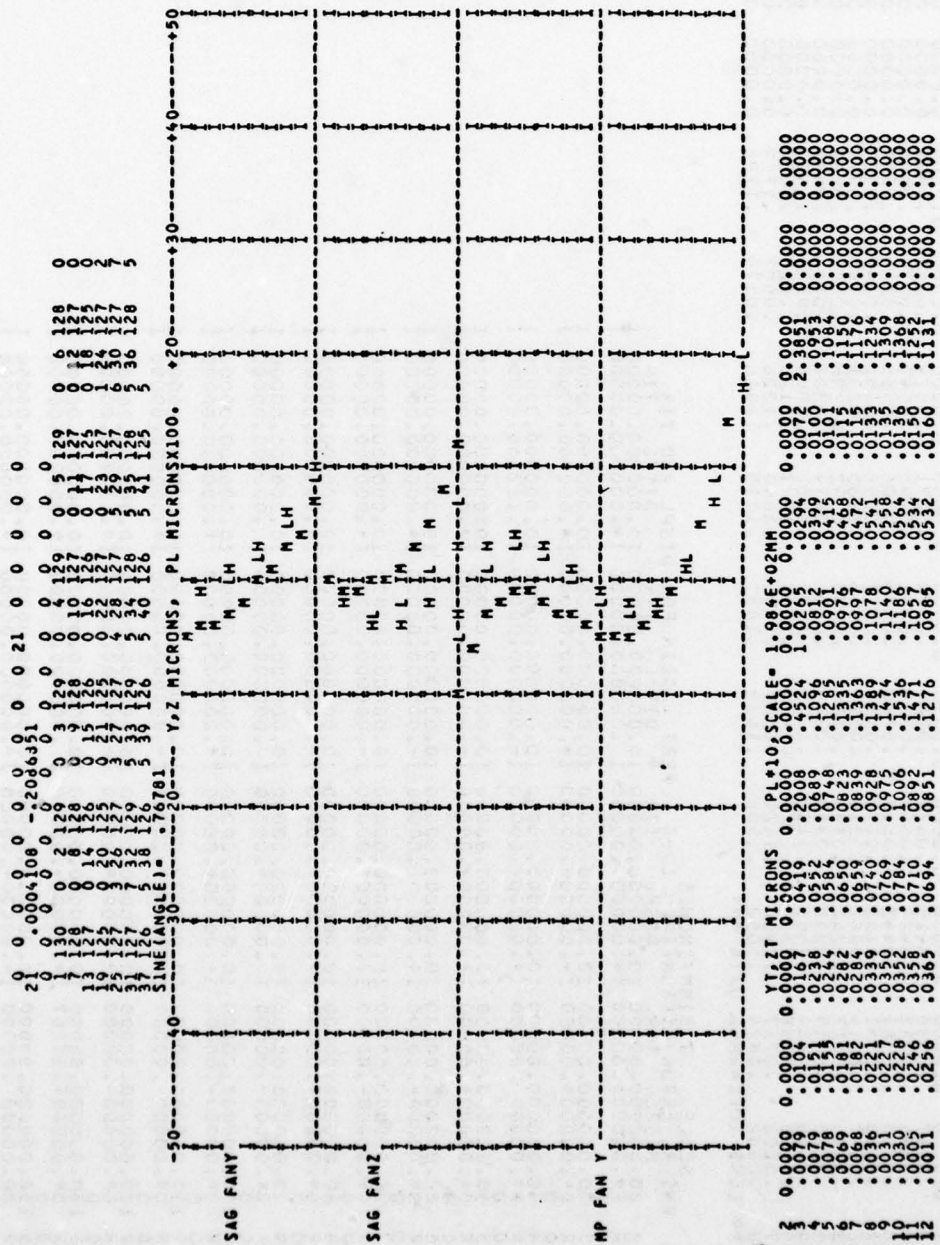


2 .0057608 .3497788 .0020828 .3497788 -.0016193 .3497788











```

00.000000*.00000 I*.00000*.00000 I*.00000 .00000 I .000000.00000 I
190.000000.00000 I0.00000.00000 I0.000000.00000 I0.000000.00000 I
00.000000 .00000 I-.00000-.00000 I-.00000 .00000 I*.000000.00000 I
200.000000*.00000 I-.00000-.00000 I0.000000-.00000 I*.000000.00000 I
00.000000*.00000 I-.00000-.00000 I0.000000-.00000 I*.000000.00000 I
210.000000.00000 I0.00000.00000 I0.000000-.00000 I0.000000.00000 I
00.000000 .00000 I-.00000-.00000 I-.000000-.00000 I*.000000.00000 I
220.000000*.00000 I*.80132*.00000 I0.000000.00000 I0.000000.00000 I
00.000000*.00000 I*.80132*.00000 I-.00000 .00000 I*.000000.00000 I
230.000000.00000 I0.00000.00000 I0.000000.00000 I0.000000.00000 I
00.000000-.00000 I-.00000-.00000 I0.000000-.00000 I*.574830.00000 I
240.000000 .00000 I0.00000.00000 I0.000000.00000 I0.000000.00000 I
00.000000 .00000 I*.00000*.12500 I-.00000-.00000 I*.000000.00000 I
250.000000*.00000 I0.00000.00000 I0.000000.00000 I0.000000.00000 I
00.000000*.00000 I*.85304*.00000 I-.00000 .00000 I*.000000.00000 I
260.000000.00000 I0.00000.00000 I0.000000.00000 I0.000000.00000 I
00.000000-.00000 I*.12582-.00000 I-.00000-.00000 I*.000000.00000 I
270.000000.00000 I0.90927-.00000 I0.000000-.00000 I0.000000.00000 I
00.000000.00000 I0.00000.00000 I0.000000.00000 I0.000000.00000 I
280.000000*.00000 I-.00000-.00000 I-.00000 .00000 I-.000000.00000 I
00.000000*.00000 I0.00000.00000 I0.000000-.00000 I0.000000.00000 I
290.000000*.00000 I0.00000.00000 I0.000000-.00000 I0.000000.00000 I
40.000000.00000 I0.00000.00000 I0.000000.00000 I0.000000.00000 I
00.000000 .00000 I*.00000-.00000 I*.00000-.00000 I*.000000.00000 I
50.000000.00000 I0.00000.00000 I0.000000.00000 I0.000000.00000 I
00.000000 .00000 I*.00000-.00000 I-.00000 .00000 I*.109380.00000 I
90.000000*.00000 I0.00000.00000 I0.000000.00000 I0.000000.00000 I
00.000000*.00000 I0.00000.00000 I-.00000-.00000 I*.000000.00000 I
120.000000.00000 I0.00000.00000 I0.000000.00000 I0.000000.00000 I
00.000000-.00000 I-.00000-.00000 I0.00000*.00000 I*.000000.00000 I
160.000000.00000 I0.00000.00000 I0.000000.00000 I0.000000.00000 I
00.000000-.00000 I-.00000*.00000 I*.00000 .00000 I*.000000.00000 I
200.000000.00000 I0.00000.00000 I0.000000.00000 I0.000000.00000 I
00.000000-.00000 I-.00000*.00000 I*.000000.00000 I*.242840.00000 I
210.000000.00000 I0.00000.00000 I0.000000.00000 I0.000000.00000 I
00.000000*.39151 I*.00000*.00000 I0.000000.00000 I0.000000.00000 I
240.000000.00000 I0.00000.00000 I0.000000.00000 I0.000000.00000 I
00.000000-.00000 I*.00000.00000 I*.000000.00000 I*.704100.00000 I
260.000000.00000 I0.00000.00000 I0.000000.00000 I0.000000.00000 I
00.000000*.73232 I*.00000*.00000 I0.000000.00000 I0.000000.00000 I

```

```

1 SEE UPDATE 10/ 1/71
MIT 6
NST 6 NWT MT NPASS M5 M NHELD NLOOP NFT NINC NN4 M1 M2 M3 M4 M5 M6 M7 M8 MDR

```